UNIVERSITY OF OKLAHOMA

GRADUATE COLLEGE

# SYNTHESIS, STRUCTURE AND ELECTROCHEMICAL PERFORMANCE OF POLY(ETHYLENIMINE)-BASED ELECTROLYTES

A Dissertation

SUBMITTED TO THE GRADUATE FACULTY

in partial fulfillment of the requirements of the

degree of

Doctor of Philosophy

By

MICHAEL JASON ERICKSON
Norman, Oklahoma
2004

UMI Number: 3148890

UMI Microform 3148890



ProQuest Information and Learning Company
300 North Zeeb Road
P.O. Box 1346
Ann Arbor, MI 48106-1346

# SYNTHESIS, STRUCTURE AND ELECTROCHEMICAL PERFORMANCE OF POLY(ETHYLENIMINE)-BASED ELECTROLYTES

A Dissertation APPROVED FOR THE
DEPARTMENT OF CHEMISTRY AND BIOCHEMISTRY

By


Daniel Glatzhofer

Roger Frech

John Furneaux

Ken Nicholas

Ralph Wheeler

**Acknowledgements**

I would like to thank a few people whose support made this dissertation possible. As my main research advisor, Dr. Glatzhofer has provided an exceptional amount of encouragement and support throughout my graduate school experience. He is an excellent example of what a mentor should be. As co-advisor of my research, Dr. Frech has provided wisdom, guidance and research tools. For their advising services, I would like to express my gratitude to my other committee members, Dr. Nicholas, Dr. Wheeler and Dr. Furneaux. I would like to thank Albert Snow for his early guidance in Dr. Glatzhofer's lab. Discussions with Chris Burba have also been very useful. The support from other past lab mates is appreciated. The Department of Chemistry and Biochemistry support staff deserve recognition for their technical and non-technical assistance provided throughout my graduate school experience. Arlene Crawford in particular has been especially helpful. I would like to express thanks to others in the Department of Chemistry and Biochemistry that have provided assistance. Finally, I would like to thank my family, especially Kendra, for their support.

**Table of Contents**

## ABSTRACT

Ion conducting polymers have found application as the electrolyte host in lithium batteries and proton exchange membrane fuel cells as a result of desirable processing and adequate ionic conductivity. Poly(ethylenimine) (PEI) is an example of an ion conducting polymer whose potential has not been fully explored as an electrolyte host. Through previously unexplored chemical modifications to the PEI structure and/or addition of ionic conductivity promoting small molecules, the physical properties and ion conduction of PEI-based electrolytes have been improved. Addition of a cyanoethyl ($-CH_2CH_2CN$) side chain to the nitrogen of the PEI repeat units resulted in a new polymer called poly((*N*-cyanoethyl)ethylenimine) (PCEEI). This polymer, when complexed with lithium triflate, has altered ionic conductivity from PEI and poly(acrylonitrile). Infrared spectroscopy has also revealed a significant coordination of lithium ion to the nitrile of the PCEEI side chain in PCEEI:LiTf electrolytes and has been quantified and compared with LiTf speciation data. In another polymer electrolyte system studied, PEI was cross-linked with tetraethylene glycol diacrylate (TEG) and plasticized with diglyme to produce gel-type electrolytes. With dissolved LiTf, high room temperature ionic conductivity was observed in this system ($10^{-4}$ S/cm). Infrared spectroscopy allowed analysis of lithium ion coordination to the individual gel components and correlation of the ionic conductivity to LiTf speciation. A lithium polymer battery with lithium and $LiV_3O_8$ electrodes was designed, and a variety of PEI-based polymers were tested as the electrolyte host including poly(*N*-methylethylenimine) (PMEI), cross-linked PMEI,

PCEEI, cross-linked PCEEI and diglyme infused TEG cross-linked PEI. Good to excellent first discharge capacities were observed. Proton exchange membranes consisting of PEI with a di-aldehyde based cross-linker in the presence of varying compositions of $H_3PO_4$ gave membranes with high proton conductivity ($10^{-2}$ S/cm) at 150 °C. The chemical structure of these electrolytes was studied with infrared and nuclear magnetic resonance spectroscopies, and, when viewed in light of the conductivity data, revealed a system whose mechanism of ion conduction changes at different phosphoric acid compositions. Membrane electrode assemblies containing the cross-linked PEI-$H_3PO_4$ membranes were incorporated and tested in a fuel cell and resulted in performance comparable to a commercially available membrane.

## Chapter 1: INTRODUCTION

Environmental concerns about global warming, a declining supply of fossil fuels and the increased demand for high performance miniaturized electronics are driving portable power suppliers to explore alternative power source chemistries. For example, nickel- and lithium-based rechargeable batteries are being optimized for companies such as General Motors[1], Honda[2], Ford[3] and Toyota[4] for incorporation into hybrid vehicles to improve power density, weight and fuel efficiency. The same auto manufacturers are developing new polymer-based hydrogen fuel cell systems to serve as powertrains in prototype vehicles with the goal being to eliminate the direct consumption of fossil fuels and to improve the overall energy efficiency of the vehicle[1-4]. Portable electronics like laptop computers, mp3 players and cell phones have recently swamped the marketplace and have pushed portable power suppliers to improve battery specifications by incorporating electrodes and electrolytes that are capable of yielding higher energy densities. Advances made in portable energy storage and production devices are linked directly to the advances of the chemistries of their components.

While a fuel cell is an energy conversion device and a battery is an energy storage device, both harness chemical reactions to produce energy. Ions are produced and consumed by these reactions and then, for proper cell function, these ions must travel through a medium between the electrodes. This medium, including the ions, is called an ion conductor or electrolyte. Improving the efficiency of ion movement through this material is an area of research that has received significant attention because advances in known materials and development in new materials are required for battery and fuel cell

improvement. My research work has involved the creation of new polymer-based ion conductors (polymer electrolytes), the study of ion movement in the polymer electrolytes and incorporation and study of the electrochemistry of the polymer electrolytes in lithium-polymer batteries and proton exchange membrane fuel cells. A background and description of relevance for lithium-polymer batteries and proton exchange membrane fuel cells is given in this introductory chapter.

## Polymer Electrolytes for Lithium Polymer Batteries

### Battery and Li Battery Background

A battery is composed of several electrochemical cells that are connected in series and/or parallel to provide a required voltage and capacity (Figure 1). Each cell consists of two electrodes, one oxidized upon cell discharge (anode), the other reduced (cathode), separated by an electrolyte material containing dissociated salts that enables ion transfer

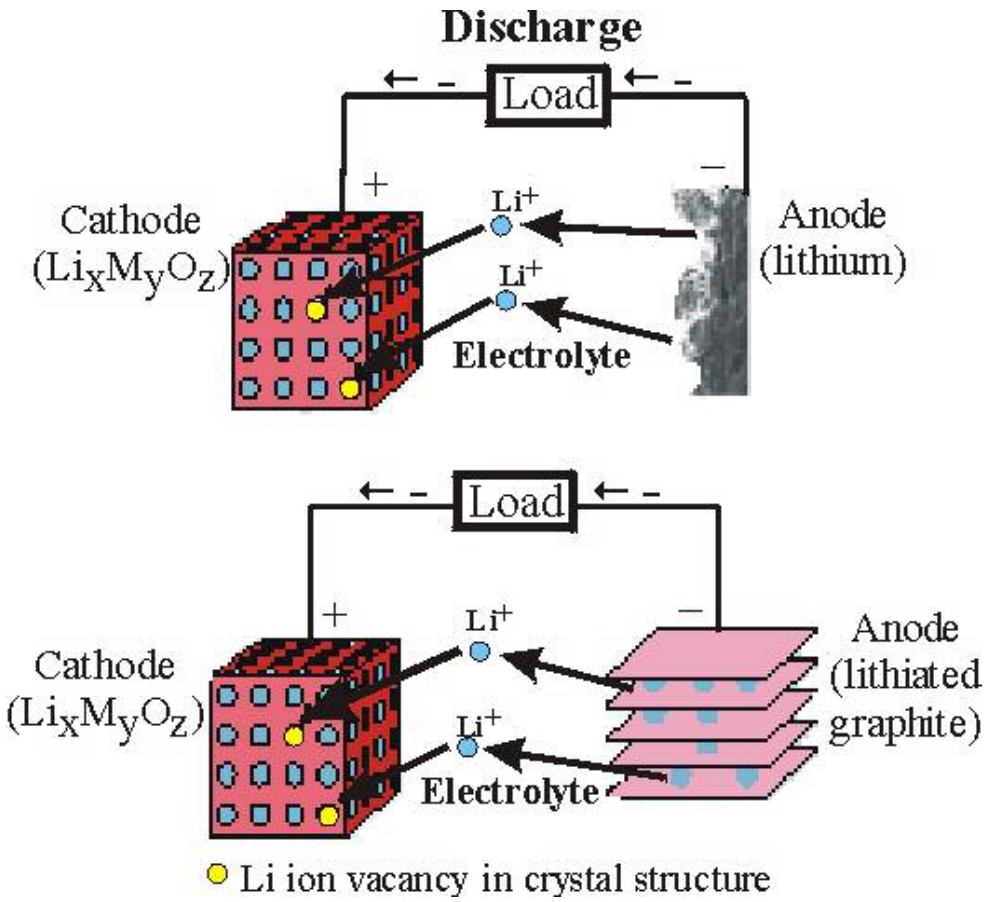


Figure 1: Discharge cycle in two battery cells with different lithium-based anodes

between the two electrodes. Once these electrodes are connected externally, the redox reactions proceed in tandem at both electrodes, thereby liberating electrons and enabling the current to perform work. Depending on whether the reactions at the electrodes are reversible, a battery is classified as either primary (non-rechargeable) or secondary (rechargeable). The amount of electrical energy that a battery is able to deliver is a function of the cell potential and capacity, both of which are linked to the chemistry of the system.[5]

Among the rechargeable battery types available, alkaline, nickel-cadmium, nickel-metal hydride and lithium are widely used today in portable energy consuming

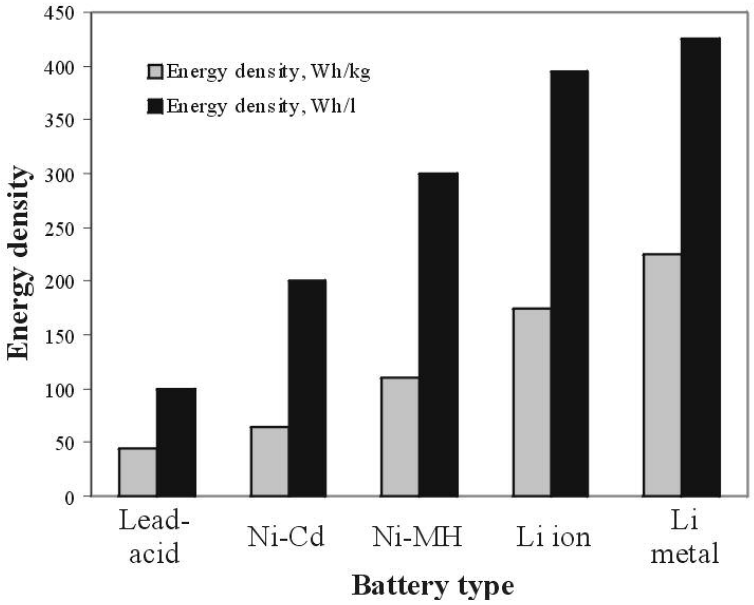


Figure 2: A comparison of approximate maximum energy densities for different battery types as a function of mass and volume[7]

devices (Figure 2). Alkaline batteries are suitable for low-power applications but have limited cycle life and are relatively low in energy density. Nickel-cadmium batteries are used where long life, high discharge rate and economical price are important, but contain environmentally unsafe cadmium metal, so their use has become limited. The nickel-metal hydride battery has a higher energy density compared to the nickel-cadmium but a reduced cycle life. Lithium-based batteries are the newest battery technology (first commercial cell-Sony, 1991) and is used where high-energy density and weight is of prime importance[6]. Among the various existing technologies, lithium-based batteries

currently outperform other systems and receive the most research attention at the fundamental and applied levels[7].

The strength of lithium batteries is a result of the lithium ion having the most negative reduction potential of all the metals (-3.04 V versus standard hydrogen electrode). This is important because it allows a lithium anode to produce a higher voltage than any other metal in systems using identical cathodes. The electrochemical capacity of lithium is also higher than other metals and allows a lithium anode to deliver the greatest quantity of charge per unit weight. Since the energy produced by a battery is the product of its voltage times the charge it delivers, lithium's large electrochemical capacity and capability of generating high cell voltages allows lithium batteries to produce higher energy per unit weight than its nearest competitor, the nickel-metal hydride battery.[7]

**Lithium Battery Materials**

The electrode materials (Figure 3), while not the main focus of the research presented here, play a vital role in cell performance as they dictate, along with the electrolyte to a lesser extent, the amount of current that can be provided and the voltage

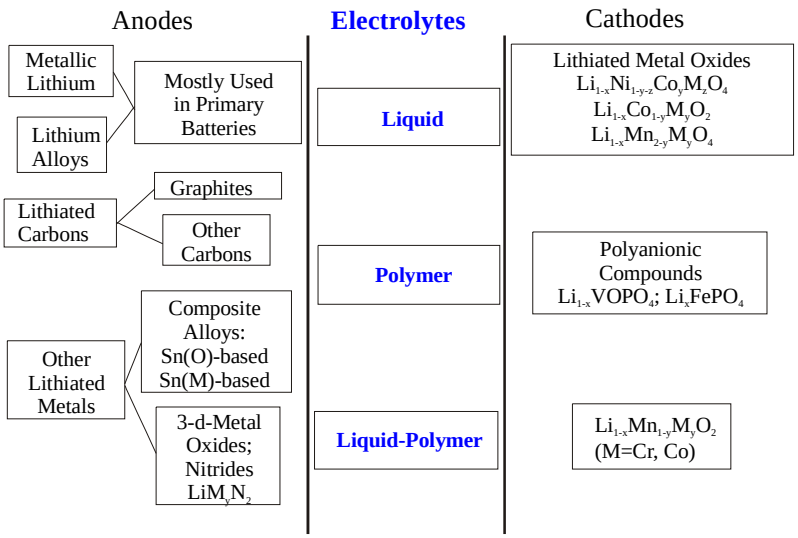


Figure 3: Common electrode material types and generic electrolyte types found in lithium batteries

at which the current is provided. The three different types of materials considered for anode materials in secondary lithium cells are carbon based, stabilized metallic Li and metal oxides. Carbon-based anodes allow for the intercalation of Li ions, have an electrochemical potential close to that of metallic Li and eliminate the problematic Li metal from the cell. Commercial secondary batteries also use metallic Li stabilized as an alloy with a metal such as aluminum or with a solid polymer electrolyte (versus the more common liquid electrolyte) to control undesired Li plating. Metal oxides such as Li transition metal nitrides and manganese vanadates and molybdates are the newest materials to be studied as anodes owing to their ability to provide a higher capacity per unit weight than graphite and improved cycling over Li metal.[9]

Common cathode materials (Figure 3) used in secondary Li batteries are typically of the composition $Li_xM_yO_z$ where M is a transition metal that can be reversibly oxidized and reduced with cycling. $LiCoO_2$, $LiV_3O_8$ and $LiMnO_2$ are typical cathodes in secondary

cells and allow cell operating voltages between 2.5 and 4.5V when using a Li-metal or carbon anode. These solids have layered or tunneled crystal structures that act as a host for the intercalation and de-intercalation of lithium ions upon cycling.[5] Cathode materials must not only provide the necessary electrochemical voltage but also must have sufficient electronic conductivity and are typically constructed with conductivity-boosting carbon[10].

The role of the electrolyte is to separate the electrodes, preventing direct reaction, while allowing lithium ions to pass between the electrodes. Li ion rate of flow through the electrolyte will govern the current generated by the cell, so the rate of flow (often described using ionic conductivity) must be sufficient to satisfy the current requirements for the cell. The electrolyte solution must also be electrochemically stable within the redox window created by the cathode and the anode (typically, -3 to 1 V vs. S.H.E.). A suitable Li salt is one that has a low lattice energy that allows for sufficient solubility and cation-anion separation in either the solid or liquid solution. Typically, a Li ion paired with a large, electrochemically stable anion with a delocalized charge is suitable. Examples include: $LiClO_4$, $LiPF_6$, $LiBF_4$, $LiCF_3SO_3$ (LiTf) and $Li(CF_3SO_2)_2N$ (LiTfsi).[11]

Liquid electrolytes are the most common electrolyte type in secondary Li batteries. They consist of a single or, more typically, a combination of aprotic organic solvents such as ethylene carbonate, propylene carbonate, dimethyl carbonate, diethyl carbonate, dimethoxyethane and diethoxyethane. These solvents with a suitable dissolved Li salt generally allow high ion mobility and are electrochemically stable within the redox window of most cathodes and anodes. Although liquid electrolytes generally yield acceptable ion mobility and electrochemical stability, they are not completely ideal. One of the main drawbacks of the use of liquid electrolytes is that they require a robust metal

battery casing to reduce potential leakage. All of the commonly used liquid electrolytes pose potential fire and toxicity threats. The metal casing significantly affects the battery by increasing the weight, limiting the shape and adding expense.[9]

**Polymer Electrolytes**

Solid polymer electrolytes (PEs) (Figure 4), which consist of Li salts dissolved in polymer, are currently being incorporated into lithium batteries and overcome problems related to using a liquid electrolyte. A polymer electrolyte is suitable in a Li battery when it has good mechanical properties (to assure easy battery fabrication), high ionic mobility, high lithium transport under a potential, wide electrochemical stability, low cost and benign chemical composition. Cross-linked and non-crosslinked poly(ethylene oxide) (PEO), poly(vinylidene fluoride) (PVDF), poly(bis(methoxyethoxy-ethoxy)phosphazene) (MEEP) and poly(acrylonitrile) (PAN) are the most common polymers studied, while the salts employed are typically the same as for liquid electrolytes.[9] For room temperature batteries, the goal for ionic conductivity (a measure of the dissociated ion mobility) of a PE is $10^{-3}$ S / cm.[7] Currently, no PE satisfies this requirement. Commercial Li polymer batteries are typically operated above room temperature to obtain the necessary current rate provided by higher ionic conductivity. As an alternative, a variety of liquid-polymer 'hybrid' electrolytes (Figure 4) are being developed to satisfy the room temperature conductivity requirement. These solid-like materials incorporate organic solvents called plasticizers, usually the same as in liquid electrolytes, into the PE framework to increase their ionic conductivity. Depending on the plasticizer content, improvements in

conductivity are about an order of magnitude less conductive than their liquid counterparts.[7,9,12-14] The lightly plasticized systems can be

| **Polymer Membrane** | **Polymers** | **Liquid component** | **Salts** | **Interacting components** | **Maximum conductivity, RT** |
|---|---|---|---|---|---|
| Dry polymer | PEO, PAN, MEEP, others | none | LiTfsi, LiTf, $LiPF_6$, $LiClO_4$ | Polymer:salt | $10^{-5}$ S/cm |
| Composite, polymer + silica | Same as above | none | Same as above | Polymer:silica, Polymer:salt | $10^{-4}$ |
| Liquid-polymer gel | Same as above | Carbonates, glymes | Same as above | Polymer:salt:liquid | $10^{-3}$ |
| Poly-olefin | PE, PVDF | Same as above | Same as above | Liquid:salt | $10^{-3}$ |

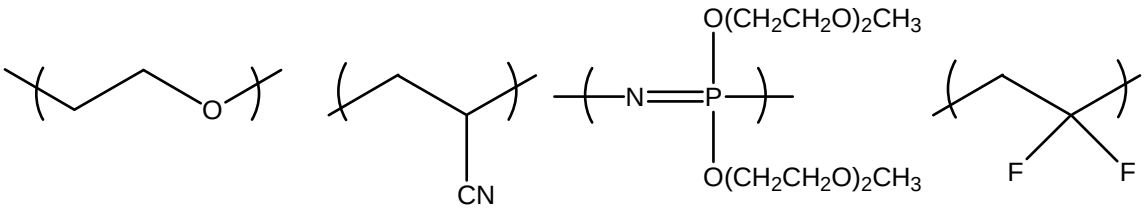


**PEO** **PAN** **MEEP** **PVdF**

Figure 4: Examples of the different components comprising the different types of polymer electrolytes, types of interactions and typical maximum conductivities with structures of select polymer studied

used in a Li-metal configuration, whereas the much softer gels require a Li-ion configuration because of an increased risk of lithium dendrite formation with metallic lithium.[7] A plasticized PE system is not always ideal because of weakened physical properties, so lithium battery producers seek both capable non-plasticized and plasticized systems that reduce the magnitude of their drawbacks. This requires additional fundamental research that involves understanding and improving Li ion conduction through new and modified PEs.

Other solid electrolytes exist in the form of crystalline solids, glasses and molten solids. In general polymer electrolytes have a mechanical advantage at lower temperatures, but their ionic conductivity can be 100 to 1000 times less.[15] Although higher conductivities are preferable, a thin film formed with a polymer electrolyte can compensate for the lower values. A polymer electrolyte can provide the following properties compared to other types of solid electrolytes: adequate conductivity for practical purposes, low electronic conductivity, good mechanical properties, chemical, electrochemical and photochemical stability and ease of processing.[9]

**Polymer Electrolyte Theory**

Ion mobility in a polymer electrolyte directly impacts cell performance. For a salt to be mobile in a polymer electrolyte, some general rules apply. First, the salt must incorporate itself into the polymer host through dissolution. In order for a salt to dissolve, the free energy of dissolution, $\Delta G$, must be negative (spontaneous) as given by the equation, $\Delta G = \Delta H - T\Delta S$. The entropy of dissolution of a salt into a polymer is

considered negligible because entropy increases upon salt dissolution and also decreases upon salt coordination to the polymer. A negative enthalpy (heat loss) is required and is regarded to be the result of cation solvation and electrostatic interactions between the dissolved ions.[11]

Dissolution of a salt in a solvent such as a polymer typically indicates a degree of cation-anion dissociation and solvation of each component. The dissociation is essential for cell function because ion-paired salts are not charge carriers or influenced by an electrical potential. Ion association in polymer electrolytes and other types of solutions is very important to the ion movement under a potential, and many studies (including those in this dissertation) have investigated this phenomenon. Lithium salts are known to be in various states of coordination when dissolved in a polymer host as shown by many vibrational spectroscopic studies.[16-18] If this coordinative environment were static and fixed, ion movement would be negligible.

The mobility of the salt is also related to diffusion. It has been shown in polymer electrolytes that ion diffusion is greater in low molecular weight polymers and can be described by the following relationship:

Eq. 1 $$D \propto 1 / M^2$$

where D is the diffusion coefficient (amount of a substance that diffuses across a unit area in a unit time under the influence of a gradient of one unit, usually $cm^2s^{-1}$) of the ion in question and M is the molecular weight of the polymer. This relationship is true for polymers up to a certain molecular weight where the chain entanglement limit (point at

which chains no longer slip along each other and further lengthening of the chains doesn't make a difference in properties) is reached and fluid-like chain diffusion makes little contribution to mechanisms for ion transport.[19]

The mechanism of ion movement has been described with various models. A common model is based on the Vogel-Tamman-Fulcher (VTF) equation,

Eq. 2 $$\sigma = \sigma_o \exp[-B / (T - T_o)]$$

where $\sigma$ is the ionic conductivity, $\sigma_o$ is a reference ionic conductivity, B is a constant with the dimensions of energy, T is the temperature at which the measurement is taken and $T_o$ is the reference temperature. This equation has been used to describe the diffusion of uncharged molecules through fluids and polymers, and it is assumed that ions are transported by the semi-random motion of short polymer segments like crank-shaft torsional motion in three adjacent bonds in the backbone of a polymer. Segmental motions promote ion mobility by making and breaking the co-ordination bonds between ions and polymer and providing free volume into which the ion can diffuse under the influence of an electric field. Figure 5 shows this type of movement.[15]

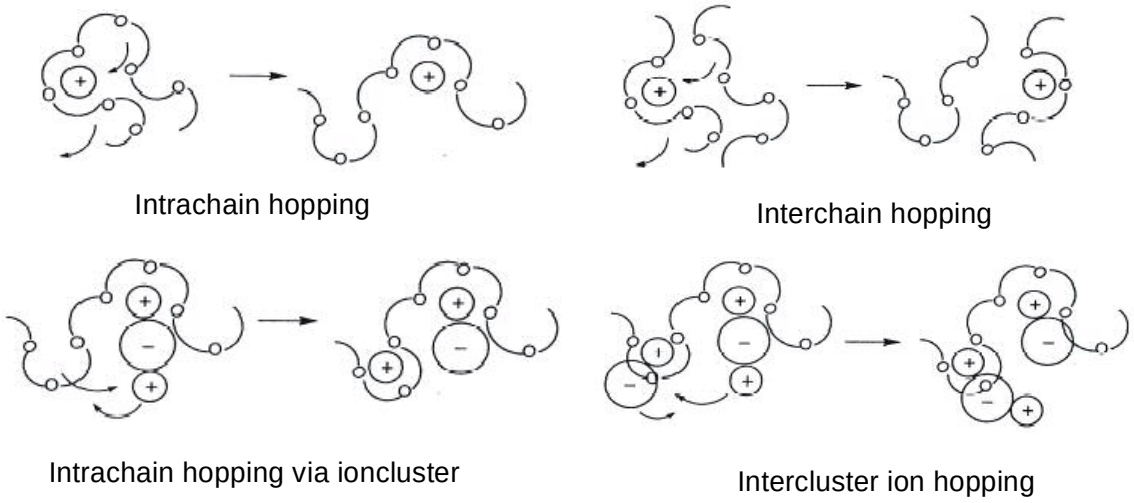


Figure 5: Representation of the types of cation transport in a polymer electrolyte[15]

The polymer's glass transition temperature, $T_g$, influences the movement of ions through a polymer. Above this temperature, segmental motion, or the rolling of chains over one another, and increased random motion[20] occurs and, consequently, improves ion mobility. Non-cross-linked solvent-free polymer electrolytes in lithium batteries have a $T_g$ below room temperature. The addition of a small organic molecule to enhance ion mobility typically lowers $T_g$ through an increase in the system's structural arrangement entropy. $T_g$ increases as the degree of cross-linking of a polymer increases, and, in some cases, the cross-linked polymer may decompose before the $T_g$ is reached because the polymer is considered to have very high molecular weight. The ion mobility in a cross-linked polymer with a small molecule additive has been shown not to be related to $T_g$. This is unlike non-plasticized cross-linked and non-cross-linked polymer electrolytes.[15]

Ion mobility is also influenced by whether a polymer is amorphous, semi-crystalline or crystalline. As the crystallinity of a polymer increases, the ordering of the polymer chains increases and results in increasingly larger rigid domains.[20] Ideally, a

polymer used in an electrolyte for a battery would be totally amorphous because increased chain freedom allows an enhanced radius of gyration for the polymer chain and whatever salt is coordinated. However, elimination of crystallinity may result in a breakdown of the polymer physical properties. A widely used semi-crystalline polymer used in lithium batteries is poly(ethylene oxide). It has a range of crystallinity with different salts[11], and it is the crystallinity that provides a sufficient physical barrier between the cathode and anode in Li batteries while not being so crystalline that it prohibits significant ion transport.

The magnitude of ion movement in solution, polymer or liquid, is measured by ionic conductivity as indicated earlier. Mobile electrons are not typically found in polymer electrolytes for batteries because of their low electrical permittivity[11], so the ionic conductivity is actually the measurement of electrical current transported by ion movement. For a dissociated salt, each ion is able to carry charge, and the molar ionic conductivity ($\Lambda_o$) is given by the following equation[22]

Eq. 3 $$\Lambda_o = v_+\lambda_+^o + v.\lambda_-^o$$

where $v_+$ and $v_-$ refer to the number of moles of cation and anion in the solution and $\lambda_+$ and $\lambda_-$ refer to the cation's and anion's individual contribution to the conductivity. Ionic conductivity, $\sigma$, of a homogeneous polymer electrolyte as a function of temperature and pressure can be modeled after the Kohlrausch summation[22],

Eq. 4 $$\sigma(T,P) = \Sigma\, c_i q_i u_i$$

where T is temperature, P is pressure, $c_i$ is the concentration of charge carriers of type I, $q_i$ is the charge and $u_i$ is the charge mobility. Included in the summation is all charged species. Determining $c_i$ is straightforward in polymer electrolytes where complete salt dissociation occurs and allows direct determination of ion mobility because the charge and the conductivity are known. The situation is more complicated when ion association occurs and more complicated techniques and models are needed. In general, it should be noted that the ion mobility plays a key role in this equation and re-emphasizes the need for PE with high ion mobility to give a highly conductive material.

**Poly(ethylene oxide)-based Polymer Electrolytes**

Initial lithium polymer batteries used predominately high molecular weight PEO (highly crystalline) with a lithium salt as the electrolyte because the electrochemical stability of the PEO ether linkages is high (360 kJ/mol) and high conductivity ($10^{-5}$ S/cm) could be achieved at high temperature (60 - 100 °C) when the crystalline phases are melted.[15] Operating at high temperature, though, resulted in the loss of the mechanical properties of the PE as a result of the crystalline melt. PEO has a $T_g$ of –67 °C and $T_m$ of 65 °C. Currently, ethylene oxide-based polymers are still popular because of alternative synthetic routes that have given mechanically more stable cross-linked and / or amorphous material. Also, new lithium salts have been used to form amorphous complexes with high molecular weight PEO.[7] Figure 6 compares the thermal conductivity dependence of dry PEO and two different salts to crosslinked PEO with plasticizer, liquid electrolytes and a PVDF-based gel.[7]

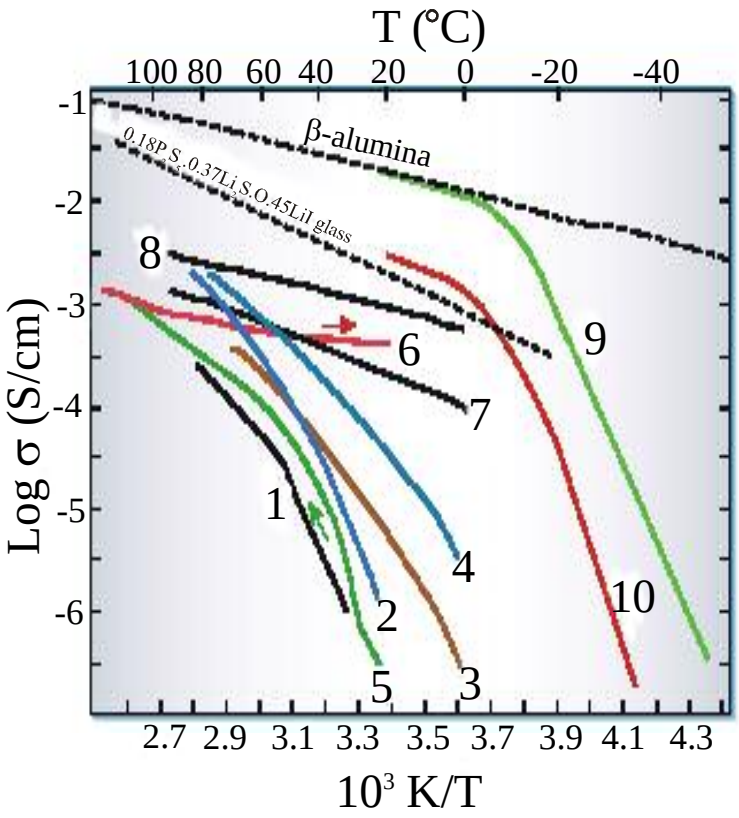


Figure 6: **1**. PEO-LiTf; **2**. PEO-LiTfsi; **3**. PEO polymer with ethylene oxide side chains; **4**. PEO-LiTfsi + 25 w/w glyme plasticizer, molecular wt. 250; **5**. liquid crystalline PE, heating curve; **6**. liquid crystalline PE, cooling curve; **7**. cross-linked PEO-LiTfsi with w/ 70% propylene carbonate; **8**. liquid electrolyte, propylene carbonate/dimethyl ether-LiTf; **9**. ethylene carbonate, dimethyl carbonate-$LiPF_6$ at low temperature; **10**. gel electrolyte P(VDF-HFP)/ethylene carbonate/dimethyl carbonate-$LiPF_6$

Lithium salt conductivity in PEO involves a dynamic coordination of the lithium ion with ether oxygens of the PEO backbone and concurrent segmental motion. Crystal structures of low molecular weight PEO model compounds suggest that the lithium ion is four-fold coordinate in solution and five-fold coordinate in the crystalline state. For

example, the lithium ion in a solution of 2-methoxyethyl ether (diglyme) and LiTf was found to prefer coordination to three diglyme oxygens and one oxygen from the triflate in the form of an ion pair.[26] Much work has gone into improving polymers to serve as an electrolyte that have used the PEO structure and conductivity as a model.

**Poly(ethylenimine)-based Polymer Electrolytes**

Poly(ethylenimine) (PEI)-based polymer electrolytes have been largely overlooked as candidates for lithium-polymer batteries because of lackluster conductivity in preliminary studies, but our group has begun to re-examine PEI through modification of the amine functional group. Structurally, PEI is analogous to the well-studied PEO in that the oxygen in PEO has been replaced by a synthetically modifiable NH group. Two general structural forms of PEI exist: branched (BPEI) and linear (LPEI) (Figure 6).

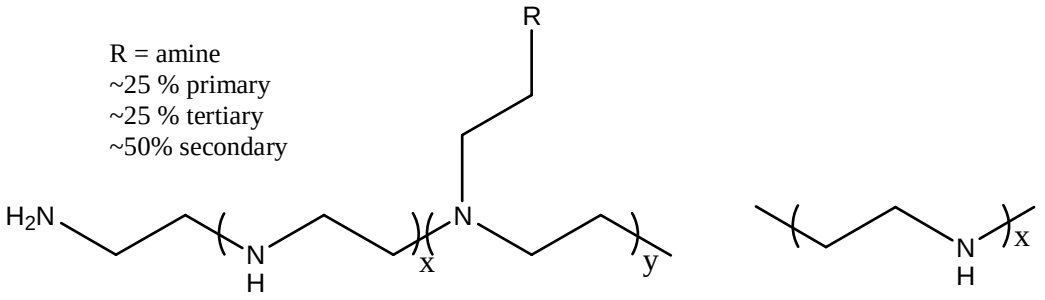


BPEI LPEI

Figure 6: Representative structures of branched and linear PEI

Branched PEI is available commercially, synthesized from the acid catalyzed polymerization of aziridine and has been suggested to contain 25% primary amines, 50%

secondary amines and 25% tertiary amines.[27] High molecular weight linear PEI has very limited commercial availability, contains only secondary amines and is obtained by the acidic hydrolysis of side chains of commercially available poly(2-X-oxazoline)s.[28,29] A poly(2-X-oxazoline) is synthesized by the acid catalyzed ring opening polymerization of a 2-X-oxazoline, where X has been H, ethyl and phenyl.[28] Crystal structures of anhydrous LPEI, LPEI-HCl and LPEI-x$H_2O$ have been published.[30-32] Of note is that the current published proposed crystal structure LPEI is a double stranded helix.[30] Anhydrous LPEI is semi-crystalline and has a melting point of 58.5 °C and a glass transition ($T_g$) at -23.5 °C[28], while BPEI is amorphous. Modifications have been made to PEI in the form of acylations[27], reductive alkylations[33] and cross-linking[34].

Comparing PEI and PEO, the relative strength of the coordination of lithium ion to the electron lone pair of the PEI amine group to a lone pair of the PEO oxygen is debatable. In terms of $pK_a$, a protonated amine is about 10, while a protonated ether is about –4.[35] If the lithium ion was regarded as simply a large proton, then amine coordination is stronger. HSAB theory says that harder acids (low polarizability, high electronegativity) prefer to bond to harder bases (low polarizability, high electronegativity). Lithium ion has a $\eta$ (absolute hardness, one half the difference between the ionization potential and the electron affinity) value of 35.1, while a tertiary amine's $\eta$ is 6.3 and an ether's $\eta$ is 8.0.[36] This indicates that the ether oxygen is more compatible with the lithium ion. The answer to which is stronger coordinating is not certain.

Limited work outside of OU has been published on the formulation and study of LPEI and BPEI based salt complexes as ion-conducting films. Table 2 shows some comparative data for LPEI salt systems from as reported by other groups.[37-39]

| **Lithium salts** | **Concentration (mole%)** | **Melting Temperature** | **Enthalpy (cal/g)** | **Percent Crystallinity** | **Glass Temperature** | **σ, 60°C** |
|---|---|---|---|---|---|---|
| none | 0 | 76.4 | 53.33 | 80.0 | -35 | - |
| LiF | 10 | 76.7 | 35.09 | 50.7 | none | - |
| LiCl | 10 | 68.5 | 27.99 | 40.5 | -16 | - |
| LiBr | 10 | 65.1 | 20.63 | 29.8 | -15 | - |
| LiI | 10 | 61.5 | 15.08 | 21.8 | -15 | - |
| NaI | 10 | ~50 | - | - | - | $10^{-6}$ |
| LiSCN | 10 | 59.2 | 19.78 | 28.6 | -30 | $10^{-6}$ |
| $LiClO_4$ | 10 | 64.7 | 19.79 | 28.6 | -9 | $10^{-7}$ |
| $LiBF_4$ | 10 | 59.6 | 27.19 | 39.3 | -23 | $10^{-5}$ |
| LiTf | 10 | 52.8 | 6.17 | 8.9 | -13 | $10^{-6-7}$ |

Table 2: A comparative table of thermal and conductivity data for LPEI:salt systems[37-39]

In all cases, added salt decreases the melting temperature and increases the glass transition temperature. The reported conductivity was the lowest for the samples with $LiClO_4$ and LiTf. Complexes of LPMEI (poly(N-methylethylenimine)) (Figure 7) with

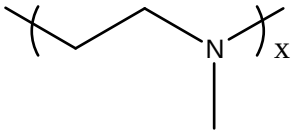


Figure 7: Linear PMEI

$LiClO_4$ and LiTf salts have been characterized by their ionic conductivity, thermal characteristics and polymer-salt interactions. With both $LiClO_4$ and LiTf salt complexes, the glass transition temperature increased with increasing salt composition, especially so with $LiClO_4$. The highest conductivity value, $10^{-6}$ S/cm, at 60 °C was obtained with a 16N:1Li sample. Conductivity over a range of temperatures and compositions indicated that PMEI:LiTf complexes were more highly conductive than the $LiClO_4$ counterpart.[40] Complexes of BPEI with LiTf have been examined, as well, and selected data is presented in Table 3.

| **N:Li** | **$T_g$, °C** | **σ, 20°C** | **σ, 60°C** |
|---|---|---|---|
| 25 | -36 | $7.4\times10^{-7}$ | $1.4\times10^{-5}$ |
| 16 | -27 | $4.5\times10^{-7}$ | $3.4\times10^{-5}$ |
| 8 | -5 | - | $8.5\times10^{-7}$ |

Table 3: Glass transition temperatures and conductivity data for BPEI:LiTf at different salt compositions[41]

The best conductivity in this system was observed at low salt composition.[41] Lower than desired conductivity values resulted in most early studies dismissing PEI-based salt systems as viable polymer electrolytes for the lithium polymer battery.

Work in the groups of Drs. Glatzhofer and Frech has been focused on improving the ionic conductivity and physical properties of PEI through the functionalization of the amine nitrogen and studying the manner in which Li salts interact in the functionalized PEI -salt systems. But first, the synthesis and purification of high molecular weight LPEI was needed, so it was optimized in their labs.[42] LPEI-LiTf and -NaTf complexes were examined to provide a baseline for understanding ethylenimine-based systems.[43] Infrared and Raman spectroscopies were used to probe the triflate ion association and the N-H stretch. It was found, through curve fitting of triflate bands that are sensitive to association, that the triflate anion is predominately ion paired at a 20N:1Li composition and, at higher LiTf composition, 5N:1Li, the triflate anion is mostly of the aggregate form, $Li_2Tf^+$. One difference found between PEI and PEO is the presence of extensive hydrogen bonding in non-complexed PEI as seen in the N-H stretching region. The loss of hydrogen bonding was observed in this region with the addition of salt. X-ray diffraction measurements of LPEI-LiTf and LPEI-NaTf systems showed that that the samples were highly amorphous.[43]

The first functionalized LPEI in their labs was LPMEI. The synthesis, using the Eschweiler Clarke N-methylation reaction, of LPMEI was optimized[42], and LPMEI-LiTf complexes were studied. Over a composition range of 5N:1Li to 20N:1Li, LiTf ion pair was found to be the dominate triflate species using infrared and Raman spectroscopies. The $T_g$ for LPMEI was –91 °C and increased to 3 °C at a 5N:1Li composition. The ionic

conductivity increased with decreasing LiTf composition (minimum studied- 20N:1LiTf) in the temperature range studied.[44] Figure 8 shows a comparative plot of conductivity values published in the Glatzhofer/Frech lab for LPEI and LPMEI and conductivities published by others for PEO.[43-45] LPMEI-LiTf is more conductive than LPEI-LiTf in the temperature regions studied, while the PEO-LiTf conductivity data is greater in value than both.

In an effort to improve the conductivities to at least the PEO level, further modifications to the LPEI structure were made. One published example is poly(*N*-(2-(2-methoxyethoxy)ethyl)ethylenimine) (LPEI-G2) that was made by the reductive alkylation of LPEI with 2-(2-methoxyethoxy)acetic acid and sodium borohydride. This structure contains a tertiary amine, with each repeat unit containing an ethylene oxide side chain. The resulting amorphous polymer had a $T_g$ of –76 °C that didn't change significantly with salt addition. The composition of non-lithium associated triflate decreased as LiTf was added, and, at high LiTf composition (5O:1Li), mostly LiTf ion pair was observed.

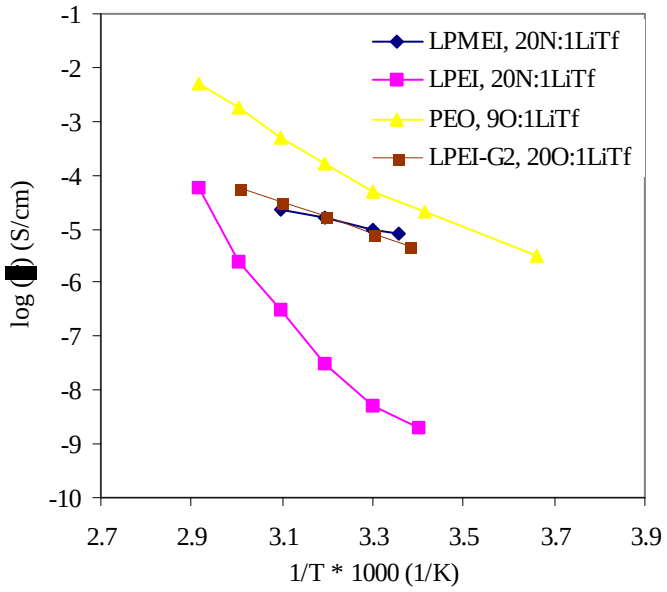


Figure 8: Comparison of the temperature dependent ionic conductivity in LPMEI, LPEI, PEO and LPEI-G2 electrolytes

Figure 8 includes the observed conductivity for the highest conductivity LPEI-G2 system published.[46]

Other functionalized PEIs have been produced. The degree of ion association, first and second order thermal transitions and ionic conductivity has been examined in electrolyte systems using the functionalized PEI. Crystals of PEI model compounds with LiTf and NaTf have been grown and characterized and provide intricate pictures of the Li ion coordinative environments. For example, a tetramethylethylenediamine(TMEDA)-LiTf crystal was grown in which the lithium ion was four coordinate with two oxygens from separate triflates and two nitrogens from a single molecule of TMEDA.[47] Vibrational spectroscopy of the crystals has led to correlations of vibrational modes in the solution and crystalline phases. Crystallography data has also led to computational work

that has aided in the assignment of previously ambiguous vibrational modes in PEI/PMEI salt systems.[48]

A number of obstacles are still being addressed in the poly(ethyleneimine)-based systems including less than satisfactory ionic conductivity, dimensional instability of the non-cross-linked polymers and electrochemical stability and performance in battery cells. These issues including the development of novel cross-linked and non-cross-linked, plasticized and non-plasticized modified PEI polymer electrolytes and studies of ion, polymer structure and electrochemistry in batteries with these polymer electrolytes will be presented in Chapters 2 through 4.

## Polymer Electrolytes for Proton Exchange Membranes Fuel Cells

### Fuel Cell Background and Operation

Fuel cells are electrochemical devices that convert chemical energy of reactants directly into electricity and heat in a highly efficient manner. Fuel cells and batteries are similar in that both systems consist of two electrodes separated by an electrolyte and electrical energy can be withdrawn from electrode-based reactions. In contrast to batteries, fuel cell reactants are delivered externally and operation is continual provided an unimpeded supply of reactants. Also, battery performance decreases with decreasing charge, but a fuel cell functions consistently as long as reactants are supplied and cell component do not deteriorate in function.

There are several different types of fuel cells, and they are usually distinguished by the electrolyte. Six common types are listed in Table 1.[49]

| Fuel cell type | Mobile ion | Operating temperature |
|---|---|---|
| Alkaline (AFC) | $OH^-$ | 50-200 °C |
| Proton exchange membrane (PEMFC) | $H^+$ | 30-100 °C or higher |
| Direct methanol (DMFC) | $H^+$ | 20-90 °C |
| Phosphoric acid (PAFC) | $H^+$ | ~220 °C |
| Molten carbonate (MCFC) | $CO_3^{2-}$ | ~250 °C |
| Solid oxide (SOFC) | $O^{2-}$ | 500-1000 °C |

Table 1: Common fuel cell types with the mobile ion and typical operating temperatures[49]

Operational efficiency is often dictated by operating temperature because electrode and electrolyte performance is often more optimal at different temperatures in different systems. My research project in this area deals exclusively with PEMFCs. The electrolyte in a PEMFC is a solid polymer in which protons are transported through the polymer under a potential.

In a PEMFC, hydrogen fuel is oxidized with oxygen as indicated in Figure 7. The chemical reactions of a fuel cell occur at the surface of (typically) platinum coated on electronically-conducting carbon-based electrodes and are fed by a continuous supply of hydrogen and oxygen. PEMFC operation and the reactions involved with their standard reduction potentials are presented in Figure 7.

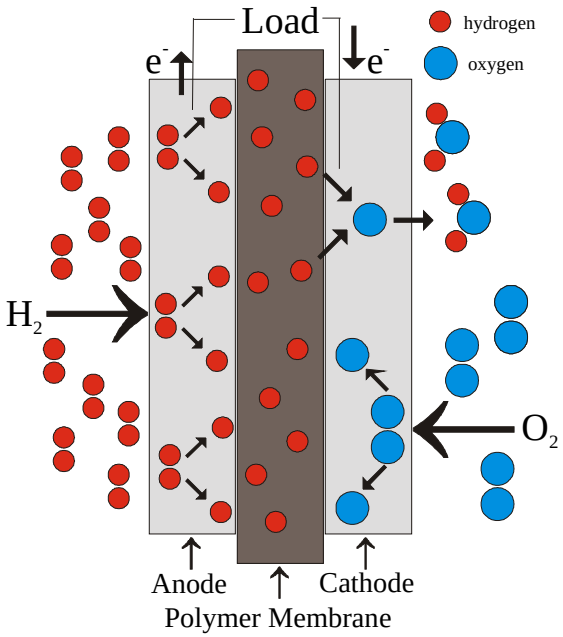


| | | | |
|---|---|---|---|
| Oxidation half reaction | $2H_2$ | $\rightarrow 4H^+ + 4e^-$ | E° (V) = 0 |
| Reduction half reaction | $O_2 + 4H^+ + 4e^-$ | $\rightarrow 2H_2O$ | E° (V) = +1.23 |
| Cell reaction | $2H_2 + O_2$ | $\rightarrow 2H_2O$ | E° (V) = +1.23 |

Figure 7: PEMFC operation and calculation of theoretical voltage for a PEMFC (STP)

Both the anode and cathode consist of a fine dispersion of platinum chemically fixed on an electronically-conducting carbon sheet. The $H^+$ exchange membrane is a sheet of proton-conducting polymer. These three sheets are compressed into a layered material called a membrane electrode assembly. At the anode, hydrogen molecules are introduced and absorb on platinum particles. The chemical absorption of $H_2$ on the surface of a Pt particle allows the $H_2$ to dissociate into two absorbed hydrogen atoms

bonded to two neighboring Pt atoms. In a similar way, oxygen is absorbed at the cathode and dissociates into atomic oxygen. Electrons are released from the atomic hydrogen into the conductive platinum on carbon at the anode and then flow through the external circuit (and whatever load) to the higher relative voltage platinum of the cathode where reduction of atomic oxygen occurs. Protons delivered from the PEM combine with the reduced oxygen to form $H_2O$[50].

**Fuel Cell Theory**

Fuel cell operating performance is described by the electrical power and energy output of the cell. These values are calculated from the following formulas:

Eq. 6 $$\text{Power} = VI$$

Eq. 7 $$\text{Energy} = VIt$$

(V = voltage, I = current, t = time)

The energy of the chemical input and output for the cell is based on the chemical energy of the $H_2$, $O_2$ and $H_2O$ and is described by Gibbs free energy which is the energy available to do external work, neglecting any work done by changes in pressures and/or volume. In a fuel cell, the 'external work' involves moving electrons around an external circuit- any work done by a change in volume between the input and output is not harnessed by the fuel cell. In a fuel cell, it is the change in the Gibbs free energy of formation, $\Delta G$, which gives energy. This change is the difference between the Gibbs free energy of the products and the Gibbs free energy of the inputs or reactants.

Eq. 8 $$\Delta G = \Delta G_{f,\ products} - \Delta G_{f,\ reactants}$$

The Gibbs free energy for the reaction $H_2 + 1/2O_2 \rightarrow H_2O$ is –237.2 kJ/mol at 25 °C and varies with temperature. In this reaction, two electrons pass through the external circuit for each water molecule produced and each molecule of hydrogen used. So, for one mole of hydrogen used, two moles of electrons pass through the external circuit. If –e is the charge on the electron, then the charge that flows is

Eq. 9 $$-2Ne = -2F \text{ coulombs}$$

(N = Avogadro's number, F = Faraday's constant, or the charge on one mole of electrons)

If E is the voltage of the fuel cell, then the electrical work done moving this charge around the circuit is

Eq. 11 $$\text{Electrical work done} = \text{charge} \times \text{voltage} = -2FE \text{ joules}$$

If the system is reversible, then this electrical work will be equal to the Gibbs free energy released $G_f$. So

Eq. 12 $$G_f = -2FE$$

and

Eq. 13 $$E = -G_f/2F$$

For a hydrogen fuel cell operating at 25 °C ($G_f$ = -237.2 kJ/mol, F = 96,485 C/mol), the theoretical E is equal to 1.23 V.[49]

The operating voltage of a fuel cell can be related to its efficiency at different temperatures. The efficiency of the fuel cell is given by the following equation:

Eq. 14 $$\text{Efficiency, } n = \mu_f V_c / 1.23 \times 100$$

where $\mu_f$ is the ratio of the mass of fuel reacted in the cell to the mass of fuel input to the cell, $V_c$ is the actual voltage and 1.23 is the theoretical voltage at 25 °C taken from equation 13. This efficiency assumes no irreversible fuel cell behavior.

Electrical energy is obtained from a fuel cell only when a current is drawn, but at the same time, cell voltage drops due to fuel cell irreversibilities as shown in Figure 8 which shows a typical fuel cell's performance as a function of different applied external loads. Voltage drop originates from four sources and is reflected by the shape of the performance curve seen in Figure 8. Activation losses ($\Delta V_{act}$) are caused by the speed of the

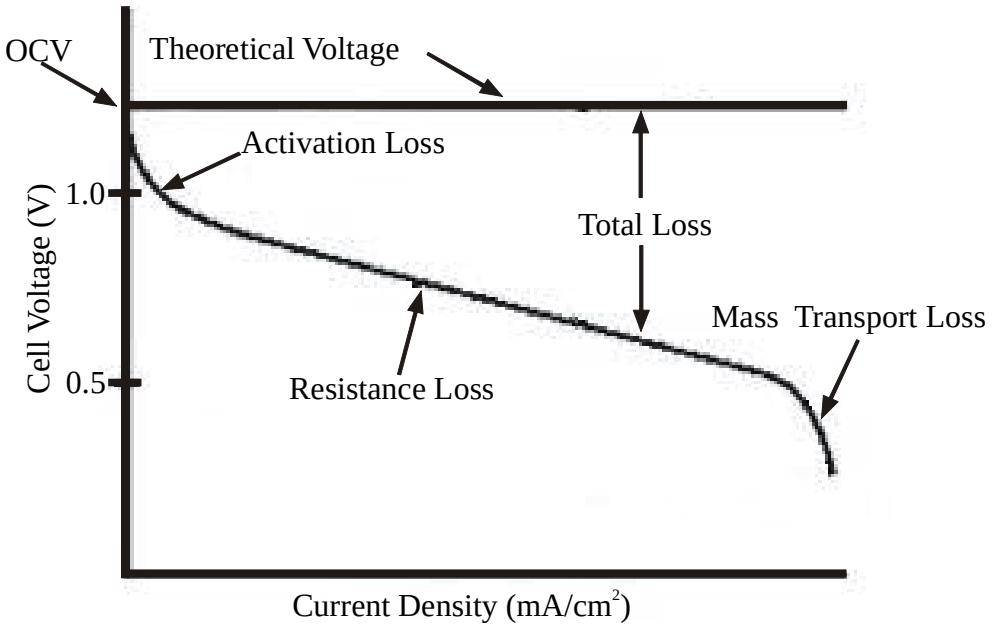


Figure 8: Theoretical and typical performance curves for a fuel cell and labeled voltage drop mechanisms

reactions taking place on the surface of the platinum particles and formation of intermediates such as water and peroxides on the electrodes. Some of the voltage lost goes to driving the chemical reaction that transfers the electrons to or from the platinum. Crossover of fuel ($H_2$ and $O_2$) through the polymer membrane and internal electrical currents ($\Delta V_{crossover}$) both cause voltage to drop as the electrolyte is intended to transport only protons. Ohmic losses ($\Delta V_{ohm}$) occur because of the resistance to the flow of electrons through the electrode material, electrical connections and the resistance of proton transport through the electrolyte. Voltage drop due to mass transport loss ($\Delta V_{trans}$) results when a change in concentration of the reactants at the surface of the electrodes

occurs. This results from high currents being drawn and insufficient quantities of fuel being available at the electrodes. The experimental voltage is then given by[50]

Eq. 15 $$V = E - \Delta V_{act} - \Delta V_{crossover} - \Delta V_{ohm} - \Delta V_{trans}$$

**Current Proton Exchange Membranes**

Current membranes for proton exchange membrane fuel cells use a poly(perfluorosulfonic) acid based polymer called Nafion (Figure 9) that consists of three regions. It has a hydrophobic Teflon-like, fluorocarbon backbone with the repeat unit -$CF_2CFXCF_2$- where X is a side chain. The side chain usually consists of

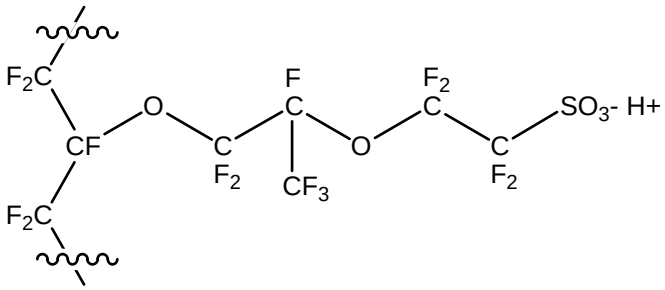


Figure 9: Side chain structure of Nafion

the –$OCF_2CF_2OCF_2CF_2$- unit linking it to the third region, which is a sulfonic acid group, -$SO_3^-$ $H^+$. This sulfonic acid group promotes proton mobility if the polymer is in the hydrated form. If the polymer is dehydrated, the protons are less mobile. The mechanism for proton conduction is typically thought to consist of protons bonded to water molecules that then hop along sulfonic acid groups in close proximity.[52] This polymer, when incorporated into a proton exchange membrane, is used commonly in commercial fuel cells because it strong and stable in both oxidative and reductive environments and

the proton conductivities for a well humidified membranes can be as high as 0.2 S/cm at PEM fuel cell operating temperatures.[53]

Nafion does have significant problems. The temperature range over which the membrane can be used efficiently is below 100°C because water evaporation results in membrane dehydration and a decrease in proton conductivity. For example, the conductivity at 80°C is diminished by more than 10 times relative to that at 60 °C.[54] This is unfortunate as the fuel cell performs more efficiently at higher temperatures as reported by Rikukawa and Sanui.[54] Specifically, operation at elevated temperatures increases the rates of reaction, reduces problems related to catalyst poisoning by carbon monoxide in the 150 – 200 °C range, reduces the use of expensive catalysts and minimizes problems due to water flooding. In addition to these problems, the Nafion membrane is very expensive and currently averages \$25 $kW^{-1}$ in a fuel cell.[53]

Research is being done to identify acceptable, lower cost membranes with better thermal characteristics. Sulfonated and non-sulfonated acid doped polybenzimidazole membranes currently are popular in the chemical literature. Polybenzimidazole (Figure

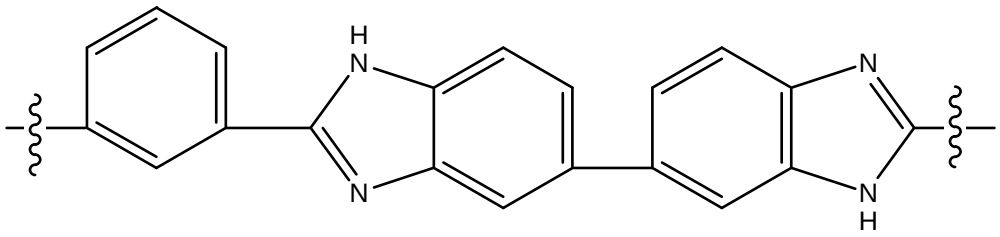


Figure 10: Repeat unit of poly(benzimidazole)

10) is an amorphous thermoplastic polymer with a glass transition temperature of 425-426 °C that incorporates water and acids to give a material with high conductivity and thermal stability.[55]

**PEI-based Proton Exchange Membranes**

Our lab has been working on proton exchange membranes incorporating poly(ethlyenimine) as the polymer host. These membranes are being prepared as alternatives to current proton conducting membranes for PEMFCs. The high ratio of nitrogen to carbon in PEI makes the polymer susceptible to high proton uptake, and the low $pK_a$ of the protonated secondary amine (for PEI, $pK_a \sim 3$[56]) allows for dynamic proton coordination. PEI is able to form polymer-acid blends with select acids.

Interest expressed by the scientific community in poly(ethylenimine)-based proton conductors is limited. Lassegues et. al. in 1988 examined the conductivity, thermal properties and chemical structure of highly branched poly(ethyenimine) strong acid complexes and reported a maximum conductivity value of $2.7 \times 10^{-3}$ S/cm at 100 °C. Also, it was observed that the mechanical properties decreased with increasing $H_3PO_4$ composition.[57] In 1991, Lassegues evaluated the electrochemical stability of a BPEI, $H_3PO_4$ blend with cyclic voltammetry and found that no polymer degradation occurred up to 1.5 V vs. $H_2$ and proton reduction started at 0.3 V vs. $H_2$ giving an electrochemical stability domain of 1.2 V.[58] Poly(ethylenimine) as a proton conductor was not again evaluated until 1995, when Tanaka compared the conductivity in linear and branched poly(ethylenimine)-$H_3PO_4$ systems. The conductivities of the LPEI systems showed

stronger temperature dependence than those of the BPEI systems, but the overall gross features were similar.[59]

In 2000, Tanaka reported a cross-linked LPEI-$H_3PO_4$ system in which ethylene glycol diglycidyl ether (a di-epoxide) was used as the cross-linker and resulted in non-homogeneous membranes as a result of an unconventional preparation. Tanaka's membranes were made by cross-linking PEI with the diepoxide, dehydrating the resulting gel, pulverizing the dehydrated gel, soaking the pulverized material in phosphoric acid/methanol, removing methanol, pulverizing the dry material once more and then compacting the powder into sheets. The ionic conductivity of the cross-linked LPEI-$H_3PO_4$ material was compared to the non-cross-linked LPEI-$H_3PO_4$ and showed that, for the cross-linked systems, conductivity was one to two orders of magnitude lower than the non-cross-linked material. Also, the conductivity was found to be higher in samples with a lower cross-link density at high phosphoric acid compositions at 50 °C. At the highest temperature reported, 127 °C, the best cross-linked LPEI-$H_3PO_4$ sample (2.01 $H_3PO_4$ phosphorous to PEI nitrogen) had a conductivity of $6\times10^{-4}$ S/cm.[60] No other methods of preparation of cross-linked PEI:acid membranes are reported in the chemical literature.

Work described in Chapter 5 involves cross-linking LPEI in the presence of $H_3PO_4$, to give homogeneous membrane material. The proton conductivity, ionic speciation, thermal stability and performance in a PEMFC will be described.

**References**


1. www.ford.com/en/innovation
2. www.gm.com/automotive/innovations/new_devices

3. www.hondacorporate.com/environ.tech
4. www.toyota.co.jp/en/tech/environment
5. Treptow, R.S. *J. Chem. Ed.* **2003**, 80, 1015.
6. Winter, M. Broddy, R.J. *Chem. Rev.* **2004**, 104, 4245.
7. Tarascon, J.M. Armand, M. *Nature* **2001**, 414, 359.
8. Shriver, D. F. Atkins, P. Langford, C. H. 'Inorganic Chemistry: Second Edition' W. H. Freeman and Company: New York, 1994.
9. Schalkwijk van, W. A.; Scrosati, B. 'Advances in Lithium-Ion Batteries' Kluwer Academic/Plenum Publishers: New York, 2002.
10. Hong, J. K.; Lee, J. H. Oh, S. M. *J. Power Sources* **2002**, 111, 90-96.
11. Shriver, D.F. Bruce, P.G. 'Solid State Electrochemistry' Cambridge University Press: New York, 1995.
12. Vincent, C. A. *Solid State Ionics* **2000**, 134, 159-167.
13. Song, M.-K. Kim, Y.-T. Kim, Y. T. Cho, B. W. Popov, B. N. Rhee, H.-W. *J. Electrochem. Soc.* **2003**, 150, A439-A444.
14. Abbrent, S. Lindgren, J. Tegenfeldt, J. Wendsjo, A. *Electrochim. Acta* **1998**, 43, 1185-1191.
15. Gray, F. 'Polymer Electrolytes' The Royal Society of Chemistry: Cambridge, 1997.
16. Zhou, J. Fewick, P.S. *Solid State Ionics* **2004**, 166, 275.
17. Chu, P.P. Reddy, M. Jaipal, N. Tsai, J. *J. Poly. Sci., Part B: Poly. Phys.* **2004**, 42, 3866.
18. Subban, R.H.Y. Arof, A.K. *Eur. Poly. Journal* **2004**, 40, 1841.
19. Shi, J. Vincent, C.A. *Solid State Ionics* **1993**, 60, 11.
20. Painter, P.C. Coleman, M.M. 'Fundamentals of Polymer Science, 2nd Edition' Technomic Publishing, Inc: Lancaster, Pennsylvania, 1997.
21. Lindley, D. Moore, T.H. 'Dictionary of Science' Helicon Publishing Unlimited: New York, 1998.
22. Atkins, P. 'Physical Chemistry, Sixth Edition' W.H. Freeman and Company: New York, 1998.
23. Lang, M.C. Noel, C. Legrand, A.P. *J. Poly. Sci., Poly. Phys. Ed.* **1977**, 15, 1319.
24. Bauat, R. Tincer, T. *J. App. Poly. Sci.* **2003**, 90, 488.
25. Kweon, J.O. Noh, S.T. *J. App. Poly. Sci.* **2003**, 90, 270.
26. Rhodes, C.P. Frech, R *Macromolecules* **2001**, 34, 2660.
27. Johnson, T.W. Klotz, I.M. *Macromolecules* **1974**, 7, 149.
28. Saegusa, T. Ikeda, H. Fujii, H. *Macromolecules* **1972**, *5*, 108
29. Tanaka, R. Ueoka, I. Takaki, Y. Kataoka, K. Saito, S. *Macromolecules* **1983**, *16*, 849-853.
30. Chatani, Y. Kobatake, T. Tadokoro, H. Tanaka, R *Macromolecules* **1982**, 15, 170-176.
31. Chatani, Y. Irie, T. *Polymer* **1988**, 29, 2126-2129.
32. Chatani, Y. Kobatake, T. Tadokoro, H. *Macromolecules* **1983**, 16, 199-204.
33. Saegusa, T. Yamada, A. Taoda, H. Kobayashi, S. *Macromolecules* **1978**, 11, 435-436.
34. Takahashi, T. Davis, G. T. Chiang, C. K. Harding, C. A. *Solid State Ionics* **1986**, 18-19, 321-325.

35. Bruice, P.Y. 'Organic Chemistry, Third Edition' Prentice Hall: Upper Saddle River, New Jersey, 2001.
36. Smith, M.B. March, J. 'March's Advanced Organic Chemistry: Reactions, Mechanisms, and Structure, 5th Edition' John Wiley and Sons: New York, 2001.
37. Chiang, C.K. Davis, G.T. Harding, C.A. *Solid State Ionics* **1986**, 18-19, 300.
38. Chiang, C.K. Davis, G.T. Harding, C.A. *Macromolecules* **1985**, 18, 825.
39. Harris, C.S. Shriver, D.F. Ratner, M.A. *Macromolecules* **1986**, 19, 987.
40. Tanaka, R. Fujita, T. Nishibayashi, H. Saito, S. *Solid State Ionics* **1993**, 60, 119.
41. Paul, J.L. Jegat, C. Lassegues, J.C. *Electrochim. Acta* **1992**, 37, 1623.
42. Snow, A.G. 'Synthesis and Spectroscopic Studies of Polymer Electrolyte Hosts: Linear Poly(ethylenimine), Linear Poly(*N*-methylethylenimine) and Linear Poly(2-(2-methoxyethoxy)ethylenimine)' Dissertation, University of Oklahoma, **2002**.
43. York, S. Frech, R. Snow, A. Glatzhofer, D. *Electrochim. Acta* **2001**, 46, 1533.
44. Sanders, R.A. Snow, A. Frech, R. Glatzhofer, D. *Electrochim. Acta* **2003**, 48, 2247.
45. Bandara, L.R.A.K. Dissanayake, M.A.K.L. Mellander, B.E. *Electrochim. Acta* **1998**, 43, 1447.
46. Snow, A.G. Sanders, R.A. Frech, R. Glatzhofer, D.T. *Electrochim. Acta* **2003**, 48, 2065.
47. Sanders, R. A. Frech, R. Khan, M. A. *J. Phys. Chem., Part B* **2003**, 107, 8310.
48. York, S. S. Boesch, S. E. Wheeler, R. A. Frech, R. *Macromolecules* **2003**, 36, 7348.
49. Larminie, J. Dicks, A. 'Fuel Cell Systems Explained' John Wiley and Sons Ltd.: West Sussex, England, 2003.
50. Winter, M. Broddy, R.J. *Chem. Rev.* **2004**, 104, 4245.
51. Vaughn, D.J. *DuPont Innovation* **1973**, 4, 10.
52. Kruer, K.D. *J. Mem. Sci.* **2001**, 185, 29.
53. Mehta, V. Cooper, J.S. *J. Power Sources* **2003**, 114, 32.
54. Rikukawa, M. Sanui, K. *Prog. in Poly. Sci.* **2000**, 25, 1463.
55. Wainright, J.S. Fontanella, J.J. Wintersgill, M.C. Savinell, R.F. Litt, M. *Electrochim. Acta* **1998,** 43, 1289.
*56. Unpublished results*
57. Daniel, M.F. Desbat, B. Cruege, F. Trinquet, O. Lassegues, J.C. *Solid State Ionics* **1988**, 28-30, 637.
58. Schoolman, D. Trinquet, O. Lassegues, J.C. *Electrochim. Acta* **1992**, 37, 1619.
59. Tanaka, R. Yamamoto, H. Kawamura, S. Iwase, T. *Electrochim. Acta* **1995**, 40, 2421.
60. Tanaka, R. Yamamoto, H. Shono, A. Kubo, K. Sakurai, M. *Electrochim. Acta* **2000**, 45, 1385.

## Chapter 2: SOLID POLYMER/SALT ELECTROLYTES BASED ON LINEAR POLY((*N*-2-CYANOETHYL)ETHYLENIMINE)

Modified from *Electrochim. Acta* **2003**, 48, 2059.

Exploration of the chemical literature reveals a lack of diversity in the types of modifications performed on the PEI structure. Most reported modifications are reductive alkylations[1-3] and substitution-based alkylations[4-5] with a scattering of other types. Reductive alkylations with polymers can require cumbersome workup procedures to remove used reductant salts because of PEI's tendency to form salt complexes and fundamental polymer physical properties making workup sometimes difficult. Alkylation by $S_N2$ substitution of the PEI secondary amine to yield tertiary amine tends to result in an amount of undesired quaternized tertiary amine as result of over-alkylation. As part of our effort to investigate novel PEI-based electrolytes, new synthetic routes that yield highly substituted PEI with minimal side products and workup steps are desired. One such un-tapped type of reaction that delivers exclusively mono-substitution to secondary amines is the Michael reaction[6] in which a nucleophilic species adds to the 4-position of an $\alpha$, $\beta$ unsaturated conjugated structure (Figure 1).

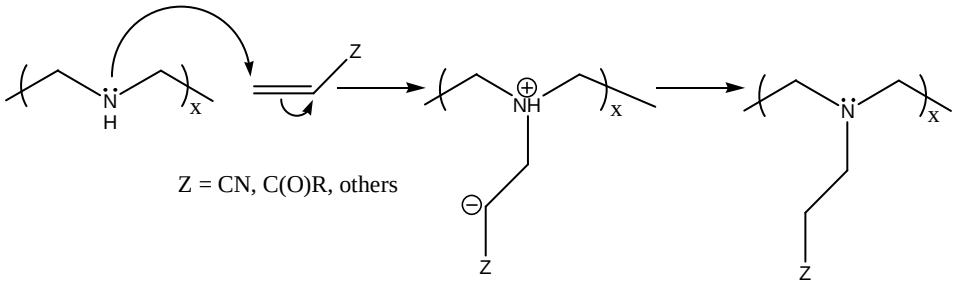


Figure 1: Michael reaction of a PEI secondary amine with an α, β unsaturated structure

The reaction of a secondary amine with a Michael acceptor yields only tertiary amine. Any tertiary amine involved in conjugate addition results in the formation of unstable zwitterions that rapidly reverse to starting material leaving no quaternary product.

One of the goals for modified PEI structures is the improvement in the ionic conductivity and physical properties of their PEs over popular, current state of the art PEs. Poly(acrylonitrile) (PAN) has been widely examined as a PE host, with numerous studies expounding its potential utitility in Li-polymer batteries[7-10]. The nitrogen of the nitrile group provides functionality that facilitates salt dissolution and provides hopping sites for the lithium ion. Non-plasticized PAN PEs are reported to have conductivities approaching $10^{-5}$ S/cm above its glass transition temperature of 80 °C[11]. Problems associated with PAN PEs include preparation that requires addition of plasticizer[10] or special hot pressing techniques[11] for salt incorporation. Also, PAN PEs have ionic conductivity that is insufficient for cell operation at room temperature.

**PCEEI Synthesis and Electrolyte Preparation**

As a poly(ethylenimine) version of PAN, linear poly((*N*-cyanoethyl)ethylenimine) (PCEEI) (Figure 2) was synthesized to take advantage of the desirable properties of PAN and LPEI. Reaction of dissolved LPEI, from the hydrolysis of PEOz, in methanol with a slight 1:1 excess of acrylonitrile resulted in an amber colored highly viscous liquid after removal of the liquid component (Figure 2).

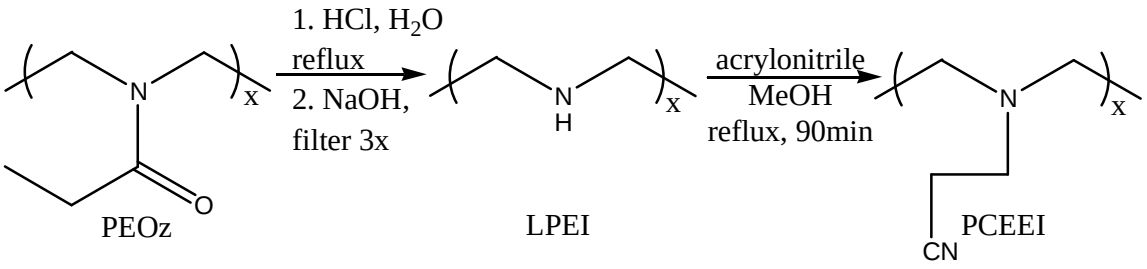


Figure 2: Hydrolysis of PEOz and neutralization to form LPEI and the ensuing Michael reaction to form PCEEI

Repeat unit percent substitution with cyanoethyl groups was determined to be ~95% with NMR. The resulting polymer was soluble in acetonitrile, tetrahydrofuran and other organic solvents allowing PE formation from the casting of organic solvent solutions of dissolved lithium salt (LiTf or LiTfsi) onto preferred substrates and removal of the solvent under dry air and vacuum atmospheres as opposed to cumbersome hot pressing procedures. Resulting films were homogenous at compositions of 2.5RU:1Li and lower. LiTf was chosen as the electrolyte salt because of triflate's highly delocalized charge, thermal and chemical stability and frequency sensitive triflate vibrational modes that allow study of aggregation states with infrared spectroscopy.

**Thermal Characterization**

Thermal transitions in PCEEI and PCEEI:LiTf PEs were examined using differential scanning calorimetry (DSC). A melting temperature for PCEEI was not observed because of its amorphous structure. Table 1 compares the glass transition temperature, $T_g$, of PCEEI (-36 °C) with those of LPEI[12] and PEOz[14], PCEEI's parent polymers, as well as PAN[7] and LPMEI[13] (a simple substituted LPEI).

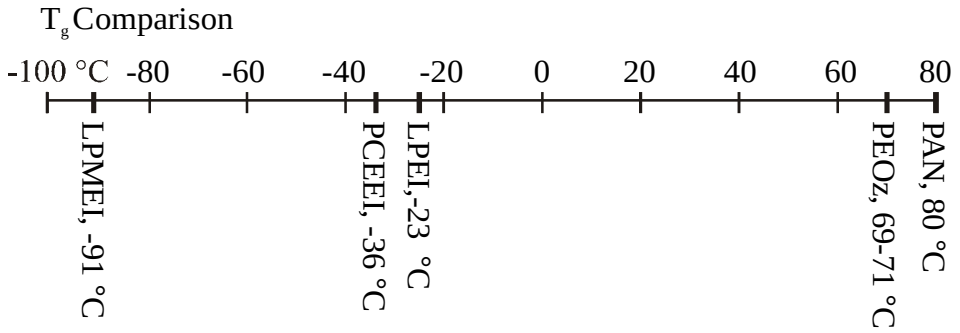


Table 1: Comparison of the glass transition temperatures of LPMEI, PCEEI, LPEI, PEOz and PAN

PCEEI's $T_g$ is significantly lower than that of PAN indicating a lower temperature for the onset of segmental motion likely resulting in PCEEI's lower room temperature viscosity. A lowering of the $T_g$ in PCEEI from that of LPEI was expected because of the reduction of N-H hydrogen bonding, but the magnitude was less than expected compared with the completely substituted LPMEI's $T_g$ of –91 °C. An ordering of the side chain nitrile groups (Figure 3) and an increase in free volume may account for this increase in $T_g$ from LPMEI[15].

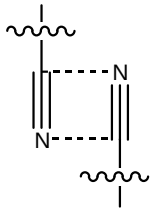


Figure 3: Possible ordering of the nitrile groups

For comparison, PEOz is a highly crystalline polymer with a $T_g$ range of 69-71 °C[14].

Glass transitions of PCEEI:LiTf and NaTf electrolytes were obtained in the range of 5RU:1cation (RU = polymer repeat unit) to 80RU:1cation as listed in Table 2. Published PMEI salt complex $T_g$'s[13]

| RU:cation | PCEEI:LiTf | PMEI:LiTf | PCEEI:NaTf | PMEI:NaTf |
|---|---|---|---|---|
| ∞ | -36 °C | -91 °C | -36 °C | -91 °C |
| 80 | -31 °C | - | -28 °C | - |
| 15 | -15 °C | -53 °C | -9 °C | -89 °C |
| 5 | 16 °C | 3 °C | 6 °C | - |

Table 2: Glass transition temperatures for PCEEI and PMEI electrolytes as a function of salt composition[13]

are also listed in Table 2. PMEI:LiTf samples exhibit a marked increase in $T_g$ with increasing LiTf compositions indicating increased polymer structuring/ordering. This ordering results in the need for more thermal energy to promote the phenomenon of polymer segmental motion. This salt dependent effect is also observed in PMEI:LiTf but

with a greater magnitude from pure polymer to the 5:1 composition. Increases observed were 52 °C for the PCEEI system and 94 °C for the PMEI system. The methyl side chain may allow for increased polymer segmental motion at low salt compositions when compared to the larger cyanoethyl group of PCEEI. At higher salt compositions, the presence of crystalline domains may account for PMEI's higher $T_g$[13]. The introduction of the sodium salt to PCEEI yields a similar increase in $T_g$ with increasing salt composition but with a slightly smaller magnitude.

The temperature range in which a PE remains chemically/physically stable is important because it dictates the potential temperature range of the battery in which it is incorporated. Thermogravimetric analysis (TGA) was used to characterize this temperature range for PCEEI and PCEEI:LiTf PEs. Figure 4a, 4b and 4c display thermograms of PCEEI, PCEEI:LiTf 20RU:1Li and PCEEI:LiTf 10RU:1Li from room temperature to 525 °C with a heating ramp of 10 °C/min.

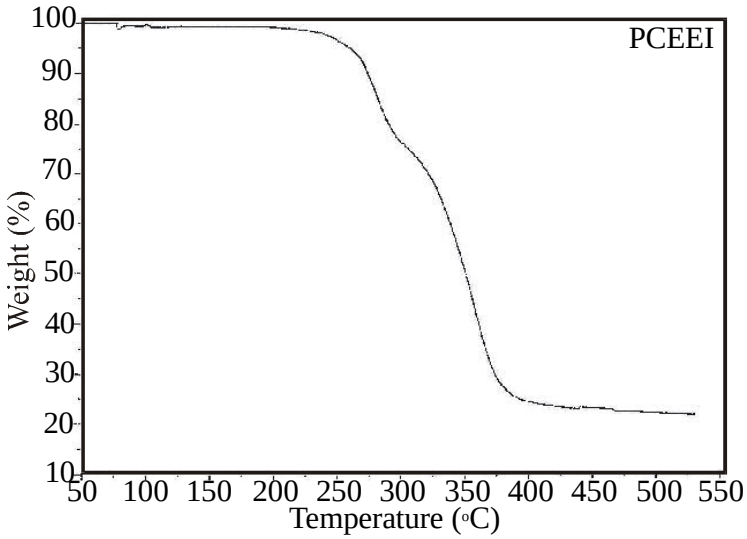


Figure 4a: Thermogram for PCEEI with an onset temperature of degradation of 210 °C

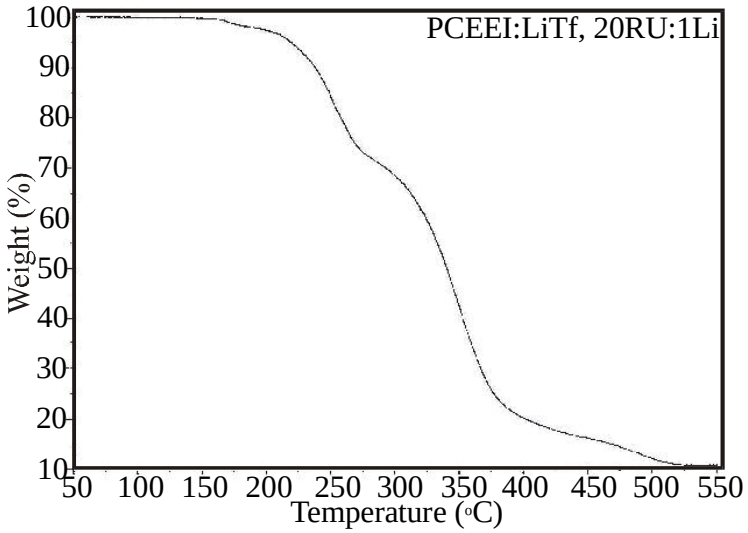


Figure 4b: Thermogram for PCEEI:LiTf (20RU:1Li) with an onset temperature of degradation of 170 °C

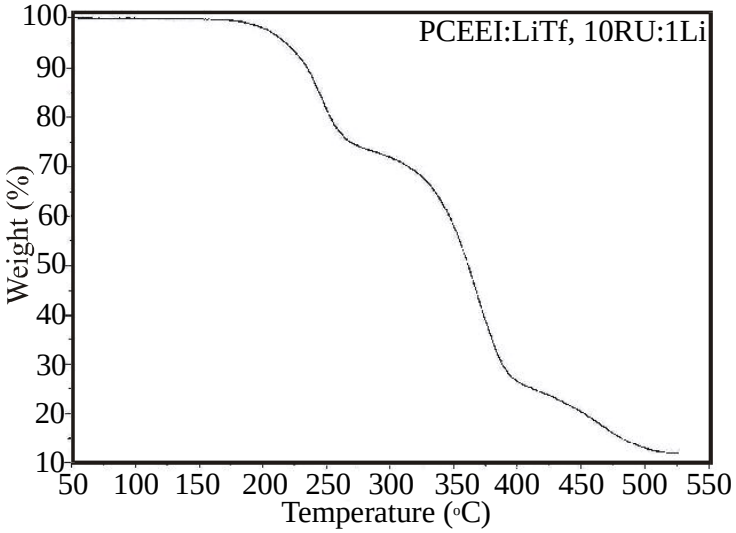


Figure 4c: Thermogram for PCEEI:LiTf (10RU:1Li) with an onset temperature of degradation of 175 °C

PCEEI is thermally stable up to approximately 210 °C where the onset of weight loss begins. Two distinct regions of weight loss appear with the first beginning around 210 °C and the second at 275 °C. For the 20 and 10RU:1LiTf compositions, the onset of weight loss decreases to about 170 °C with a second weight loss dip appearing around 260 °C. Speculatively, the first band may be the result of de-cyanoethylation, and the second may be backbone decomposition.

## $Li^+$ Interactions

LiTf in solution can exist in multiple states of aggregation. Estimations of the number and types of aggregation of the triflate anion in PEs have been reported in the literature and infrared spectroscopy has been used for this determination[16-18]. The sulfonate stretch, $\nu_s(SO_3)$ (Figure 5), is a vibrational mode that is sensitive to cation

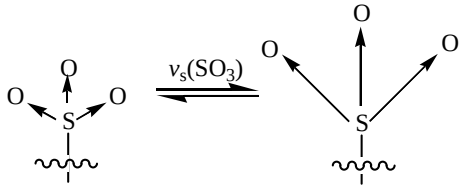


Figure 5: $\nu_s(SO_3)$ vibrational mode

coordination and, through band deconvolution and assignment of band frequencies, gives relative populations of ‘free’ triflate, ion pair/triple ion I, triple ion II (Figure 6) and higher aggregates (not shown). With this method, ion pair and triple ion I are indistinguishable because both types of triflate coordinate to one lithium ion resulting in the same type of influence on the $\nu_s(SO_3)$.

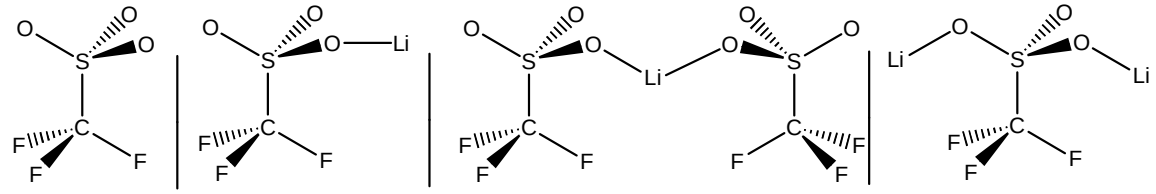


Figure 6: Potential triflate species

This method of estimation of triflate aggregation was employed for PCEEI:LiTf complexes. A series of PCEEI:LiTf samples were made with different salt compositions, an infrared spectrum was taken for each and bands in the $\nu_s(SO_3)$ region were deconvoluted with curve fitting software. As seen in Figure 7, a very broad, weak polymer band

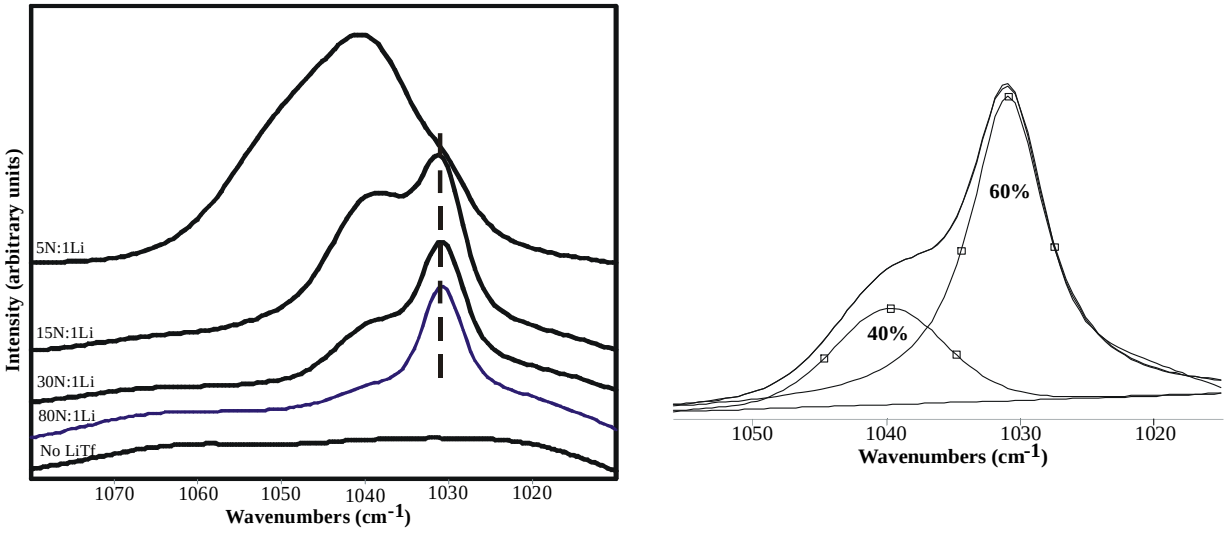


Figure 7: $\nu_s(SO_3)$ region for PCEEI:LiTf and an example of the fitting of a spectrum in this region

is observed in this region for pure PCEEI, while additions of LiTf dwarf this band with increased LiTf composition. Increases in the frequency of the $\nu_s(SO_3)$ bands are also observed and is consistent with what is reported in the literature. A sample of the curve fitting results for a 20N:1Li sample is also shown in Figure 7. The curve fitting results are listed in Table 3.

| | **Band center frequency ($cm^{-1}$) (% integrated area)** | | |
|---|---|---|---|
| **Sample (N:Li)** | **'free' triflate** | **ion pair/triple ion I** | **triple ion II** |
| 0 | - | - | - |
| 80 | 1031 (~99%) | - | - |
| 30 | 1031 (60%) | 1039 (40%) | - |
| 15 | 1031 (33%) | 1039 (67%) | - |
| 5 | 1031 (1%) | 1039 (69%) | 1053 (30%) |

Table 3: Relative populations of different triflate species at different LiTf compositions

The band at 1031 $cm^{-1}$ was verified to be non-lithium coordinated, 'free', triflate by obtaining spectra of PCEEI:tetrabutyl amine triflate (TBAT). Tetrabutyl ammonium cations are non-coordinating and allow the identification of non-coordinatively influenced $\nu_s(SO_3)$. In contrast to PAN:LiTf electrolytes, where 'free' triflate or LiTf ion pair is not observed at compositions from N:Li = 10 to 60:1[11], 'free' anion in PCEEI:LiTf electrolytes is the dominant triflate species at low salt compositions, 80 to 30N:1Li. LiTf species in PCEEI appear to be more similar in the nature and degree of ion association to LiTf species in LPEI, where the dominant species present, as determined by curve fitting,

was the ion pair at a 10N:1Li salt composition[19]. As in PCEEI, LiTf aggregation increases with increasing salt composition in LPEI:LiTf electrolytes, but, at a 5N:1Li composition, the triple ion II species dominates in the absence of 'free' triflate. Spectra of PCEEI:LiTf 15N:1Li were taken from room temperature to 120 °C in increments of 10 °C and little change is noted except for a slight increase in the ratio of ion pair/triple ion I and triple ion II to 'free' triflate. Examination of the aggregate sensitive $\delta_s(CF_3)$ bands in PCEEI:LiTf samples reveals comparable behavior but is complicated due to polymer bands in this region.

It has been reported in the chemical literature[8,10] that a high frequency shoulder exists on the free $\nu_s(C\equiv N)$ band in PAN:LiTf electrolytes at high LiTf compositions and has been attributed to nitrile coordination with lithium ion. At sufficiently large salt composition, this shoulder has been reported to be higher in relative intensity than the free nitrile band at 2244 $cm^{-1}$. Shifting intramolecular vibrational frequencies in a phase containing nonbonding ions (e. g., metal cations in solution) is generally believed to arise due to polarization of the molecule in the Coulomb field of a cation[20]. The high frequency shift has been rationalized through the study of model compounds such as acetonitrile with Lewis acids. In free acetonitrile, the nitrogen lone pair is suggested to have more *s* character than a pure *sp* orbital, while the corresponding nitrogen orbital that participates in the sigma bond with the carbon atom has more *p* character than a true *sp* orbital. Complex formation would then increase the *p* character of the lone pair orbital and hence increase the *s* character of the bonding orbital resulting in the strengthening and increase in the force constant of the C≡N bond[21]. The frequency of the vibrational mode is directly proportional to the square root of the force constant, yielding a higher frequency shift to

the coordinated nitrile. Shortening of the C≡N bond has also been observed in acetontitrile:Lewis acid crystal structures[21].

At LiTf compositions of 15N:1Li and higher, a higher frequency shoulder on the PCEEI $\nu_s$(C≡N) band develops and increases in relative intensity with increasing salt composition (Figure 8). Spectra taken of the 15N:1Li electrolyte from room temperature to 120 °C in increments of 10 °C reveal no change in the ratio of coordinated nitrile to non-coordinated nitrile.

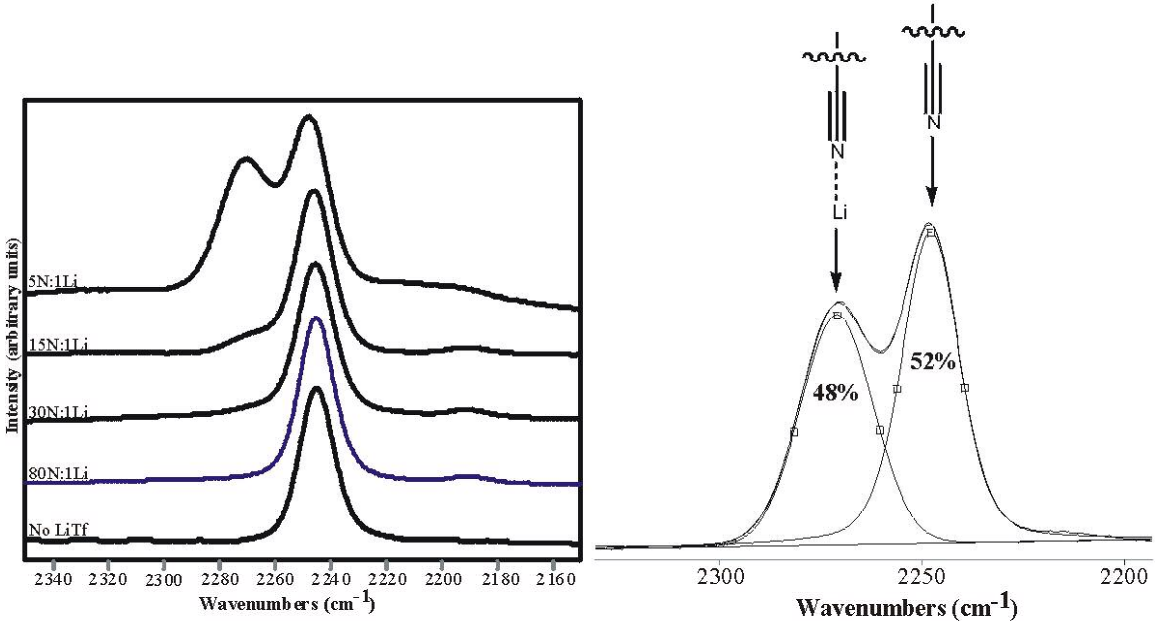


Figure 8: $\nu_s$(C≡N) of PCEEI:LiTf and an example of the spectral fitting

The peak areas were quantified and the results are listed in Table 4. It is clear that as the amount of LiTf present increases, the percentage of coordinated nitrile increases. At the high LiTf composition, the percentage of coordinated nitrile exceeds the percentage of non-coordinated nitrile. The ratio of the moles of coordinated nitrile to the total moles of

LiTf at the 5N:1Li composition is 1.3. This suggests that, in some cases, more than one nitrile must be coordinating to a single lithium ion. This should result in a physical cross-linking at high LiTf compositions which is validated by an increase in $T_g$

| **N:Li** | **Li:(C≡N)** | **'free' $v_s$(C≡N)** | **coordinated $v_s$(C≡N)** | **moles (C≡N)-Li: moles LiTf** |
|---|---|---|---|---|
| 80 | 0.025 | ~100% | - | 0 |
| 30 | 0.067 | ~100% | - | 0 |
| 15 | 0.13 | 91% | 9% | 0.23 |
| 5 | 0.40 | 48% | 52% | 1.3 |

Table 4: A comparison of the N:Li ratio, Li:(C≡N) ratio, the percent nitrile coordinated and the moles C≡N)-Li: moles LiTf ratio

It also is likely that at the dilute composition, 80N:1Li, lithium is coordinating to the backbone nitrogen because 'free' triflate is the only anion species present.

Qualitative determination of the extent of lithium coordination to either the nitrogen of the tertiary amine or the cyano nitrogen requires a comparison of vibrational modes. Data collected has been inconclusive and other studies, such as using Raman to examine the $v_s$(C-N) vibrational mode, are necessary for reasonable comparisons. Model compounds of cyanoethylated *N,N*'-dimethylethylenediamine and diethylamine and LiTf were made into solutions with the hope of forming crystals and exploring the lithium coordination but crystals have been elusive.

**Ionic Conductivity**

With a considerable amount of non-ion paired LiTf present, ~100% at low salt composition, and the amorphous nature of the electrolytes, it seemed likely that the ionic conductivity for PCEEI:LiTf electrolytes would be an improvement over PAN

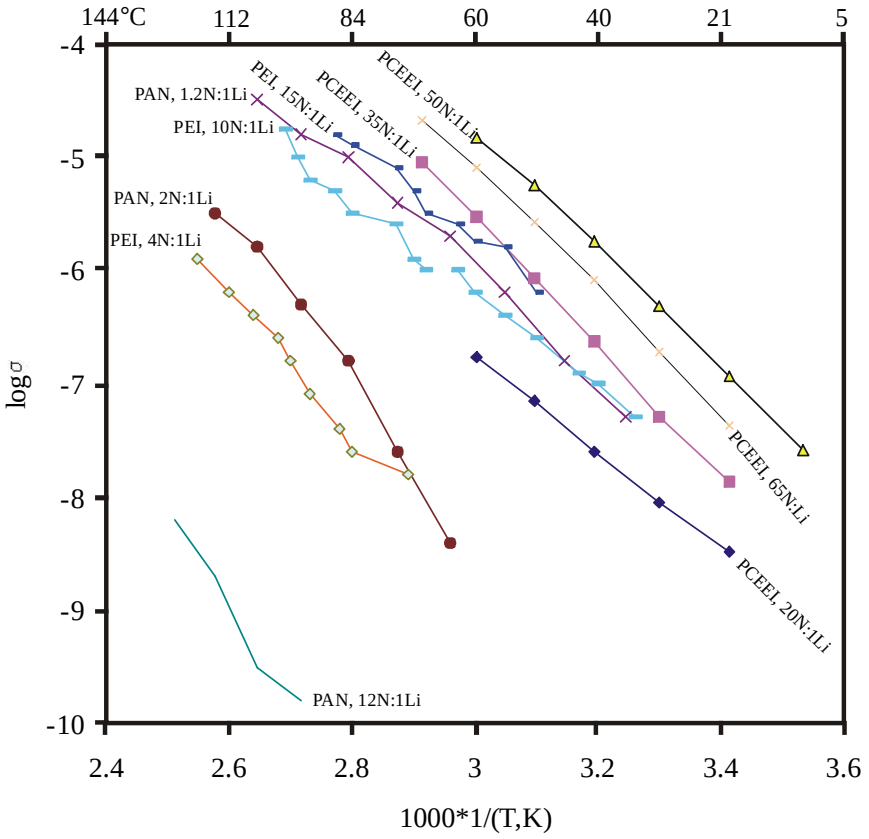


Figure 9: A comparison of the temperature dependent conductivity for PAN, PEI and PCEEI electrolytes[11, 12]

electrolytes. At low LiTf compositions, PAN electrolytes are reported to have poor ionic conductivity, unmeasureable at room temperature to ~$10^{-9}$ S/cm at over 100 °C, while, at higher LiTf compositions, it improves dramatically from $10^{-8}$ S/cm at 30 °C to $10^{-5}$ S/cm

at 105 °C[11] (Figure 9[11, 12]). LPEI:LiTf electrolytes display the opposite trend with ionic conductivity increasing as salt composition decreases[12]. As seen in Figure 9, LPEI:LiTf is significantly more conductivity than PAN:LiTf in comparable temperature ranges and LiTf compositions. The highest conductivity was reported as $3.2\times10^{-5}$ S/cm at 105 °C for the PAN 1.2N:1Li sample[11] and $1.6\times10^{-5}$ S/cm at 88 °C for the LPEI 10N:1Li sample[12]. PCEEI:LiTf electrolytes exhibit higher ionic conductivity than PAN:LiTf and PEI:LiTf electrolytes in select temperature ranges for the 30, 50 and 65N:1Li sample compositions (Figure 9). Ionic conductivity in PCEEI:LiTf electrolytes increases as salt composition decreases until the low compositions are reached, 50 and 65N:Li, where the 50N:1Li sample is higher in conductivity over the temperature range measured. This could be due to error in the measurement process. The room temperature ionic conductivity of all four PCEEI:LiTf samples was on the order of $10^{-8}$ S/cm, well below the lofty goal of $10^{-3}$ S/cm set for dry polymer electrolytes. Apparent activation energies for the ionic conductivity were in the range of 38 to 93 kJ/mol. In samples of PAN:LiTf (33 – 67% salt by weight), activation energies were reported to be between 55 and 144 kJ/mol[7].

**Conclusion**

PCEEI is a new polymer synthesized by a Michael reaction of PEI with acrylonitrile, which utilizes the functionizable secondary amine in the backbone of PEI. Pure PCEEI has a $T_g$ of –36 °C, and addition of significant amounts of triflate salts increases this value to close to room temperature. At 210 °C, PCEEI undergoes a form of polymer degradation, while, with LiTf salt addition, onset for this degradation is between 170 and 175 °C. Infrared spectroscopy revealed a high ratio of ‘free’ triflate to other

triflate species at low salt compositions. Ion pair/triple ion I and 'free' triflate are approximately equal in number at high salt compositions. This data, coupled with the observed nitrile coordination at high salt compositions, suggests that at high LiTf compositions lithium ion is highly coordinated. Calculations from spectral fitting data indicate, at a 5RU:1Li composition, a ratio of 1.3 Li-coordinated nitrile to total lithium ion exists. This suggests that some lithium ions are coordinatively shared between nitrile groups . As the composition of LiTf in the PCEEI:LiTf samples is increased, the ionic conductivity decreased over a wide temperature range. This information, coupled with the increases in $T_g$ with increasing salt composition and the high lithium coordination by nitrile at high salt composition, suggests that the lithium ion becomes less mobile at higher salt compositions as a result of the immobilizing of the lithium ion and coordination-based cross-linking. The ionic conductivity of PCEEI:LiTf electrolytes is greater over select temperature ranges than in PAN:LiTf and LPEI:LiTf.

Improvements in the physical properties of PCEEI with crosslinking and construction and cycling of individual battery cells with non-crosslinked and crosslinked PCEEI are reported in Chapter 4.

**References**


1. Saegusa, T. Yamada, A. Taoda, H. Kobayashi, S. *Macromolecules* **1978**, 11, 435.
2. Tanaka, R. Ueoka, Y. Kataoka, K. Saito, S. *Macromolecules* **1983**, 16, 849.
3. Snow, A. G. Sanders, R. A. Frech, R. Glatzhofer, D. T. *Electrochim. Acta* **2003**, 48, 2065.
4. Johnson, T. W. Klotz, I. M. *Macromolecules*, **1974**, 7, 149.
5. Takahashi, T. Davis, G. T. Chiang, C. K. Harding, C. A. *Solid State Ionics* **1986**, 18-19, 321.

6. Smith, M. B. March, J. 'March's Advanced Organic Chemistry' John Wiley & Sons: New York, 2001; p 1022.
7. Forsyth, M. Sun, J. MacFarlane, D. R. *Solid State Ionics* **1998**, 112, 161.
8. Ferry, A. Edman, L. Forsyth, M. MacFarlane, D. R. Sun, J. *Electrochim. Acta*, **2000**, 45, 1237.
9. Appetecchi, G. B. Croce, F. Marassi, R. Panero, S. Ronci, F. Savo, G. Scrosati, B. *Solid State Ionics* **2001**, 143, 73.
10. Wang, Z. Weidong, G. Chen, L. Yujan, M. Huang, X. *J. Electrochem. Soc.* **1996,** 149, 5, E148.
11. Ferry, A. Edman, L, Forsyth, M. MacFarlane, D. R. Sun, J. *J. App. Phys.* **1999**, 86, 2346.
12. Tanaka, R. Fujita, T. Nishibayashi, H. Saito, S. *Solid State Ionics*, **1993**, 60, 119.
13. Sanders, R. A. Snow, A.G. Frech, R. Glatzhofer, D. T. *Electrochim. Acta*, **2003**, 48, 2247.
14. Aldrich chemical catalogue, 2003-2004, p1522.
15. Painter, P.C. Coleman, M.M. 'Fundamentals of Polymer Science, Second Edition' Technomic Publishing Company; Lancaster, 1997 p 293.
16. Schantz, S. Sandahl, J. Borjesson, L. Torell, L. M. Stevens, J. R. *Solid State Ionics*, **1988**, 28-30, 1047.
17. Frech, R. Huang, W. *Solid State Ionics* **1994**, 72, 103.
18. Huang, W. Frech, R. Wheeler, R. A. *J. Phys. Chem.* **1994**, 98, 100.
19. York, S. Frech, R. Snow, A. Glatzhofer, D. T. *Electrochim. Acta* **2001**, 46, 1533.
20. Ostrovskii, D. Brodin, A. Torell, L.M. Appetecchi, G.B. Scrosati, B. *J. Chem. Phys.* **1998**, 17, 7618.
21. Evans, J.C. Lo, G.Y.S. *Spectrochim. Acta* **1965**, 21, 1033.

# Chapter 3: GEL ELECTROLYTES BASED ON CROSS-LINKED TETRAETHYLENE GLYCOL DIACRYLATE/POLY(ETHYLENIMINE) SYSTEMS

Modified from *Polymer* 2004, 45, 3389.

The development and study of polymer electrolytes (PEs) has been extensive because of their potential application as ion transport membranes in batteries and other electrochemical devices. PEs are desirable because they offer flexibility, decreased weight and improved safety as compared with other materials used as electrolytes in electrochemical devices[1], but most PEs have lower than necessary ionic conductivity needed for high energy density electrochemical devices. Polymeric gel electrolytes have been developed and make certain improvements in the physical properties and conductivity of PEs. A polymeric gel electrolyte typically consists of a polymer matrix infused with a high boiling point organic solvent and a suitable salt.[2] Ionic conductivity for these gel electrolytes can typically range from $10^{-3}$ and $10^{-4}$ S/cm and lower at room temperature.[3-6] For gel electrolytes to be a practical substitute for PEs, they also must be dimensionally stable solids with electrochemical stability in a wide voltage range. Further exploration of new and improved materials, along with further understanding of the link between molecular level interactions and ionic conductivity, is still necessary for the further development of polymeric ion transport membranes for electrochemical devices.

**Cross-linked PEI Synthesis and Electrolyte Preparation**

A Michael reaction[7] involving the nucleophilic amine functionality in PEI with the electrophilic acrylate functionality of TEG serves as the means of synthesis of the cross-linked material described in this chapter (Figure 1). To our knowledge, the use of

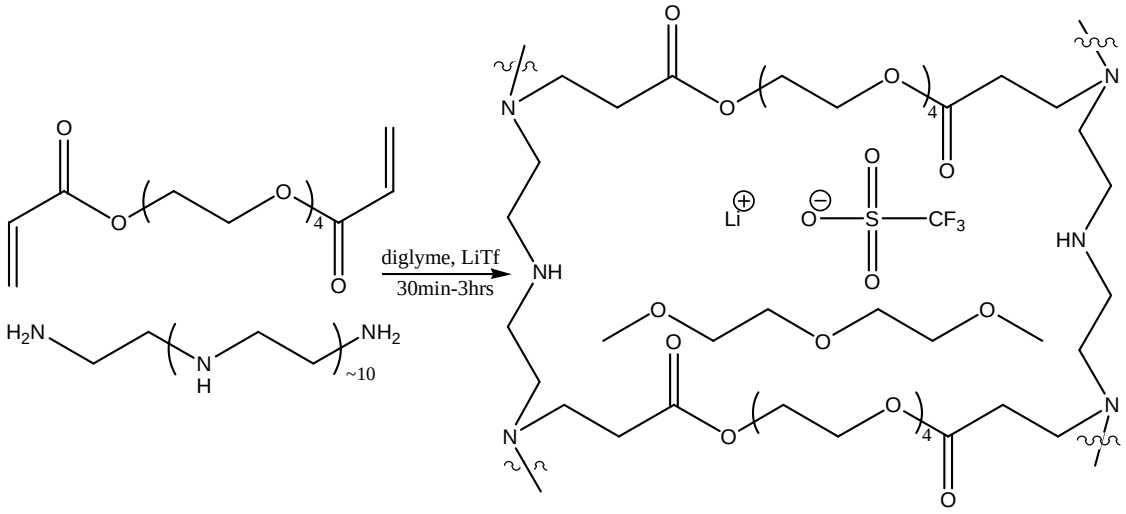


Figure 1: Synthesis of TEG cross-linked PEI gel electrolyte

TEG to produce gel electrolytes by condensation polymerization/cross-linking using the acrylate functionality as a Michael acceptor has not been reported. TEG has been described in the chemical literature for the preparation of cross-linked polymer gel electrolytes as a cross-linking agent.[3,8-12] However, in these examples the alkene of the acrylate functionality has been used in addition polymerization reactions, typically radical, with other alkenes, and other TEG alkenes, in the presence of electrolyte and a solvent to yield gel electrolytes. These gel electrolytes require initiation of polymerization by an initiator[3,8-11] or a UV lamp[12]. With our system, only mixing is required for cross-linking. Ionic conductivity measurements are presented for TEG cross-

linked PEI gel electrolytes. Interactions of lithium ion with triflate, diglyme and the cross-linked polymer matrix have been examined with vibrational spectroscopy and will be used to help clarify certain aspects of ionic conduction occurring in these gel electrolytes.

All samples cited in this chapter were prepared with a constant theoretical cross-linking ratio of five moles of PEI nitrogen to one mole of TEG (2.5N:1acrylate functionality), abbreviated 5N:1TEG (this composition was used because it produced samples that subjectively had good physical properties). The diglyme composition of each sample is listed as a ratio of the number of PEI nitrogens to diglyme oxygens (no TEG or $Tf^-$ oxygens included). A sample with five nitrogens for every two diglyme molecules is abbreviated N:O = 5:6. When indicating the molar composition of a sample, the contribution of TEG is excluded because the molar ratio of PEI to TEG is held fixed in all samples.

IR and Raman spectroscopies were used evaluate the degree of cross-linking of the cured gel electrolytes. A complete disappearance of the alkene stretching bands of TEG at 1637 and 1619 $cm^{-1}$ and the alkene $CH_2$ twist at 810 $cm^{-1}$ was noted in the IR spectra for all samples discussed in this paper. An absence of the alkene stretching mode at 1636 $cm^{-1}$ was also observed in Raman spectra. In both IR and Raman spectra, a higher frequency shift of the $\nu_s$(C=O) from 1724 $cm^{-1}$ in pure TEG to 1734 $cm^{-1}$ in the cross-linked samples was observed. Curve fitting of each carbonyl stretching mode indicated only one component contributes to the peak area in the samples prepared with diglyme but no LiTf. The combined evidence suggests essentially complete reaction of

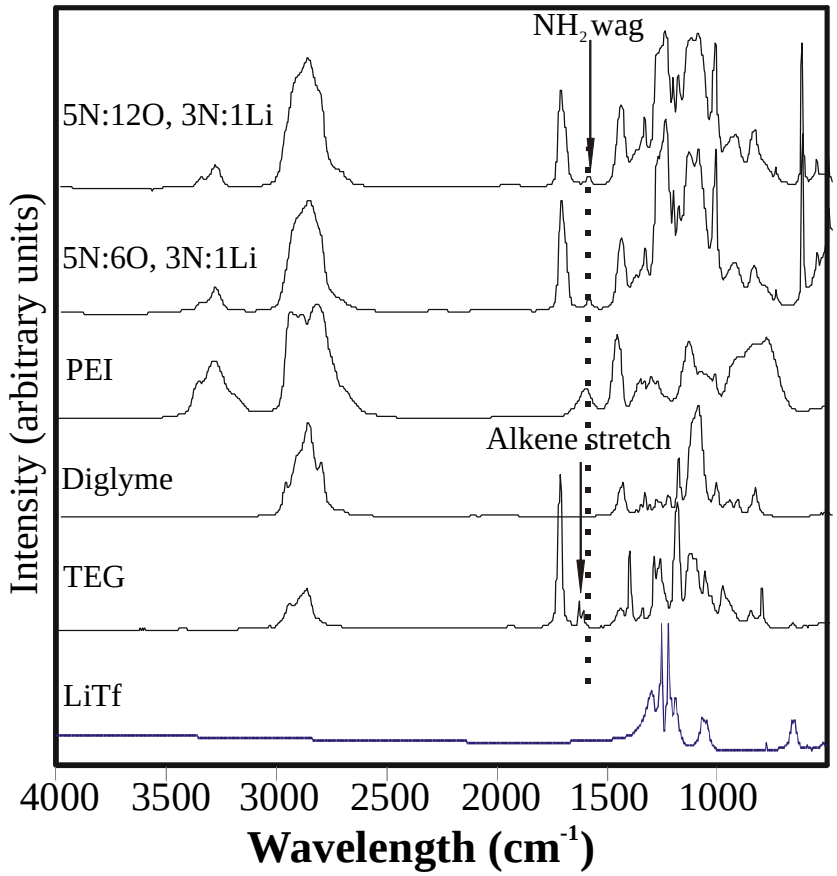


Figure 2: Stack plot of each component in the gel electrolytes and a high and low diglyme composition gel

the acrylate groups of TEG with the amine groups of PEI. An infrared spectra stack plot of each of the gel components as well as two gels with different diglyme compositions is presented in Figure 2 to show the spectral origins of the gel electrolytes and the disappearance of the alkene stretch.

All gel electrolytes described in chapter were free-standing and flexible materials. When blotted by tissue paper, diglyme bleeding out of the polymer matrix was not

observed. Decreasing the diglyme composition yielded a tougher material, while increasing the LiTf composition had little effect except at the very high concentrations (N:Li = 1.5 and 2) where the material softened at 60 °C.

**Ionic Conductivity**

Ionic conductivity measurements were taken for a variety of sample compositions at different temperatures. Each sample tested had a composition of 5N:1TEG, while the compositions of diglyme and LiTf were varied. Conductivity measurements were taken for all samples at 20 °C and, for select samples, over a temperature range of 0 to 60 °C.

**Ionic Conductivity at 20 °C**

The ionic conductivity of samples with a diglyme composition of N:O = 5:6 increased with increasing amounts of LiTf present at 20 °C as shown in Table 1.

| xN:1Li | wt% PEI | wt% TEG | wt% diglyme | wt% LiTf | % 'free' ion | % ion pair | % aggregate | σ, S/cm |
|---|---|---|---|---|---|---|---|---|
| **5N:12O** | | | | | | | | |
| 30N:1Li:72O | 19.9 | 27.9 | 49.8 | 2.4 | 100 | | | $1x10^{-5}$ |
| 20N:1Li:48O | 19.7 | 27.6 | 49.2 | 3.5 | | | | $2x10^{-5}$ |
| 10N:1Li:24O | 19.0 | 26.6 | 47.5 | 6.8 | 93 | 7 | | $6x10^{-5}$ |
| 5N:1Li:12O | 17.8 | 24.9 | 44.4 | 12.9 | 78 | 22 | | $1x10^{-4}$ |
| 3N:1Li:7.2O | 16.4 | 22.9 | 41.0 | 19.7 | 51 | 48 | 1 | $2x10^{-4}$ |
| 2N:1Li:5O | 15.1 | 21.1 | 37.7 | 26.2 | 31 | 65 | 4 | $2x10^{-4}$ |
| 1.5N:1Li:3.6O | 13.7 | 19.1 | 34.2 | 33.0 | 28 | 64 | 8 | $5x10^{-5}$ |
| **5N:6O** | | | | | | | | |
| 30N:1Li:36O | 26.5 | 37.1 | 33.2 | 3.2 | 100 | | | $2x10^{-6}$ |
| 20N:1Li:24O | 26.1 | 36.6 | 32.6 | 4.7 | | | | $4x10^{-6}$ |
| 10N:1Li:12O | 24.9 | 34.9 | 31.2 | 9.0 | 67 | 33 | | $8x10^{-6}$ |
| 5N:1Li:6O | 22.9 | 32.0 | 28.6 | 16.6 | 61 | 39 | | $1x10^{-5}$ |
| 3N:1Li:3.6O | 20.6 | 28.8 | 25.7 | 24.9 | 44 | 51 | 5 | $2x10^{-5}$ |

Table 1: Weight percentage of each component, relative peak areas of the triflate anion species and the 20 °C ionic conductivity for each gel electrolyte

Additional increases in LiTf composition were not possible due to limited LiTf solubility. Increasing the diglyme composition from N:O = 5:6 to 5:12 increased the conductivity about an order of magnitude for comparable LiTf compositions, (Table 1). The trend in conductivity values at 20 °C for the N:O = 5:12 samples was different than that of the trend observed in the N:O = 5:6 samples. Ionic conductivity increased as the LiTf composition increased to a maximum value of $2x10^{-4}$ S/cm at a composition of N:Li:O =

3:1:7.2 and decreased in value for samples with increased amounts of LiTf. Increases in conductivity with increasing amounts of diglyme are considerable, as samples with constant N:Li = 30:1 and N:O ratios of 5:0, 5:6 and 5:12 had conductivities of $1x10^{-7}$ S/cm, $2x10^{-6}$ S/cm and $1x10^{-5}$ S/cm, respectively.

**Ionic Conductivity from 0 °C to 60 °C**

Plots of ionic conductivity versus temperature over a temperature range of 0°C to 60°C are presented in Figures 3 and 4 for samples with N:O = 5:6 and 5:12 and LiTf

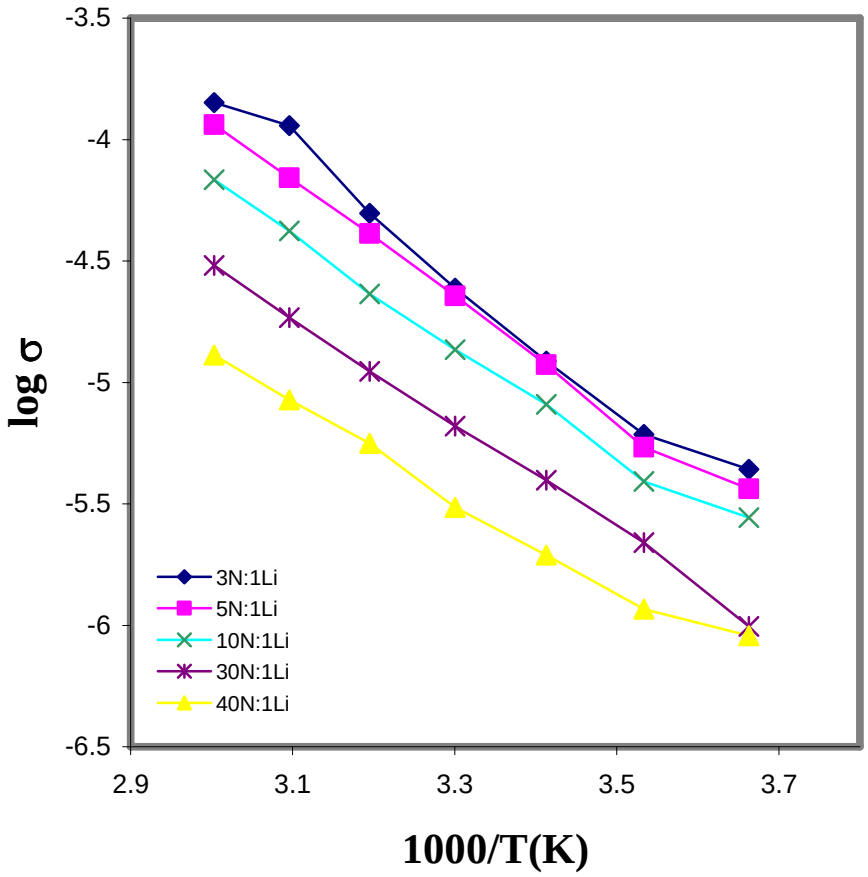


Figure 3: Ionic conductivity from 0 to 60 °C for N:O = 5:6 samples with LiTf compositions of N:Li = 3:1 to 40:1

compositions of N:Li = 3:1 to 40:1 for the N:O = 5:6 samples and N:Li = 3:1 to 30:1 for the N:O = 5:12 samples. All plots appear to display Arrhenius behavior in this

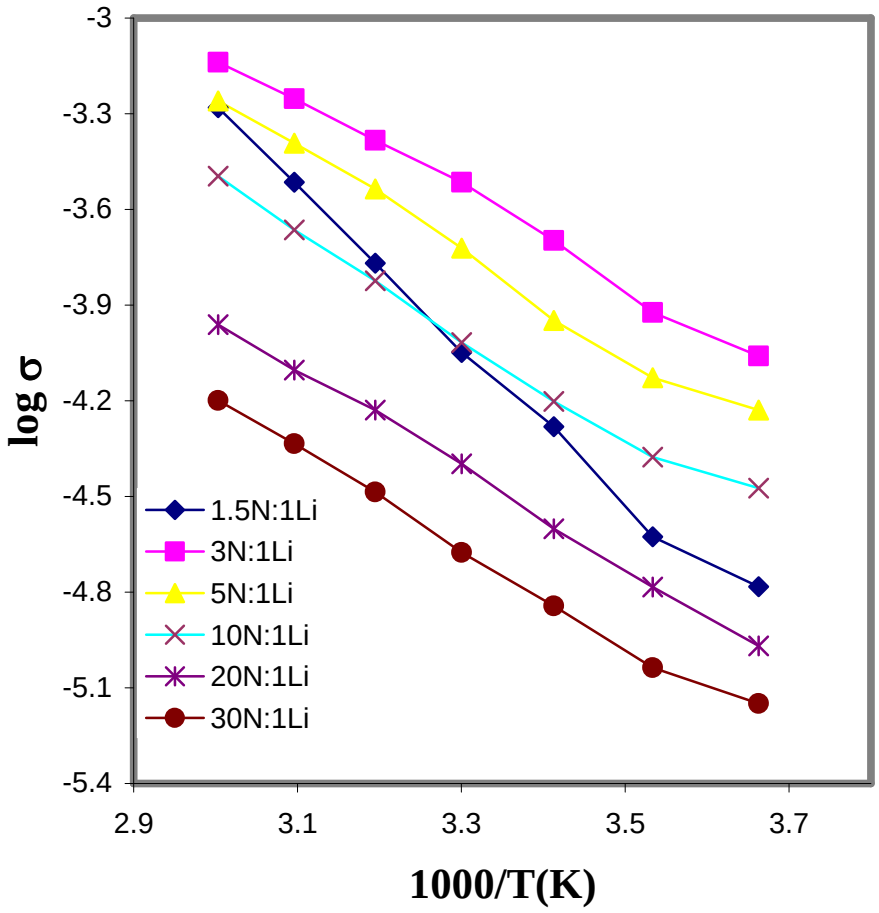


Figure 4: Ionic conductivity from 0 to 60 °C for N:O = 5:12 samples with LiTf compositions of N:Li = 1.5:1 to 30:1

temperature region although the temperature range is too narrow to distinguish between Arrhenius behavior and WLF or VTF behavior. The highest conductivity observed is $7x10^{-4}$ S/cm at 60°C for the N:O:Li = 3:7.2:1 sample. Apparent activation energies for ionic conduction were calculated for each 0 to 60 °C data set and are presented in Table 2. Higher energies are noted for the samples with the N:O = 5:6 composition relative to

| N:O = 5:12 | $E_a$ (kJ/mol) | N:O = 5:6 | $E_a$ (kJ/mol) |
|---|---|---|---|
| 1.5N:1Li:3.6 | 40 | 3N:1Li:3.6O | 42 |
| 2N:1Li:5O | 30 | 5N:1Li:6O | 40 |
| 3N:1Li:7.2O | 24 | 10N:1Li:12O | 37 |
| 5N:1Li:12O | 26 | 30N:1Li:36O | 37 |
| 10N:1Li:24O | 26 | 40N:1Li:48O | 31 |
| 20N:1Li:48O | 26 | | |
| 30N:1Li:72O | 25 | | |

Table 2: Apparent activation energies for ionic conduction for N:O = 5:6 and 5:12 samples over a range of LiTf compositions

the samples with N:O = 5:12 composition, and an increase in energy was also noted as the LiTf composition was increased in the N:O = 5:6 samples. This trend was not observed in the N:O = 5:12 samples until the LiTf composition was greater than N:Li = 3:1 where the energy of activation increased with additional LiTf for both the N:Li = 2:1 and 1.5:1 samples.

**Infrared Spectroscopy: $Li^+$ Interactions**

Lithium ion coordinative interactions in the gel electrolytes were probed using IR spectroscopy. The lithium ion can potentially interact with the triflate as a triflate ion pair or an aggregate structure, the ether oxygens in diglyme and TEG, the ester functionality in TEG and the amine nitrogens of PEI.

**$Li^+$ and $Tf^-$ Ionic Association**

The frequency of the triflate ion $\nu_s(SO_3)$ vibrational mode has been shown to be sensitive to interactions with lithium ions and is indicative of its ionic coordination ($Tf^-$ ('free'), LiTf (contact ion pair), $[Li_2Tf]^+$ (triple cation), etc.).[13,14] 'Free' triflate in this paper is defined as triflate ion not coordinated to lithium ion and was determined, as with the other triflate species, through analysis of the infrared spectral region associated with the $\nu_s(SO_3)$. Figure 5 shows IR spectra in the $\nu_s(SO_3)$ region for samples with

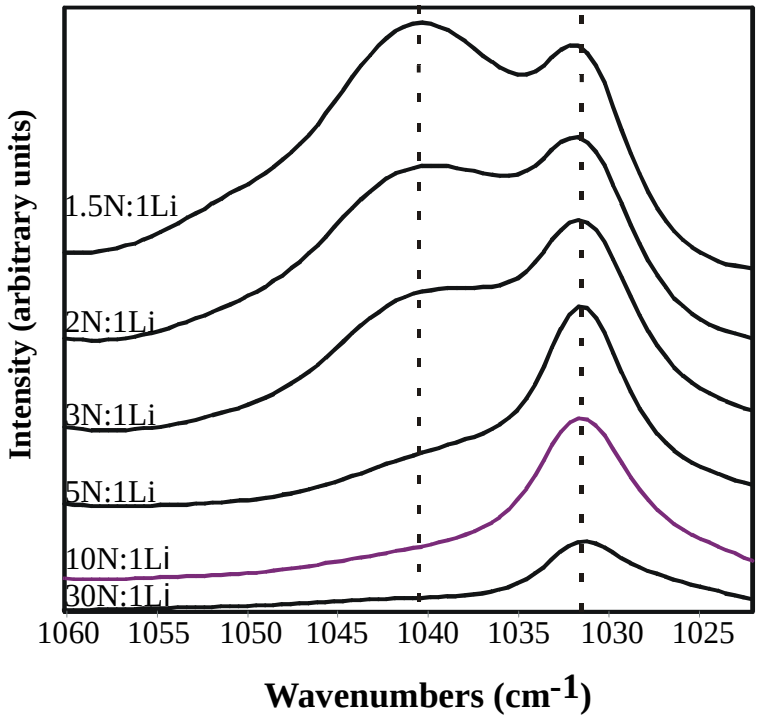


Figure 5: Comparison of the infrared spectra from N:O = 5:12 samples at the indicated LiTf compositions in the $\nu_s(SO_3)$ spectral region

compositions N:O = 5:12 and N:Li = 1.5:1 to 30:1 at room temperature. Semi-quantitative determination of the relative amounts of triflate species present was calculated by curve-fitting the $\nu_s(SO_3)$ region. Mixed Lorentzian-Gaussian bands were observed at 1031, 1039 and 1053 $cm^{-1}$ and assigned to the spectroscopically 'free' $Tf^-$, the LiTf ion pair and the $[Li_2Tf]^+$ triple ion, respectively. These values are consistent with those in chemical literature.[14, 15] Comparison of the $\nu_s(SO_3)$ region of spectra in samples with and without LiTf (5N:1TEG:4dig) indicate that the triflate bands are present in a significantly greater relative intensity to weak underlying bands even at the 30N:1LiTf composition and that these weak bands only impart a very small amount of error into the curve fitting analysis. Table 1 summarizes the curve-fitting results for both the N:O = 5:6 and 5:12 samples. At low compositions of LiTf, the only form of triflate observed was the spectroscopically 'free' form in all compositions of diglyme tested. At moderate LiTf composition (N:Li = 5:1 and 10:1 for both N:O = 5:6 and 5:12 compositions), an increase in ionic association is noted with an increase in the relative population of the LiTf ion pair without exceeding the amount of 'free' triflate present. Formation of the $[Li_2Tf]^+$ triple ion species is apparent at high LiTf compositions. Contact ion pairs predominate and increasingly become more dominant with increasing LiTf for both diglyme compositions. 'Free' triflate is notably still present in a significant percentage at the highest compositions of LiTf for both the N:O = 5:6 and 5:12 samples. Frequency shifts and band development are also noted in other lithium sensitive triflate bands, such as the $\nu_s(CF_3)$ and the $\delta_s(CF_3)$, when varying LiTf composition.

**$Li^+$ Interactions with Diglyme**

Studies of the interactions of $Li^+$ with the ether oxygens in ethylene oxide-based compounds such as PEO, tetragylyme and diglyme indicate that the frequencies and intensities of bands attributed to a mixture of $CH_2$ rocking and C-O stretching motions reflect local conformations of the ethylene oxide unit through the correlation of these frequencies with the O-C-C-O dihedral angle.[16, 17] Lithium ion interactions with the ether oxygens have been shown to affect this angle [18-20]. Figure 6 shows the $CH_2$ rocking and

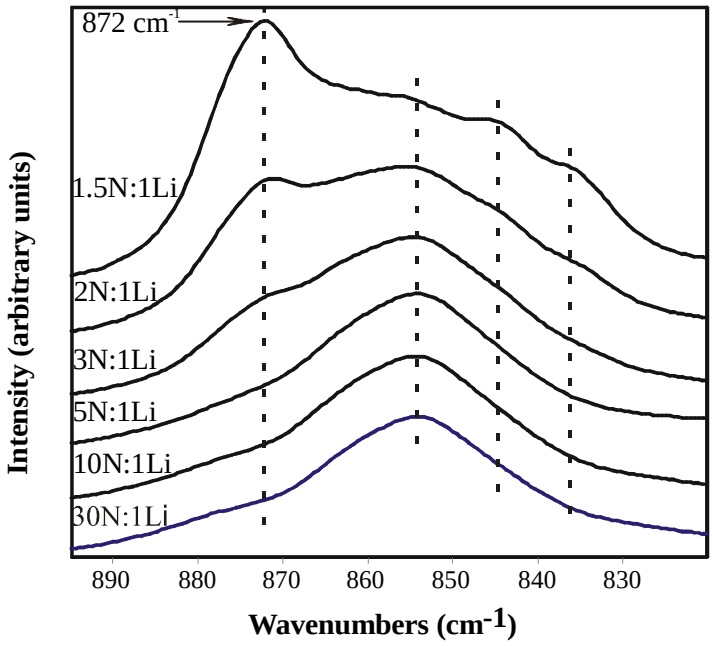


Figure 6: Comparison of the infrared spectra from N:O = 5:12 samples at the indicated LiTf compositions in the $CH_2$ rocking spectral region

C-O stretching region for samples with a constant diglyme composition of N:O = 5:12 and an increasing LiTf composition. A band, centered at 854 $cm^{-1}$, dominates at low LiTf

composition with a weak band present at higher frequency. This band has been assigned in diglyme-LiTf to be a mixture of $CH_2$ rocking and C-O stretching motions related to the TGT and TGG conformer of diglyme.[16] As the LiTf composition is increased, the higher frequency band at 872 $cm^{-1}$ increases significantly in intensity until it becomes the dominant feature at N:Li = 1.5:1. This band has been assigned in diglyme:LiTf to a $CH_2$ rocking vibration of a conformation which is not observed in pure diglyme but is adopted by diglyme in order to coordinate the lithium ion.[16] An increase in distinct band structure is also observed as two lower frequency bands at approximately 846 and 836 $cm^{-1}$ increase in intensity relative to the original dominant band at 854 $cm^{-1}$. These bands may be the result of conformers with $CH_2$ rocking and C-O stretching motions related to diglyme conformations related to the TTG and TTT conformations.[16] Only a small development in band intensity of the 872 $cm^{-1}$ band at a N:Li = 3:1 composition is noticed relative to the dominant 854$cm^{-1}$ band in the N:O = 5:6 samples from N:Li = 30:1 to 3:1. An additional band develops in the region between 900 and 1000 $cm^{-1}$ at 949 $cm^{-1}$ for both the N:O = 5:6 and 5:12 samples as LiTf composition is increased. Bands in this region also reflect local ethylene oxide conformations, which change as the lithium ion interacts with ether oxygens.

**$Li^+$ Interactions with Cross-linked Polymer**

Lithium ion interactions with the polymer matrix can be examined with IR spectroscopy. A lower frequency shoulder develops on the $\nu_s$(C=O) mode with increasing LiTf composition for both the N:O = 5:6 and 5:12 samples (Figure 7). The C=O

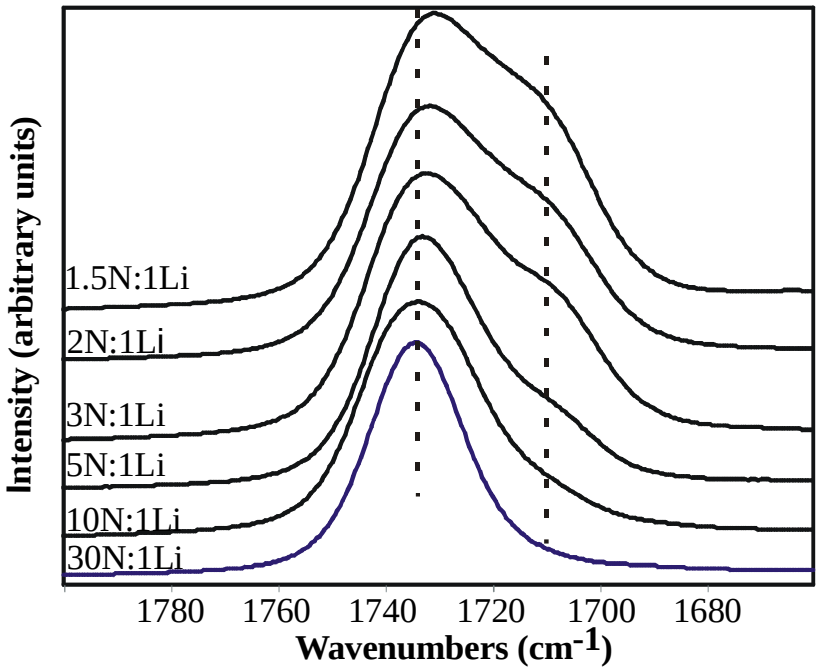


Figure 7: Infrared spectra from the $\nu_s$(CO) spectral region for N:O = 5:12 samples at the indicated LiTf compositions

stretching mode commonly develops this spectral signature in the presence of Lewis acids as a result of coordination between the Lewis acid and the more electronegative oxygen in the carbonyl.[21,22] At sufficient LiTf compositions, curve fitting the $\nu_s$(C=O) mode in the gel electrolytes reveals the presence of two bands, one at 1733 $cm^{-1}$ (indicated by a dashed line in Figure 7) and the other, typically, between 1714-1711 $cm^{-1}$.

In the absence of LiTf, only one band is observed at 1733 $cm^{-1}$. This band is assumed to be the result of non-lithium ion coordinated ester carbonyl and will be called 'free' carbonyl in this paper. The other band will be described as the lithium ion coordinated band. Curve fitting of the $\nu_s$(C=O) region for the N:O = 5:12 samples shows a distinct increase in the peak area of the coordinated band with increasing LiTf composition. As seen in Table 3, essentially all of the carbonyl groups are present in the free form at dilute LiTf compositions in the N:O = 5:12 samples. Sharp increases in the percent area of the coordinated carbonyl are noted going from the N:Li = 30:1 to the 10:1 samples. At the highest composition of LiTf, the 'free' carbonyl represents only 60% of the total peak area.

N:Li = 10:1 and 30:1 samples were prepared without addition of diglyme, and the 800-1000 $cm^{-1}$ TEG O-C-C-O conformation region was examined for evidence of increased band structure as a result of the interaction of the lithium ion with the TEG ether oxygens. One dominant band centered at 859 $cm^{-1}$ is present with bands of weak intensity on each side in both spectra and does not change appreciably as LiTf composition is increased from N:Li = 30:1 to 10:1. The spectral region between 4000 and 2000 $cm^{-1}$ remains largely unchanged for the sample compositions sited in this paper. The N-H stretching bands broaden slightly at lower LiTf compositions, while the C-H stretching region is largely unaffected by changes in LiTf composition.

**Discussion**

Examination of the various lithium ion interactions and ionic conductivity in these gel electrolytes provides insight into the relative concentration of charged species and qualitatively how ionic coordination trends correlate with ionic conductivity trends. Extensive coordination of the ionic species present can either hinder ionic mobility and decrease ionic conductivity or facilitate ion mobility and increase ionic conductivity depending on the strength of coordination.

In the binary system of diglyme-LiTf, the lithium ion has been suggested to prefer four fold coordination in solution and five fold coordination in the crystalline phase.[20] The solution phase structure of lithium ion (present as LiTf) in pure diglyme was postulated to preferentially coordinate three oxygens from diglyme and one oxygen from triflate as a contact ion pair.[20] A relatively rigid three-dimensional network of cross-linked polymer, i. e. TEG cross-linked PEI, infused with diglyme and LiTf, increases the number of coordinative sites possible for the lithium ion. Instead of the lithium ion being limited to diglyme oxygens and triflate ionic species, amine nitrogens, ester oxygens and TEG ether oxygens are available for coordination, thus not allowing treatment of the polymer matrix as an inert framework for the diglyme and LiTf.

Comparison of the spectral data from N:O = 5:12 samples of the diglyme-LiTf-TEG-PEI gels and only diglyme-LiTf samples reveals markedly different diglyme conformational behavior and triflate speciation at comparable diglyme oxygen to lithium ratios. As seen in Figure 8, diglyme-LiTf at a composition of O:Li = 5:1 exhibits a strong

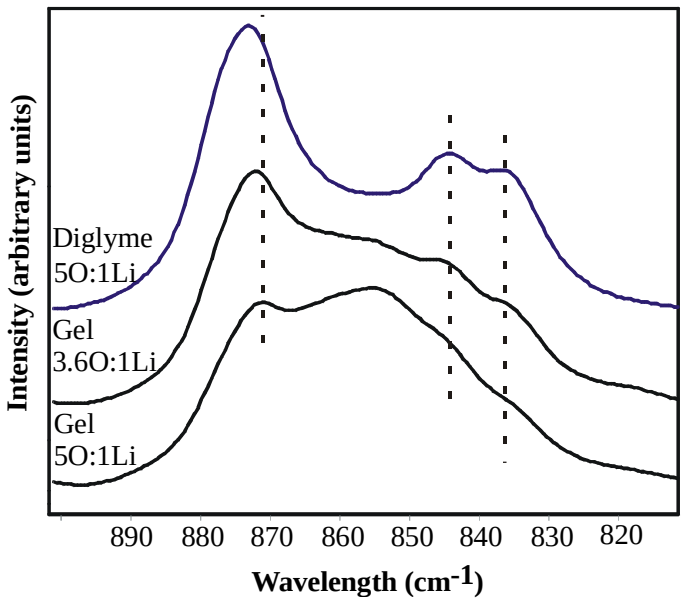


Figure 8: Comparison of the $CH_2$ rocking region of N:O samples and diglyme-LiTf at the indicated LiTf compositions

band at 874 $cm^{-1}$ with two smaller bands at 835 and 844 $cm^{-1}$. This is in contrast to the gel O:Li = 5:1 spectrum in which a slightly weaker higher frequency band at around 872 $cm^{-1}$ appears superimposed on the broad 854 $cm^{-1}$ band. Bands at 835 and 844 $cm^{-1}$ appear as only weak features on the low frequency side of the 854 $cm^{-1}$ band. The increase in band structure as LiTf composition is increased suggests an increase in the amounts of lithium ion/ether coordinative interactions.

In diglyme-LiTf, contact ion pairs are the dominant triflate species from O:Li = 80:1 to 10:1, while, at the O:Li = 5:1 composition, the triple cation $[Li_2Tf]^+$ form dominates.[23] This is significantly different from both the N:O = 5:6 and 5:12 gel samples where 'free' triflate is the only component at dilute LiTf compositions, and ion pair

develops at moderate LiTf compositions but does not dominate until high LiTf composition. The formation of higher order ionic species appears to be significantly impeded in the gel electrolyte samples when compared to the diglyme-LiTf samples.

The polymer matrix must play a key role in coordinating the lithium ion so as to produce the marked spectral differences between the diglyme-LiTf and diglyme-LiTf-TEG-PEI samples. As mentioned earlier, the polymer matrix provides several different coordinative heteroatoms as part of ester, ether and amine functionalities. Slight changes are seen in the C-N stretching region over the LiTf concentration ranges examined, but meaningful interpretation is not possible due to a medley of other bands that appear in this region. Interaction of the lithium with the TEG ether oxygens in the O-C-C-O conformation regions could not be observed because of the dominance of diglyme bands in these regions. IR spectra were taken of only TEG-LiTf at a low LiTf concentration and the maximum allowable LiTf concentration (O:Li = 10:1), and virtually no changes in band structure in the O-C-C-O conformation regions were observed when compared to pure TEG. This suggests that there are only a few conformation-restricting lithium ion interactions with the TEG ether oxygens. A slight carbonyl-lithium ion interaction did appear at the higher LiTf concentration.

The only direct evidence of lithium interaction with the polymer matrix is through observation of the shoulder that develops on the carbonyl symmetric stretch. As seen from the curve fitting results in Table 3, the peak area of the low frequency shoulder on

| N:O = 5:12 composition (N:Li) | % 'free' C=O | % $Li^+$ coordinated C=O |
|---|---|---|
| 1.5 | 61 | 39 |
| 2 | 62 | 38 |
| 3 | 65 | 35 |
| 5 | 75 | 25 |
| 10 | 79 | 21 |
| 30 | 100* | 0* |

Table 3: Curve fitting results from N:O = 5:12 samples indicating the percentage area of the $\nu_s$(C=O) represented by 'free' carbonyl and lithium ion coordinated carbonyl

the carbonyl increases significantly from essentially 0% to 39% of the total peak area over the complete LiTf composition range in the N:O = 5:12 samples. Assuming the absorptivity of the shifted carbonyl vibrational mode is approximately the same as the stationary carbonyl vibrational mode and that the lithium ion coordinates to only one carbonyl, the percentages of total lithium coordinated to carbonyls were calculated. This calculation is possible because the compositions of TEG and LiTf and the relative compositions of 'free' and coordinated carbonyl are known. Table 4 lists the percentages

| N:Li | moles of CO-Li | % $Li^+$ coordinated | % 'free' triflate |
|---|---|---|---|
| 1.5 | $3.6x10^{-4}$ | 24 | 28 |
| 2 | $3.4x10^{-4}$ | 31 | 31 |
| 3 | $3.2x10^{-4}$ | 42 | 51 |
| 5 | $2.2x10^{-4}$ | 49 | 78 |
| 10 | $1.9x10^{-4}$ | 85 | 93 |
| 30 | ~0* | 0.0* | 100* |

Table 4: Calculation of the percentage of total lithium ion coordinated to a carbonyl with a comparison to the amount of 'free' triflate present for N:O = 5:12 samples

of lithium ion coordinated to carbonyls over all the LiTf concentrations for the 5N:12O samples. At the N:Li = 1.5:1 composition, the ratio of lithium ion to carbonyl is 1.7:1, the shoulder comprises 39% of the total carbonyl peak area and 23% of the total lithium ions are coordinated to a carbonyl. At the 10N:1Li concentration, the ratio of lithium ion to carbonyl is 0.25:1, the shoulder comprises 21% of the total carbonyl peak area and 85% of the total lithium ions are coordinated to a carbonyl. This information coupled with the curve fitting data indicating the triflate speciation to be 28% and 93% 'free' triflate for the N:Li = 1.5:1 and 10:1 samples, respectively, strongly suggests that the carbonyl dominates the competition for lithium ion at moderate compositions. It also suggests that the carbonyl significantly coordinates the lithium ion not forced into coordination with triflate at high LiTf composition. Although two peaks were not observed when curve fitting the N:Li = 30:1 sample, presumably due to the very small amount of LiTf, the trend suggests that at dilute LiTf composition greater than 85% of the total lithium is

coordinated to the carbonyl. The overall coordinative influence of the carbonyl likely provides the basis for the prevalence of the lower order triflate species (free $Tf^-$ and LiTf contact ion pairs) in the gel samples as compared with the diglyme-LiTf samples.

LiTf composition affects the ionic conductivity significantly as seen in Figure 9 where molality (moles of LiTf / mass of PEI + TEG + diglyme) was used as an

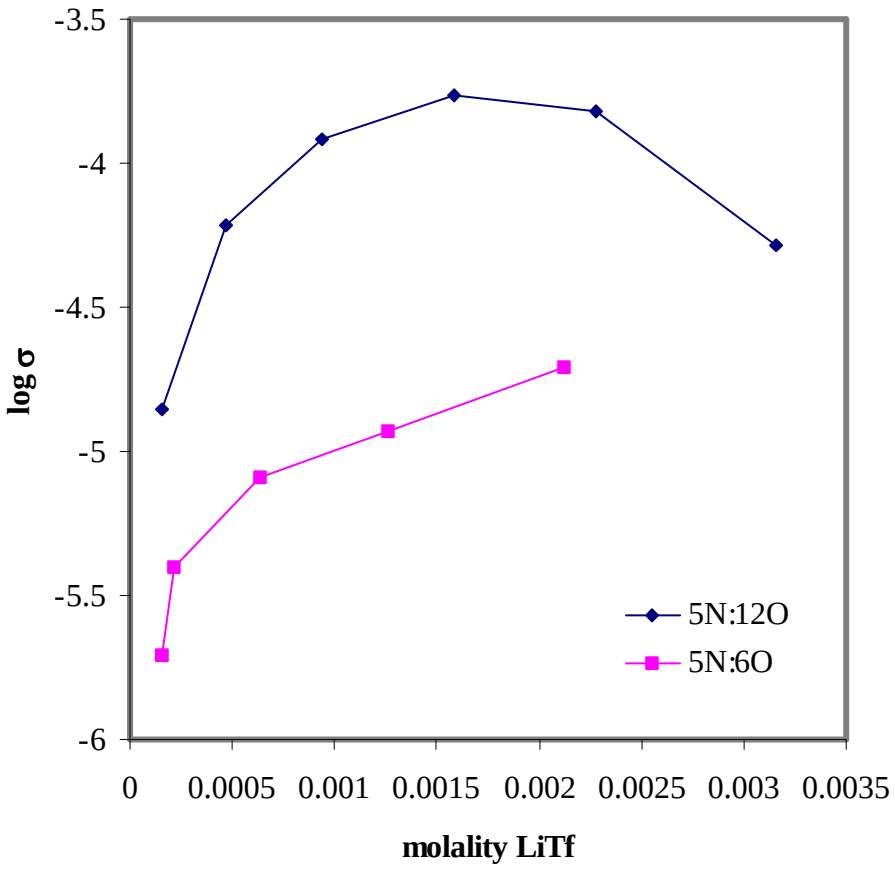


Figure 9: Natural log of the ionic conductivity versus LiTf molality for N:O = 5:6 and 5:12 samples over a range of LiTf compositions

estimation of the LiTf concentration. In the N:O = 5:12 samples, conductivity increased to a maximum and then decreased with additional LiTf. This is in contrast to the N:O = 5:6 samples where conductivity increased as the LiTf molality increased for all LiTf compositions. At higher LiTf molality, the conductivity for N:O = 5:6 samples may also decrease as similar behavior has been noted in other gel electrolyte systems.[3] The largest 'free' triflate molality (moles 'free' triflate estimated from curve fitting data / mass of PEI + TEG + diglyme + other triflate species) observed was for the N:Li = 3:1 sample, and this was also where the highest conductivity was observed. The sample with the highest molality of 'free' triflate also yielded the highest conductivity in the highest composition LiTf, 5N:6O sample.

The ionic conductivity at 20°C increased about an order of magnitude as the composition of diglyme was roughly doubled from the N:O = 5:6 to the 5:12 sample. This increase is presumably related to an increase in the mobility of the lithium and triflate ions as a result of increased amount of diglyme supported in the semi-rigid polymer matrix. The presence of more diglyme may also decrease some of the lithium ion coordination to the relatively stationary carbonyl in the polymer matrix as seen by the increase in the amount of coordinated carbonyl in the N:O = 5:6 samples at comparable LiTf compositions. Apparent activation energies for ionic conduction calculated from the variable temperature data for both the N:O = 5:6 and 5:12 samples indicate that higher activation energies are, not surprisingly, found in the N:O = 5:6 samples. This is in agreement with the lower conductivity values measured for these samples. In the N:O = 5:6 samples, the apparent activation energy actually increased with increasing LiTf concentration, which is not understood because the highest conductivity is observed with

the highest molality of 'free' triflate, and composition of LiTf. The activation energies in this gel electrolyte are on average slightly higher than those in other gel systems. For example in a glyme plasticized polymerized diacrylate system with LiTf, a typical activation energy was 28 kJ/mol[24], while in a plasticized PAN gel electrolyte activation energies were between 10 and 15 kJ/mol[25].

**Conclusions**

Novel gel electrolytes composed of a TEG cross-linked low molecular weight PEI matrix infused with varying concentrations of diglyme and LiTf have been characterized by means of vibrational and impedance spectroscopies. The ionic conductivity was found to vary with LiTf composition with the N:O = 5:6 samples showing a continual, steady increase in conductivity and the N:O = 5:12 samples exhibiting a maximum conductivity at a N:Li = 3:1 composition. The ionic conductivity was the greatest in both the N:O = 5:6 and 5:12 samples when the 'free' triflate molality was at a maximum. Increases in diglyme concentration yielded increases in conductivity. Over a temperature range of 0 to 60°C, activation energies for ionic conduction indicated more energy was required for conduction in the lower diglyme composition samples. In the N:O = 5:12 samples, the percentage of lithium ions coordinated to carbonyl groups was found to increase as the total amount of LiTf decreased and was observed to be the greatest at the N:Li = 10:1 composition where 85% of the lithium ion available was coordinated to a carbonyl group. This, along with the triflate speciation data, indicates that the lithium ion preferentially interacts with the carbonyl group relative to the triflate anion at dilute LiTf compositions. At higher LiTf compositions, a greater relative percentage of lithium ions interacting with

the triflate ions rather than the additional 'free' carbonyl groups and increasing diglyme band structure indicates a complex coordinative environment that results in material with relatively high ionic conductivity. Evaluation of the electrochemical stability and performance in batteries for this material is presented in Chapter 4.

**References**


1. Gray, F.M. 'Solid Polymer Electrolytes-Fundamentals and Technical Applications' VCH: New York, 1991.
2. Nishi, Y., In: van Schalkwijk, W.A. Scrosati, B. editors 'Advances in Lithium-Ion Batteries' Kluwer Academic/Plenum Publishers: New York, 2002.
3. Caillon-Caravanier M. Claude-Monitgny, B. Lemordant, D. *Solid State Ionics* **2003**, 156, 113.
4. Aihara, Y. Arai, S. Hayamizu, K. *Electrochim. Acta* **2000**, 45, 1321.
5. Zhou, F. MacFarlane, D.R. Forsyth, M. *Electrochim. Acta* **2003**, 48,1749.
6. Sekhon, S.S. Singh, H.P. *Solid State Ionics* **2002**, 152-153, 169.
7. Smith, M.B. March, J. 'March's Advanced Organic Chemistry: Reactions, Mechanisms and Structure' John Wiley & Sons: New York, 2001.
8. Hyun-Soo, K. Shin, J.-H. Moon, S.-I. Yun, M.-S. *J. Power Sources* **2003**, 119-121, 482.
9. Caillon-Caravanier, M. Claude-Monitgny, B. Lemordant, D. Bosser, G. *Solid State Ionics* **2002**, 149, 285.
10. Caillon-Caravanier, M. Claude-Monitgny, B. Lemordant, D. Bosser, G. *Solid State Ionics* **2002**, 149, 275.
11. Claude-Monitgny, B. Rioteau, E. Lemordant, D. Topart, P. Bosser, G. *Electrochim. Acta* **2001**, 47, 533.
12. Abraham, K.M. Alamgir, M. *J. Electrochem. Soc.* **1990**, 137,1657. 13. Frech, R. Huang, W. Dissanayake, M.A.K.L. *Mat. Res. Symp. Proc.* **1995**, 139, 523.
14. Huang, W. Frech, R. Wheeler, R. *J. Phys. Chem.* **1994**, 98,100.
15. Schantz, S. Sadahl, J. Börjesson, M.Torell, L.M. Stevens, J.R. *Solid State Ionics* **1988**, 28-30, 1047.
16. Frech, R. Huang, W. *Macromolecules* **1995,** 28, 1246.
17. Matsuura, H. Fukuhara, K. *J.Poly. Sci., Part B: Poly. Phys.* **1986**, 24, 1383.
18. Murcko, M.A. Dipaola, R.A. *J. Am. Chem. Soc.* **1992**, 114, 10010.
19. Hyun, J. Dong, H. Rhodes, C.P. Frech, R. Wheeler, R.A. *J. Phys. Chem. B* **2001**, 105, 3329.
20. Rhodes, C.P. Frech, R. *Macromolecules* **2001**, 34, 2660.
21. Schulz, W. Knoezinger, H. *J. Phys. Chem.* **1976**, 80, 1502.
22. Brown, D.G. Drago, R.S. Bolles, T.F. *J. Am. Chem. Soc.* **1968**, 90, 5706.

23. Petrowsky, M. Rhodes, C.P. Frech, R. *J. Sol. Chem.* **2000**, 30, 171.
24. Park, U.-S. Hong, Y.-J. Oh, S.M. *Electrochim. Acta* **1996,** 41, 849.
25. Reiche, A. Cramer, T. Fleischer, G. Sandner, R. Sandner, B. Kremer, F. Kaerger, J. *J. Phys. Chem. B* **1998**, 102, 1868.

# Chapter 4: PERFORMANCE OF POLY(ETHYLENIMINE)-BASED ELECTROLYTES IN LITHIUM BATTERIES

This chapter contains the discharge-charge cycling performance and analysis of cells containing several polymer electrolytes based on PEI and a comparison to a common PEO-based electrolyte. Incorporation of a polymer electrolyte as the electrode separator into a battery cell, and consequential cycling, provides a direct method for testing and comparing polymer electrolyte performance. The cells discussed contain electrodes that allow them to be cycled as secondary cells, but they can also be viewed as primary cells. The electrochemical literature contains many examples of novel polymer electrolytes to be used as the electrolyte in lithium based batteries. Polymer electrolytes are often characterized by properties such as thermal characteristics, ionic conductivity and electrochemical stability but, many times, not actual performance of the material in a cell. Although not true in all cases, difficulties in cell preparation and testing presents a hurdle for examining polymer electrolyte cell performance. Cell cycling requires an appropriate cell design, selection of compatible electrode materials and the ability to monitor and manipulate cell performance for cell characterization. No cycling performance of battery-type cells with PEI-based electrolytes is reported in the chemical literature.

## Cell Design and Li|$PEO_9Li$|$LiV_3O_8$ Benchmark

Developing a standardized method of creating cells with polymer electrolyte electrode separators capable of generating comparable performance to reported polymer

electrolyte based-cells became a priority in our lab. This necessitated the establishment of a polymer electrolyte from the chemical literature to serve as a means to compare electrolyte performance and a cell design that allows incorporation of a polymer electrolyte as the cell electrolyte. After examining the chemical literature, performance of cells containing a lithium metal negative electrode, a lithium vanadium oxide positive electrode ($LiV_3O_8$) and a high molecular weight PEO:lithium triflate electrolyte ($PEO_9LiTf$) was available from several sources[1-4]. This setup can be viewed as either a half cell (if future application of the polymer electrolyte is in a lithium ion configuration) or a full cell (if future application uses lithium metal). $PEO_9LiTf$ electrolyte has conductivity greater than $10^{-5}$ S/cm at temperatures above 70 °C[2], and cells reported in the literature were cycled from 80 to 120 °C[1-4]. This is also the temperature range that our PEI-based electrolytes are thought to require to attain the requisite conductivity ($10^{-5}$ S/cm and higher) for sufficient lithium ion mobility as determined through previous testing. So, the $Li|PEO_9LiTf|LiV_3O_8$ configuration at 100 °C was chosen to be the standard of comparison for future data collected from PEI-based electrolyte cells using the same lithium and $LiV_3O_8$ electrodes.

Several different types of cell designs are reported in the literature[2,5-6]. After developing different cell prototypes, two cell designs were picked as candidates: the tube cell and the coin cell. A tube cell is diagrammed below (Figure 1):

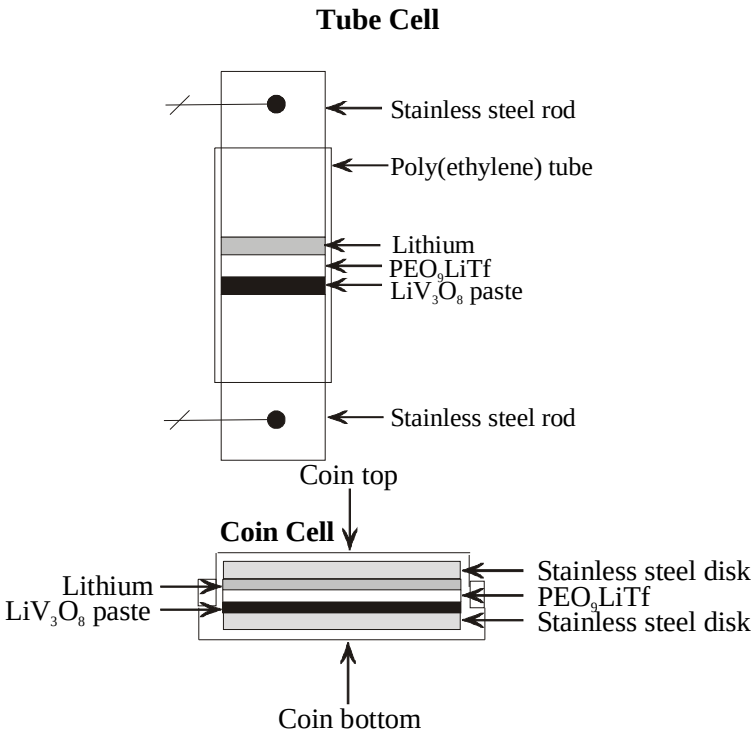


Figure 1. Tube cell and coin cell diagrams

The tube cell consisted of two steel rods inserted into a plastic tube that act to compress the lithium metal, the polymer electrolyte and the $LiV_3O_8$. The $LiV_3O_8$ electrode was prepared as a paste. This paste consisted of the active component, $LiV_3O_8$, with added graphites, 5% KS6 graphite and 5% SLP graphite, and a Teflon binder. The PEO electroloyte was incorporated by applying an acetonitrile/isopropanol solution of high molecular weight PEO and LiTf to the positive electrode followed by drying to leave a thin film ranging from 50-200μm. After considerable testing of this type of cell, it was clear that, after time, it was unsuitable because of lithium hydroxide formation from air leaks in the cell.

The second type of cell, sought to address the air leakage, uses modified coin cells obtained from Kerr-McGee. The modified cell is shown in Figure 1. A coin cell is formed by sealing two flat pans together where one pan has a plastic gasket and the other's side wall set apart far enough so that, when a special tool is used, the two plates can be compressed together to form an air-tight seal. The plastic gasket is an electronic insulator that prevents the metal cell bottom and top from coming into contact. The inside of the cell consists of two stainless steel disks sandwiching the same positive and negative electrodes and the polymer separator described above. To obtain the correct contact and pressure for the cell to function properly, a spring loaded c-clamp was used by first insulating the metal components and the applying pressure with the two heads of the c-clamp to the top and bottom of the coin cell. The force constant for the type of spring used was determined using a force gauge. The distance the spring was compressed, through Hooke's law, indirectly indicated the amount of pressure applied to the cell. The coin cell kept the interior components dry by preventing external air contamination, so this cell type was optimized for use with polymer electrolytes.

The Li|$PEO_9LiTf$|$LiV_3O_8$ cell reaction is given below.

$$Li_{(s)} + LiV_3O_{8(s)} \rightarrow Li_4V_3O_{8(s)}$$

At the start of the discharge cycle, vanadium is in the $5^+$ oxidation state, while, after complete discharge, vanadium ends up in the $4^+$ oxidation state[1]. $LiV_3O_8$ is a material that allows lithium ion intercalation and de-intercalation because of its layered structure. The $LiV_3O_8$ structure (Figure 2) is characterized by two kinds of coordination for vanadium, octahedral and trigonal bipyramidal. Strings of bipyramids and ribbons of octahedral are linked together with common corners to form puckered sheets. The sheets are linked by

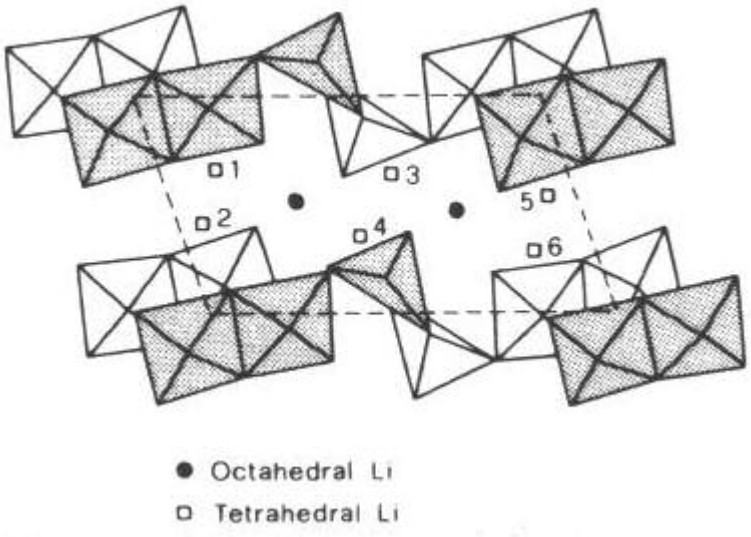


Figure 2: Representative structure of $LiV_3O_8$ showing both octahedral and trigonal bipyramids. The unit cell is dashed.[7]

lithium ions residing in both octahedral and tetrahedral sites. The presence of lithium ions in the network increases the number of metal-O bonds. This reduces the electron density on the $O^{2-}$ and reduces the possibility for the latter to form strong Li-O bonds with the ions entering the lattice during discharge. This situation contributes to fast lithium ion diffusion between sites[7]. The $LiV_3O_8$ positive electrode has a high energy density (730 W h/kg or 2500 W h/$dm^3$)[1] and lacks voltage plateaus below 1.8 V and above 3.1 V[1] (where electrolyte oxidation at the cathode is more probable). Characteristic performance of $LiV_3O_8$ versus lithium metal using $LiPF_6$ (1M)-EC:DEC liquid electrolyte is displayed in Figure 3[8].

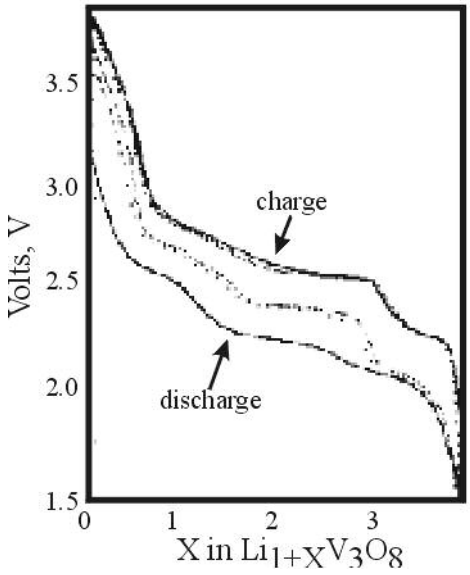


Figure 3: Representation of discharge-charge cycling plot of a Li|$LiPF_6$(1M)-EC:DEC)|$LiV_3O_8$ cell at room temperature and 200 μA/$cm^2$

Between ~2.8 and ~2.3 V on the discharge, incorporation of lithium ions into the vanadium oxide structure and reduction of $V^{5+}$ to $V^{4+}$ occurs more readily than in other regions of the discharge plot. With charging, de-intercalation of lithium from the vanadium oxide and oxidation of the vanadium occurs most readily between ~2.6 to ~2.9 V[8]. These two regions, where the majority of the exchange of lithium ions and electrons occurs, are well below the voltage range where standard liquid electrolyte breakdown occur[9]. The theoretical capacity of $LiV_3O_8$ is 280 mAh/g.

**Li|$PEO_9$Li|$LiV_3O_8$ Cell Testing**

Electrochemical stability of the Li|$PEO_9$LiTf|$LiV_3O_8$ cell was first examined so future comparison to PEI-based electrolyte cells could be made. The electrochemical stability of the $PEO_9$LiTf within a 1.5 to 3.5 volt window has been examined in the literature by cycling a cell in a voltage window with constant voltage ramps while measuring changes in current output in a manner similar to cyclic voltammetric methods[1]. With voltage cycling (Figure 4[1]) from low to high voltage, the cathodic current has an increasing slope until a maximum at ~3.1 V where it becomes negative as the voltage increases. This cathodic current behavior results from the cell being forced by the imposed voltage to extract lithium ion from the $Li_{\sim 4}V_3O_8$ ($\rightarrow LiV_3O_8$) species while plating the lithium electrode with reduced lithium ion. The slope increases from left to right because of voltage plateaus in these regions that result from favorable extraction of lithium ion from the lithium vanadium oxide plate structure (de-intercalation). The negative slope from ~3-3.5 V indicates that most of the lithium ion has been extracted from the vanadium oxide structure and less current can be generated with the same change in voltage. The anodic current (bottom part of plot) results from the electrons produced by the intercalation of lithium ion into the vanadium oxide structure and the oxidation of the lithium metal. The most negative slope of current occurs from 3 to 2.5 V, which corresponds to voltage plateaus (refer to figure 3) where incorporation of lithium ion into the vanadium oxide structure is more favorable than at other voltages. From 2.4 to 1.5 V, the current becomes less negative as the vanadium oxide structure fills up with lithium ions. The inversely symmetrical shape of both the cathodic and anodic currents

versus voltage indicate that the processes resulting in current changes are essentially reversible and little is happening electrochemically to the $PEO_9LiTf$.

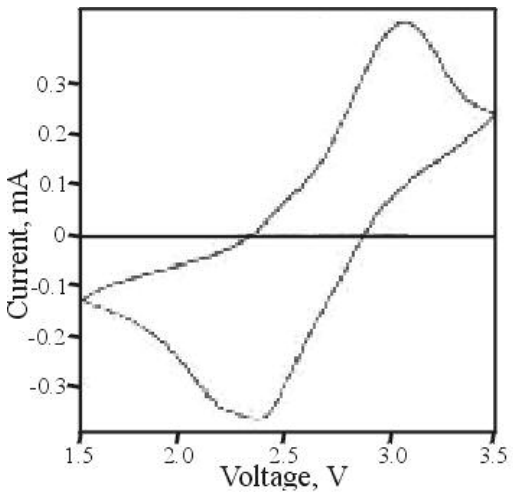


Figure 4: Representation of cyclic voltammogram for $Li|PEO_9LiTf|LiV_3O_8$ cell at a voltage scan rate of $1mV/s$[1]

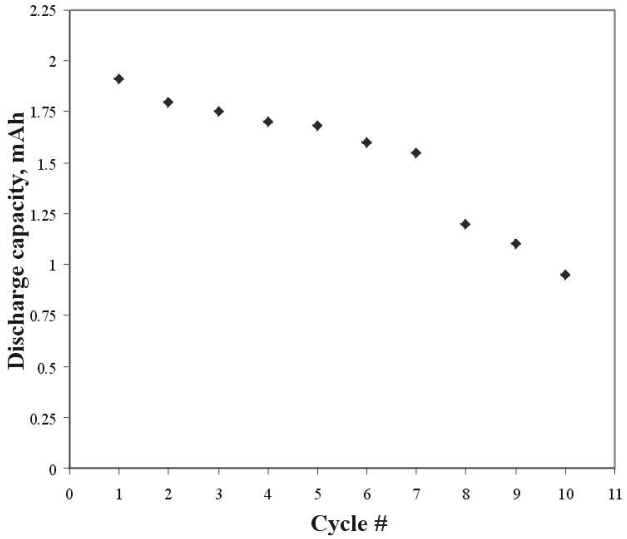


Figure 5: Typical discharge capacities of a cell composed of $Li|PEO_9LiTf|LiV_3O_8$ at 120 °C and current set at 500 $\mu A/cm^2$ (discharge)[1]

Figure 5 shows a reported Li|$PEO_9LiTf$|$LiV_3O_8$ discharge capacity plot versus cycle number at 120 °C[1]. A steady loss in capacity occurs from the initial high discharge capacity.

$PEO_9LiTf$ based cells were prepared using coin cells as described earlier. Through a significant amount of trial and error, the performance of the coin cells was found to be significantly better than in other types of cells such as the tube cell. A typical $PEO_9LiTf$ electrolyte based cell's performance is presented in Figure 6.

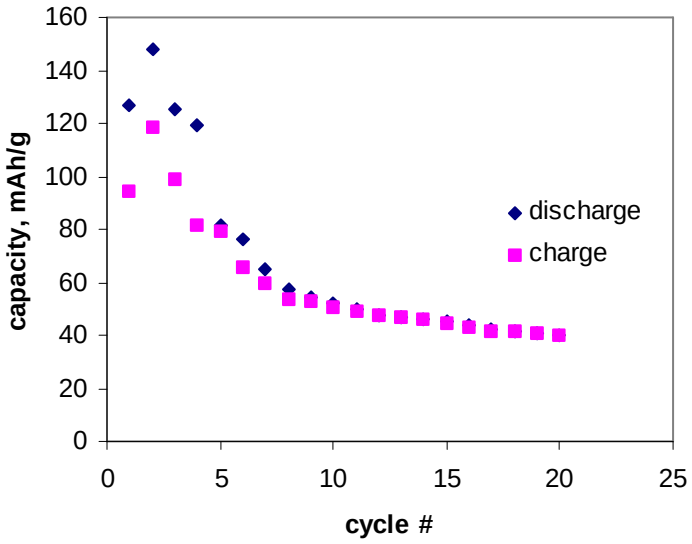


Figure 6: Typical discharge and charge capacities of a cell composed of Li|$PEO_9LiTf$|$LiV_3O_8$ at 100 °C, 7.5 lbs external pressure, current set at ±10 μA/$cm^2$ and a voltage range of 1.9 to 3.1 V

| **Cycle #** | 2 | 4 | 6 | 8 | 10 | 12 | 14 | 16 | 18 | 20 |
|---|---|---|---|---|---|---|---|---|---|---|
| **% fade** | 0 | 20 | 49 | 61 | 65 | 68 | 69 | 71 | 72 | 73 |

Table 1: Percent discharge capacity fade from largest discharge capacity

Initial high discharge and charge capacities are observed in the first few cycles followed by significant capacity fade and then relatively small capacity fade for 20 cycles (Table 1). This performance resembles reported behavior of capacity losses in that there are significant capacity losses initially followed by cycles with less fade. The capacities observed with cells with $PEO_9LiTf$ are slightly lower than reported capacities[1] but are reasonable considering optimization of $PEO_9LiTf$ based cells was not a major priority. The discharge capacity decrease from theoretical (~280 mAh/g) for these cells may be tied to incomplete charging or electrolyte breakdown at the interfaces. When a cell is cycling, oxidation or reduction of the electrolyte can occur at the interfaces resulting from oxidation or reduction of the electrolyte at the interfaces between electrode and electrolyte. This will result in the formation of electrode passivation layers that hinder lithium ion penetration complete charging or discharging[9].

**$Li|PMEI_{20}Li|LiV_3O_8$ Cell Testing**

Our initial interest in making polymer cells, other than making benchmark $PEO_9LiTf$ cells, was to evaluate the performance of cross-linked and non-cross-linked poly(N-methylethylenimine) (PMEI) (Figure 7) lithium salt complexes as the electrolyte

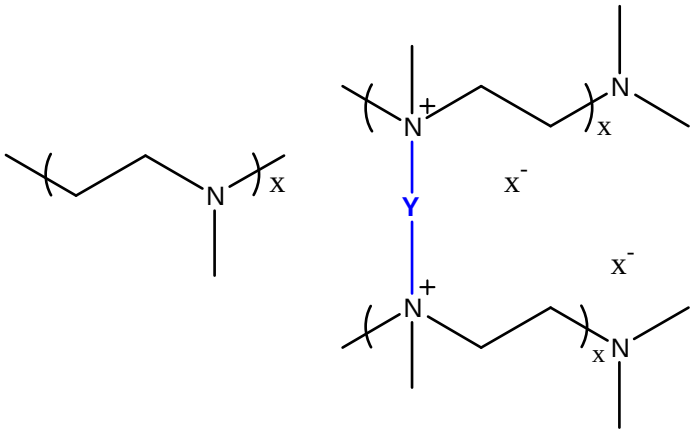


Figure 7: Linear PMEI and PMEI with a cross-link unit

in a cell. PMEI is an attractive alternative for substitution into commercial lithium polymer batteries because of its potential electrochemical stability and ease of cross-linking. The molecular weight of PMEI depends on the molecular weight of its parent polymer, poly(2-ethyl-2-oxazoline). Linear PMEI was prepared from the hydrolysis of high molecular weight poly(2-ethyl-2-oxazoline)(Average $M_w$ ca. 500,000), neutralization of LPEIHCl and Eschweiler-Clarke methylation of LPEI (Figure 8).

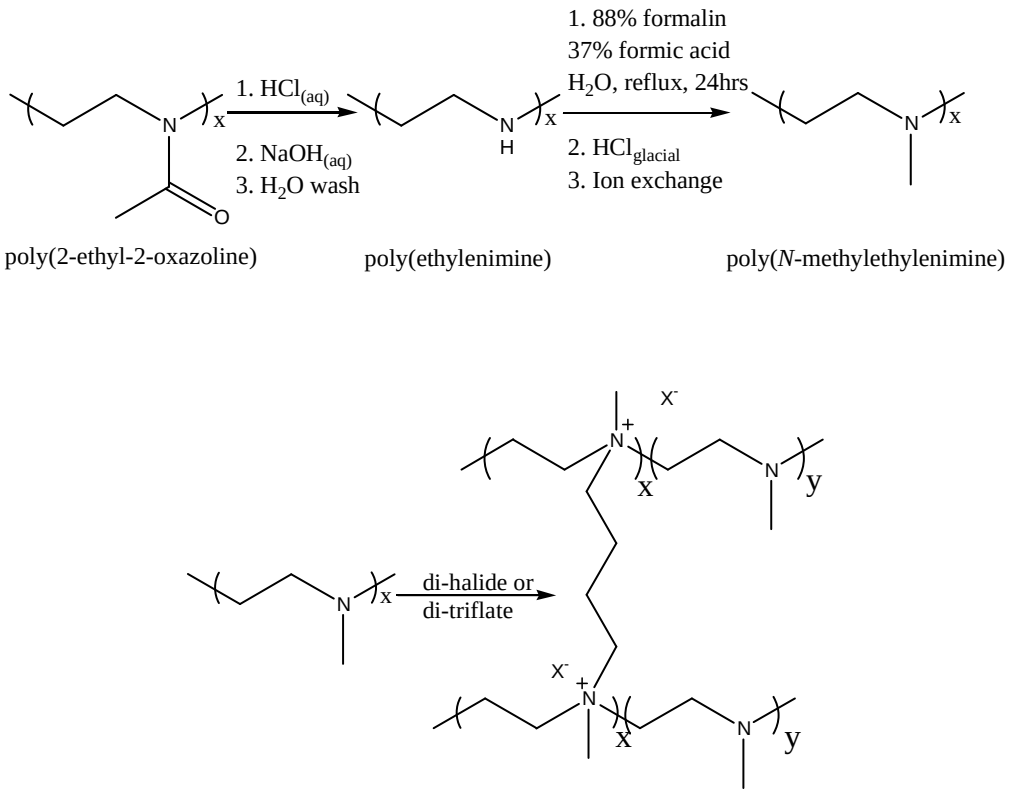


Figure 8: Synthesis of PMEI and cross-linked PMEI

High molecular weight PMEI (280,000 $M_w$) is an amber colored sticky solid that transitions into a viscous liquid just above room temperature. A liquid polymer is little better than a liquid electrolyte from a leakage prevention standpoint, so PMEI is cross-linked with a di-substituted cross-linker such as a di-triflate or a di-halide to give a material that did not melt in the room temperature to 100 °C temperature region. Li salt was incorporated during the cross-linking step to give a polymer electrolyte.

At room temperature, the ionic conductivity of cross-linked PMEI (20N:1cross-linker, 20N:1Li) was $10^{-8}$ to $10^{-9}$ S/cm, much lower than what is required to compete with other known systems. At 70 °C (70-80 °C is the max. temperature able to obtained due to

measurement setup), the ionic conductivity was $10^{-6}$ S/cm. So this provided promise that, at 100 °C, $PEO_9LiTf$ cells cycling temperature, cross-linked PMEI would like $PEO_9LiTf$. Initially, all of the cells failed because of unknown reasons that could include low ionic conductivity, electrochemical instability at elevated temperatures or design problems. So, focus was applied to the non-cross-linked PMEI electrolyte cycling performance to help understand the fundamental stability and suitability of this system.

High molecular weight linear PMEI with lithium bis-trifluorosulfonimide (LiTfsi) was chosen as the model system because high molecular weight polymer is dimensionally more similar to the cross-linked system, and LiTfsi has been shown to be more electrochemically stable than LiTf. The ionic conductivity of $PMEI_{20}LiTfsi$ is $10^{-7}$ S/cm at room temperature and $10^{-5}$ S/cm at 70 °C. To use the non-cross-linked PMEI electrolyte in a cell, a non-interactive porous polyethylene/polypropylene electrode

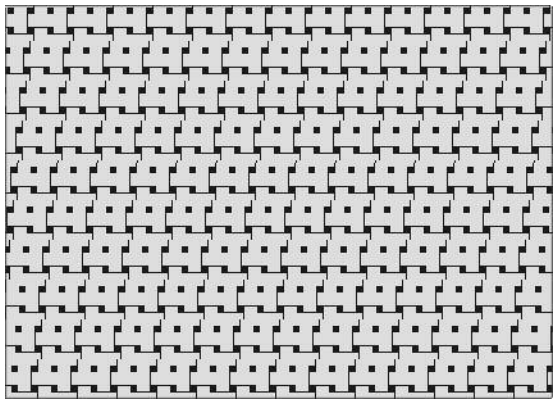

Figure 9: Representative Celgard structure; pores (black): ~0.09 × 0.04 μm

separator[10] (Celgard 3501, Figure 9[10]) saturated with $PMEI_{20}LiTfsi$ was used to prevent shorts and was incorporated in the cell in a similar manner as $PEO_9LiTf$. The

conductivity of the $PMEI_{20}LiTfsi$ saturated separator was $10^{-7}$ S/cm at room temperature and $10^{-6}$ S/cm at 80 °C. Cells were cycled at 100 °C with currents set at 10 µA.

a.

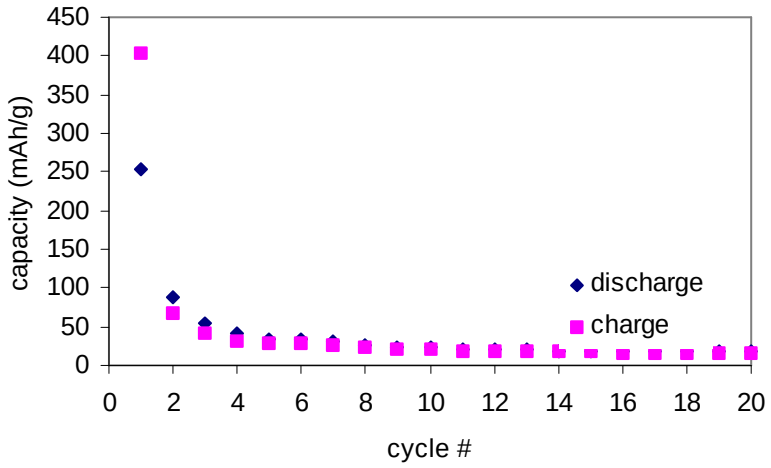


b.

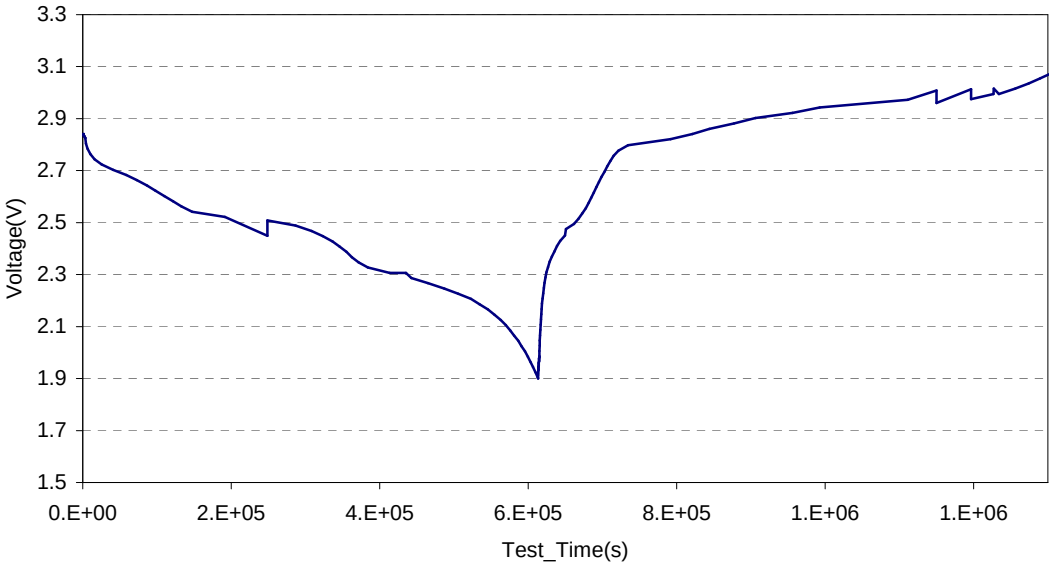


Figure 10: a. Performance of a $Li|PMEI_{20}LiTfsi|LiV_3O_8$ cell at 100 °C, pressure of 7.5 lbs, current set at ±10 µA and voltage window from1.9 to 3.1 V; b. A typical discharge-charge voltage plot versus time for a $Li|PMEI_{20}LiTfsi|LiV_3O_8$ cell

Excellent near-theoretical discharge capacities were obtained with the Li|$PMEI_{20}$LiTfsi|$LiV_3O_8$ cells, but a significant drop in capacity after the first cycle was observed in the numerous cells tested (Figure 10a). Changes in cell pressure, salt composition, and operating temperature had little affect on the capacity fade behavior. Cell pressure was optimal at 7.5 lbs, no effect was observed when ranging the salt composition between 10 to 40 N:1Li and cell capacities were decreased when operated at below 100 °C. Capacity fade is commonly reported for conventional polymer electrolyte based cells[1-4]. But, the amount of capacity fade observed for Li|$PMEI_{20}$LiTfsi|$LiV_3O_8$ is quite significant. Figure 10b shows a typical plot of voltage versus time for the first cycle for the Li|$PMEI_{20}$LiTfsi|$LiV_3O_8$ cell. In the discharge step, the discharge voltage plateau, where most of the current is generated, falls between 2.3 and 2.7 V, while, in the charge step, this plateau occurs between 2.75 and 3.0 V. This, along with high capacity fade, sets the Li|$PMEI_{20}$LiTfsi|$LiV_3O_8$ cell apart from the liquid cell data (Figure 3). A couple of possibilities exist for the observed fade and the asymmetry in the voltage plots and includes: solid-electrolyte interface (SEI) formation from potential electrolyte oxidation (or reduction) and breakdown of the physical properties of the cell components.

SEI formation occurs when a molecule at the surface of an electrode undergoes reduction(s) or oxidation(s) to form an electronically altered species that then becomes affixed to the electrode surface through ionic or covalent bonds. This is a problem because it can interfere with the passage of lithium ions in and out of the electrode if it becomes too thick[9]. In some cases, electrolyte breakdown on the electrode surface provides a stabilizing electrode cap that allows ion movement but prevents further

electrolyte breakdown[9]. To examine the possibility of SEI formation in the PMEI –based electrolyte cell, different tests were performed.

Cells were first taken apart and the electrodes were visually examined to note if any significant discoloration or obvious film formation occurred. The first thing observed was that the electrolyte turns a dark brown color and coats everything. Nothing can be learned from visual inspection of the $LiV_3O_8$ paste as it is normally a dark brown color, also. The lithium sheet was spotted with dark areas but contained no white areas indicative of LiOH formation and water contamination. The dark areas could be broken down polymer or just a layer of polymer that become affixed to the lithium as a result of pressure and heat and wouldn't affect cycling behavior. Two cycling experiments were then begun that involved assembling cells with new and old electrodes. For instance, one cell was assembled with new lithium and the $LiV_3O_8$ paste, electrolyte and separator from a cycled cell. Another cell was assembled with cycled lithium and a new $LiV_3O_8$ paste, electrolyte and separator. With the cell with new lithium and the old $LiV_3O_8$ paste, the experiment was begun on the charge step because the old $LiV_3O_8$ paste ended on a discharge step. The charge behavior observed was typical with a 2.7-3.0 V plateau. The cell with the old lithium and new $LiV_3O_8$ paste, electrolyte and separator was started on the discharge cycle but exhibited the same high voltage behavior on the charge step. Both experiments delivered typical significant capacity losses on the second discharge and indicated that something happened on either or both the discharge step (while delivering normal voltage plateaus) and the charge step where the high voltage plateau was observed. Considering the high voltage plateau also occurred with the cell starting discharged and containing the fresh lithium and cycled cathode, this suggests SEI

formation on the cathode causes abnormal lithium ion de-intercalation because of a possible higher required imposed reverse (charge) voltage to move the lithium ions through the SEI layer into the electrolyte.

In another experiment, a constant voltage ramp (± 0.1 V/hr) was applied to Li|PMEI$_{20}$LiTfsi|LiV$_3$O$_8$ cells to force repetitive cycling from 1.9 - 3.1 – 1.9 V while current output was monitored, similar to a cyclic voltammetry experiment. This experiment was done with the usual type of cell, high molecular weight PMEI, 20N:LiTfsi, 7.5 lbs pressure and 100 °C, and is shown in Figure 11.

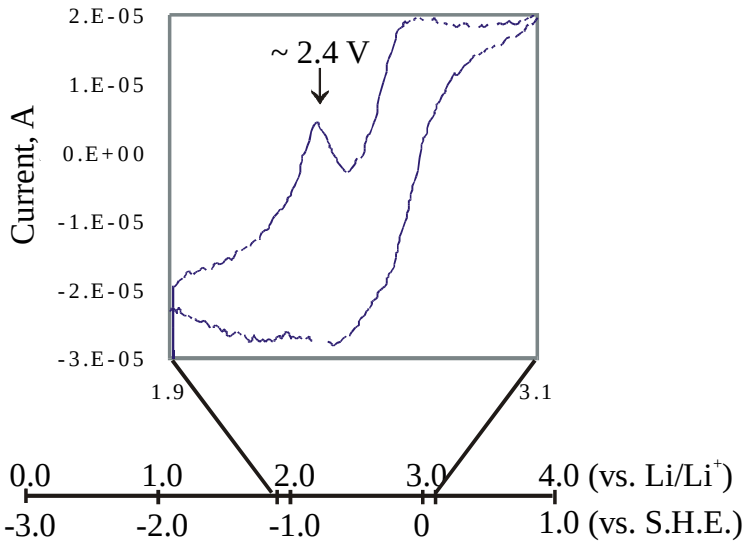


Figure 11: Cell cycled at a constant voltage ramp of ± 0.1 V/hr with voltage cutoffs of 1.9 and 3.1 V for a Li|PMEI$_{20}$LiTfsi|LiV$_3$O$_8$ cell at 100 °C and 7.5lbs pressure

On the cathodic scan, from 1.9 to 3.1 V, the slope of the current increases significantly at ~2.3 V and then becomes negative to ~2.5 V and then changes to positive and plateaus at 2.7 V. On the anodic scan, the general shape is the same, but there is no obvious current

inflection (or peak) as is observed on the cathodic scan. Upon cycling, this peak becomes smaller.

The source of this peak is not known. Speculatively, this anomalous peak may be the result of an irreversible oxidation of the tertiary amine, which has been shown in the chemical literature to occur at ~4 V (vs. $Li/Li^+$) (0.8 - 1.0 V vs. S.H.E. (reported)) for N,N,N',N'-tetramethylethylenediamine ($(CH_3)_2NCH_2CH_2N(CH_3)_2$) and in the same voltage region for other small molecule tertiary amines.[10] 4 V is outside the voltage range which the cell is cycled, so if this peak is related to an oxidation of the amine, then conditions in the cell must be sufficiently severe to alter this oxidation potential (Figure 11). Electrochemical oxidation of a pentamethyldiethylenetriamine additive in 1M $LiPF_6$/PC solutions has been demonstrated to lower the oxidation potential to approximately 3.5 V (vs. $Li/Li^+$) at room temperature[11].

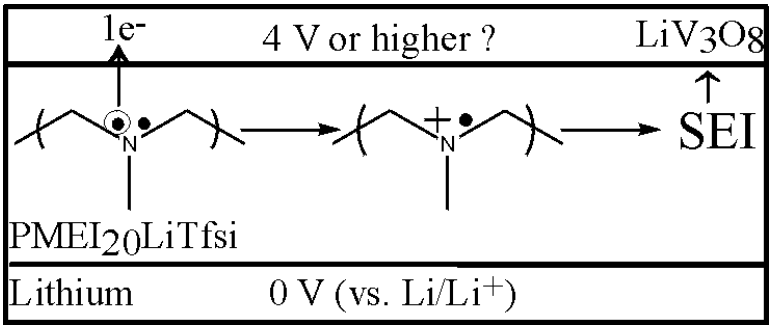


Figure 12: Potential electrode interface oxidation reaction for a cell with ~4 V window or higher

The results of this possible oxidative process could be initial formation of an amine radical cation followed by polymer breakdown by elimination, coupling or reaction with

other electrolyte components. The NMR and IR of the electrolyte taken from the electrolyte not on the electrode surface after cell cycling and disassembly showed little change from the original spectra, while isolation of the electrolyte adhered to the electrodes was difficult and was not useful.

The Celgard porous polyethylene/polypropylene separator used to prevent shorts in the non-cross-linked $PMEI_{20}$LiTfsi cells was examined to determine whether it might be degrading at 100 °C. After examining the manufacturer's web page, the Celgard separator was listed as having a melting temperature of 135 °C[10], which, at the time, did not seem significantly close to 100 °C. Much later, an article describing better the thermal characteristics of the separators was found using impedance and differential scanning calorimetry measurements[12], and separator integrity became a greater concern. As seen in Figure 13, both the sharp increase in resistance and beginnings of the endotherms start below the quoted 135 °C at the temperature scan rates of 60 °C/min and 5 °C/min[13]. At slower scan rates, it is likely that these tails begin sooner and make more of a contribution to the resistance and melt. So at a constant 100 °C, it seems quite possible that the separator may be going through some initial transition toward a melt. To address this, a non-saturated separator was placed in an oven at 100 °C for one week to see what happened. After one week, the normally tough, stretchable plastic crumbled into shreds when handled. The saturated Celgard after removal from a battery cycled at 100 °C kept its integrity but its degree of melt or breakdown at elevated temperature could not be commented on, as an SEM is needed to examine its structure.

a.

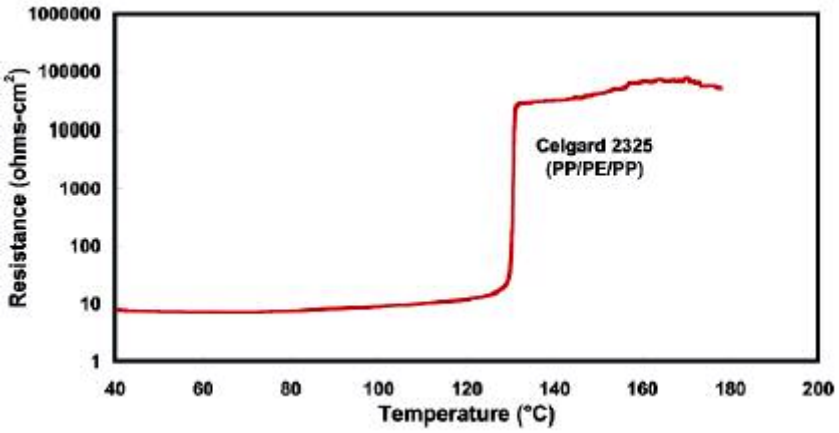


b.

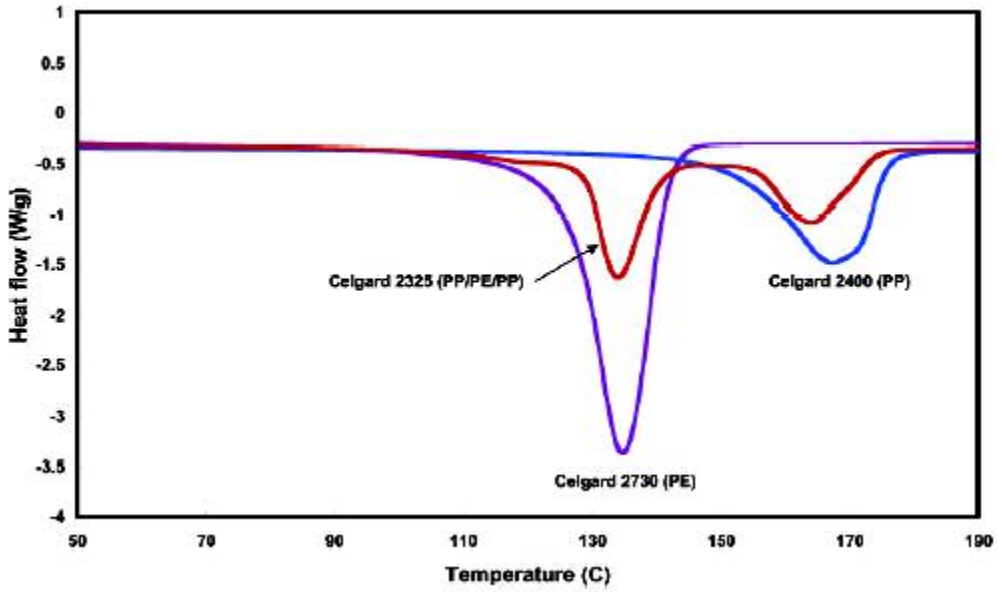


Figure 13: a. AC resistance measurements on a liquid electrolyte saturated Celgard separator at heating rate of 60 °C/min; b. Thermogram of 3 different types of Celgard at heating rate of 5 °C/min[13]

The ionic conductivity of the polymer electrolyte saturated Celgard was taken before and after cell cycling. Before cycling at 70 °C, the conductivity was $10^{-6}$ S/cm and after cycling the conductivity was $10^{-7}$ S/cm indicating an order of magnitude decrease after cycling. The significance is not known but lowered electrolyte conductivity never improves a cell. Other types of separators have been tried but have not resulted in cell performance improvement.

With additional cell assembly experience, cells were then prepared and cycled by incorporating cross-linked high molecular weight PMEI with LiTfsi. The cross-linked electrolyte for this material did not necessitate the Celgard plastic separator because of its suitable dimensional integrity, even at elevated temperatures of 100 °C. Room temperature ionic conductivity of the cross-linked material was ~$10^{-8}$ – $10^{-9}$ S/cm, while, at elevated temperatures (70 °C- again, conductivity could not be measured above this temperature due to instrument setup), it was ~$10^{7}$ S/cm. Figure 14 shows a typical cycling profile for a cell tested at 100 °C, current set at ±10 μA and no external pressure. A relatively large discharge capacity is first observed followed by cycles with smaller capacity.

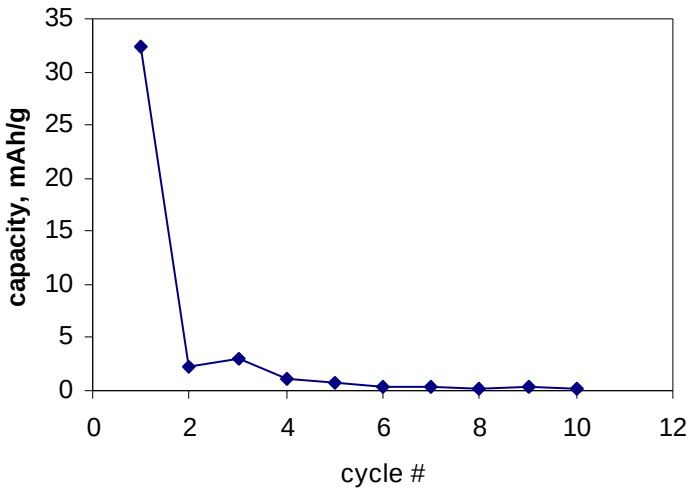


Figure 14: Cycling discharge capacities of Li|PMEI$_{20}$LiTfsi, 20N:1 dibromohexane|$LiV_3O_8$ cell with no Celgard at 100 °C, no external pressure and current set ±10 μA

The cross-linked PMEI displayed the similar type of shape as non-cross-linked PMEI when a constant voltage ramp was forced on the cell and the current was measured.

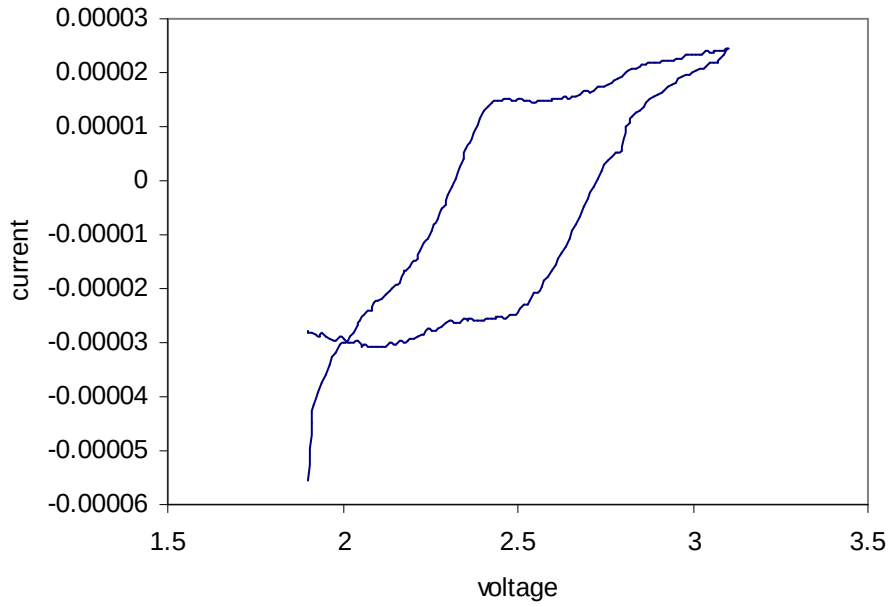


Figure 15: Cell cycled at a constant voltage ramp of 0.1 V/hr with voltage cutoffs of 1.9 and 3.1 V for a Li|$PMEI_{20}$LiTfsi, 20N:1 dibromohexane|$LiV_3O_8$ cell at 100 °C, no external pressure and current set at ±10 μA

Efforts to improve the cycling performance of the cross-linked PMEI are being made using addition of small molecule plasticizers such as cyclic carbonates to form less-debilitating passivation layers[9].

**Li|$PCEEI_{20}$Li|$LiV_3O_8$ Cell Testing**

Linear poly((N-2-cyanoethyl)ethylenimine) (PCEEI) from chapter 2 with lithium salt was also incorporated, as the electrolyte, into cells with lithium and $LiV_3O_8$ electrodes. The $PCEEI_{20}$LiTfsi electrolyte was similar in qualitative viscosity as the $PMEI_{20}$LiTfsi, so again a Celgard separator was needed. Much the same type of cycling behavior was observed for PCEEI cells as in PMEI cells in that a large discharge capacity

was observed followed by significantly smaller succeeding capacities. $PCEEI_{20}LiTfsi$ cells never attained the high first capacities as the PMEI cells, even with greater than 10 attempts at making and cycling these cells. The maximum discharge capacity observed in these cells was ~85 mAh/g $LiV_3O_8$. A typical capacity performance profile is shown in Figure 16.

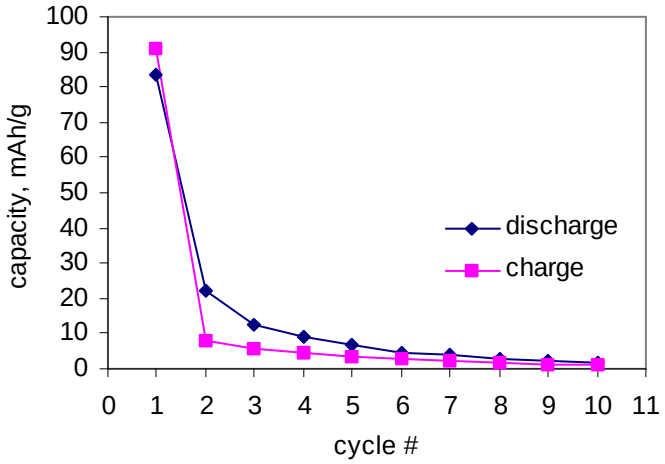


Figure 16: Cycling discharge and charge capacities of Li|PCEEI:LiTfsi|$LiV_3O_8$ cell at 100 °C, 7.5 lbs external pressure and current set at ±10 μA

The current behavior in response to constant voltage ramps is displayed in Figure 17.

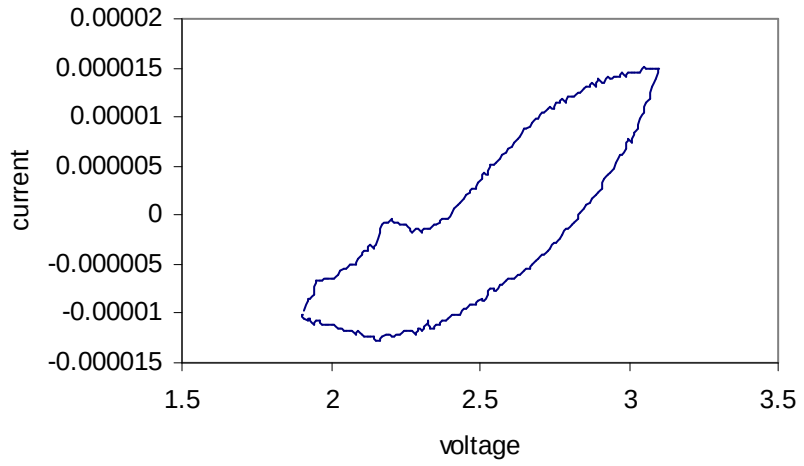


Figure 17: Cell cycled at a constant voltage ramp of 0.1 V/hr with voltage cutoffs of 1.9 and 3.1 V for a Li|PCEEI:LiTfsi|$LiV_3O_8$ cell at 100 °C, 7.5 lbs external pressure and current set at ±10 μA

A peak maximum is observed at 2.2 V and is similar to previous data in other poly(ethylenimine) based systems.

Partially substituted branched PCEEI was then cross-linked using acrolein as the cross-linker in a synthesis (Figure 18) that did not generate any charged species, unlike with the PMEI cross-linking method. This amine substitution resulted in an essentially complete conversion to tertiary amines. The films produced, after drying, are dimensionally stable above 100 °C, so they were used without the Celgard separator.

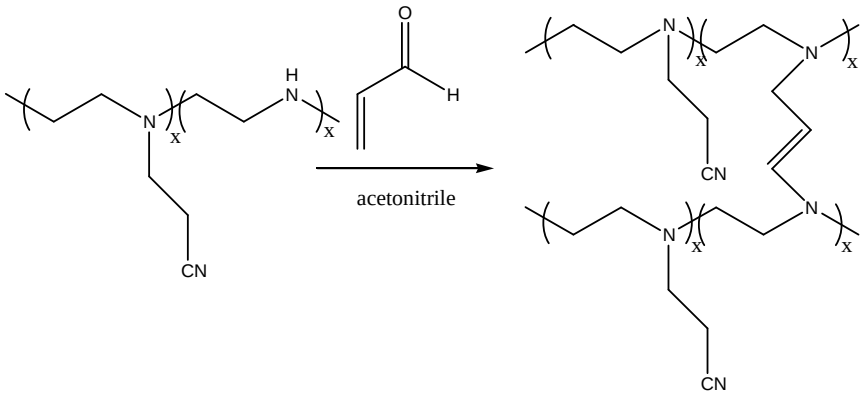


Figure 18: Synthesis of 'neutral' cross-linked poly(2-cyano-2-ethylenimine)

Figure 19 shows the discharge and charge capacities of cells with cross-linked poly(2-cyano-2-ethylenimine) infused with LiTfsi as the electrolyte and lithium and $LiV_3O_8$ as the electrodes.

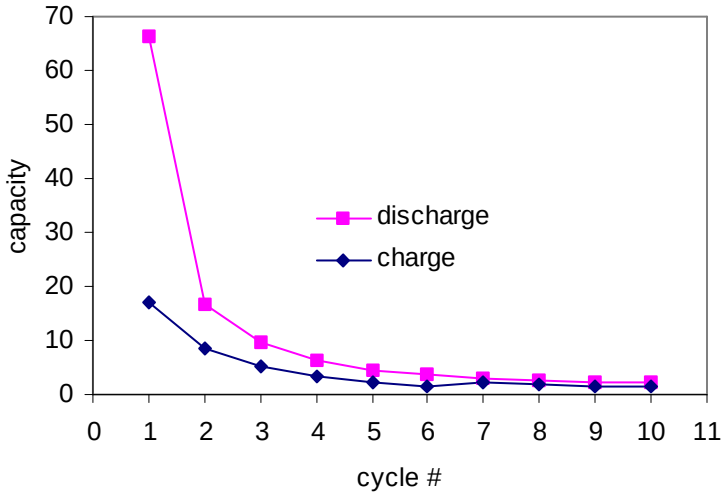


Figure 19: Cycling discharge and charge capacities of Li|cross-linked $PCEEI_{20}$LiTfsi|$LiV_3O_8$ cell at 100 °C, 7.5 lbs external pressure and current set at + and -10 μA

The discharge capacities for a typical cross-linked PCEEI electrolyte based cell are significantly larger than those for the cross-linked PMEI (figure 20) and may be attributed to the lack of charged sites in the electrolyte or improved polymer physical properties.

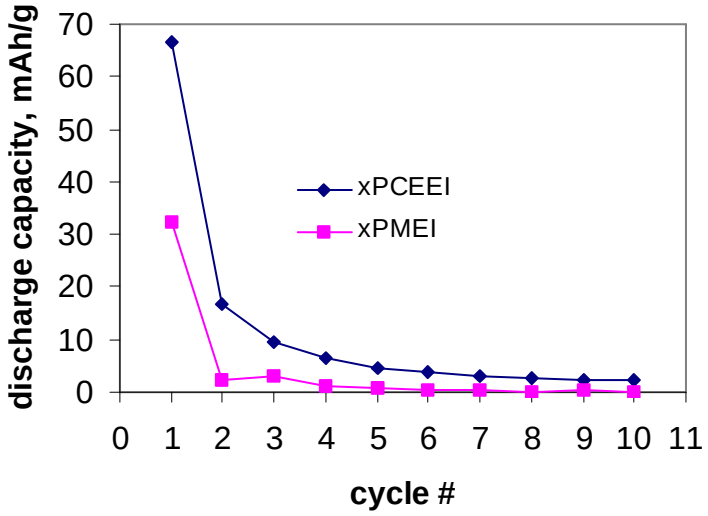


Figure 20: Comparison of the cross-linked PMEI and PCEEI's performance in cells at 100 °C, no external pressure and current set at ±10 μA

**Li|xPEI$_5$Li + diglyme|LiV$_3$O$_8$ Cell Testing**

Cells composed of the low molecular weight PEI cross-linked with tetraethylene glycol diacrylate (TEG) and infused with a diglyme placticizer and LiTf salt, from Chapter 3, were prepared with lithium metal and $LiV_3O_8$ electrodes. The molar ratios for the components of this gel were as follows: 5 moles N:1 mole TEG:4 moles diglyme: 1mole Li. This gel electrolyte was sufficiently conductive that the cells tested were run at room temperature ($10^{-4}$ S/cm at RT). Unfortunately, the same pattern of cycling behavior was observed for this system as in other PEI based systems exhibited by a large first

discharge capacity and then succeeding much lower discharge capacities. Figure 21 shows a representative plot of the discharge capacities.

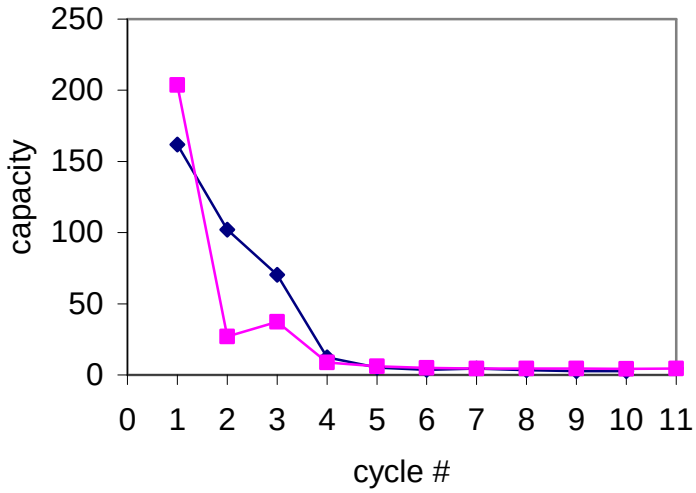


Figure 21: Cycling discharge capacities of Li|PEI+TEG+Diglyme+LiTf, 5N:TEG, 5N:1Li|$LiV_3O_8$ cell at room temperature, no external pressure and current set at + and – 10 μA

**Conclusion**

Excellent first discharges capacities are observed for the non-cross-linked polymer electrolytes (PMEI, PCEEI) and good first discharges were observed for the cross-linked polymer electrolytes (xPMEI, xPCEEI and PEI/TEG/Diglyme). Subsequent discharges in all PEI-based electrolytes are characterized by significant increases in fade from the first discharge. Similar capacity losses are observed for homemade and literature cells with $PEO_9LiTf$. Cross-linking decreases the ionic conductivity but allows elimination of the use of the Celgard separator. Cross-linked PEI-based polymers/salts were incorporated into functioning cells. The fade behavior in cells with the cross-linked

polymers is similar to that with the non-cross-linked polymers, albeit with significantly lower capacities with the PMEI system.

Sources of this fade behavior may be tied to two problem areas: Celgard breakdown/porosity loss and polymer electrolyte breakdown at the cathode interface. The conductivity of the polymer electrolyte saturated Celgard before cycling is not likely the issue because of the observed high capacity first discharges and the reasonably acceptable measured ionic conductivities at elevated temperatures. The observed breakdown of the physical properties of the non-saturated Celgard separator at 100 °C lends credence to a capacity fade mechanism where the separator gradually melts, increases significantly in ionic conductivity resulting in a process of cell charging and discharging becoming more like a process involving electrolyte polarization at the interfaces. This theory is validated to an extent by measurements of the ionic conductivity of the polymer electrolyte separator before cycling and then after cycling where the ionic conductivity of the separator decreases by about an order of magnitude for each over a 22 to 70 °C temperature range. The separator breakdown may also lead to small internal shorts that will result in lowered capacities as they develop. Removal of the separator with polymer cross-linking to examine the fade issue raises other considerations such as a significant decrease in polymer electrolyte conductivity, possible internal shorts and the remaining electrochemical breakdown of the electrolyte issue.

Polymer electrolyte breakdown and SEI formation at the electrodes is a possible issue given the pseudo cyclic voltammetry data for a variety of the PEI based polymer electrolytes. The presence of what appears to be an irreversible oxidative peak at ~2.3-2.4 V seems to be a common characteristic in all of the PEI voltage/current plots. An

oxidative process is possibly occurring and could lead to a variety of products at the cathode. This possible polymer breakdown and SEI formation may hinder the passage of lithium ions in and out of the cathode and would only increase in thickness with cycling leading to lower succeeding capacities. Once the fade issue is worked out, PEI-based electrolytes should be able to generate consistently high discharge capacities given the strong first discharge capacities.

**References**


1. Bonino, F. Selvaggi, A. Scrosati, B. *Solid State Ionics* **1988**, 28-30, 853.
2. Croce, F. Panero, P. Prosperi, P. Scrosati, B. *Solid State Ionics* **1988**, 28-30, 895.
3. Hammou, A. Hammouche, A. *Electrochim. Acta* **1988**, 33, 1719.
4. Bonino, F. Ottaviani, M. Scrosati, B. Pistoia, G. *J. Electrochem. Soc.* **1988**, 135, 12.
5. Murata, K. Izuchi, S. Yoshihisa, Y. *Electrochim. Acta* **2000**, 45, 1501.
6. Munshi, M.Z.A. Owens, B. B. *Solid State Ionics* **1988**, 27, 251.
7. Panera, S. Pasquali, M. Pistoia, G. *J. Electrochem. Soc.* **1983**, 1226.
8. West, K. Zachau-Christiansen, B. Skaarup, S. Saidi, Y. Barker, J. Olsen, I.I. Pyneburg, R. Koksbang, R. *J. Electrochem. Soc.* **1996**, 143, 820.
9. van Schalkwijk, W. A. Scrosati, B. 'Advances in Lithium-Ion Batteries' Kluwer Acedemic/Phenum Publishers: New York, 2002; pg. 7.
10. www.Celgard.com.
11. Nelsen, S. F. Hintz, P. J. *J. Am. Chem. Soc.* **1972**, 7114.
12. Foster, D. L. Wolfenstine, J. Behl, W. K. *Proc.- Electrochem. Soc.* **1999**, 98-16, 391.
13. Arora, P. Jiang, Z. *Chem. Rev.* **2004**, 104, 4419.

# Chapter 5: POLYMER ELECTROLYTES BASED ON CROSS-LINKED POLY(ETHYLENIMINE) HYDROCHLORIDE/PHOSPHORIC ACID SYSTEMS

Portions of data presented in *Solid State Ionics*, submitted.

Current state of the art proton conducting materials such as Nafion and polybenzimidazole (PBI) based membranes contain drawbacks associated with cost, preparation and performance.[1] PEI is a polymer that can be cross-linked and doped with acids to make membranes that have the potential to make improvements in these areas. The cost of producing phosphoric acid doped cross-linked PEI (xPEI:$H_3PO_4$) membranes can be as little as \$1/g[2], while Nafion costs about \$17/g[3]. Both Nafion and PBI require elaborate preparation procedures, while xPEI:$H_3PO_4$ membranes can be prepared in a very simple manner. PEI-based polymer systems also contain a higher density of proton coordination sites than both Nafion and PBI, i.e. the amine functionality, which also serve as sites for material strengthening cross-links and conductivity enhancing side chains.

Acids, such as hydrochloric, sulfuric and phosphoric, complex with PEI to form homogeneous material and, depending on composition, can saturate the polymer matrix with protons and improve the proton conductivity. Phosphoric acid was chosen as the acid in this work because of its low volatility and ability to remain hydrated up to 150 °C in the absence of water stabilizing polymers.[4] Limited work by others has been done with non-cross-linked PEI:acid membranes[5-8] and only one paper has been reported describing xPEI:$H_3PO_4$ membranes with a non-homogeneous morphology[9] (larger background is reported in introduction).

Non-cross-linked PEI:acid systems lose dimensional stability with heat and water as a result of melting and dissolution, respectively. With the addition of sufficiently robust polymer cross-links, the polymer does not melt and is not water-soluble. For suitability in PEMFCs, the cross-link unit must be pH stable, redox stable in the 0 to 1.23 V (N.H.E.) PEMFC operating window, physically stable to heat and ion currents, not exclude phosphoric acid from the polymer matrix upon cross-linking and, for ease of preparation, be prepared from aqueous solution.

**xPEI:$H_3PO_4$ Membrane Preparation**

A method was developed to generate covalent cross-linked PEI:$H_3PO_4$ and involved dissolution of linear PEI-HCl, from hydrolyzed poly(2-ethyl-2-oxazoline), and aqueous phosphoric acid followed by the addition of cross-linker, 1,1,3,3-tetramethoxypropane. Given the correct range of formulation, this procedure generates gel-like material that, when dehydrated, results in dimensionally stable membranes. The $pK_a$ of PEI-HCl is ~3, and approximately 100% of the repeat units are protonated as determined through gravimetric methods, making it an acidic polymer. Reaction of amines with 1,1,3,3-tetramethoxypropane under acidic conditions is believed to involve initial removal of the acetal functionality of 1,1,3,3-tetramethoxypropane (de-protection) to form di-aldehyde followed by iminium formation on both sides of the cross-linker upon reaction with the PEI amines and then rearrangement to form the β-aminoethenyliminium salt ([RR'NCH=CHCH=NRR']$^+$) (Figure 1).[10] This iminium salt has shown high electrochemical stability due to resonance stabilization[11] and, from our experiments, acid stability. Solutions with a variety of phosphoric acid

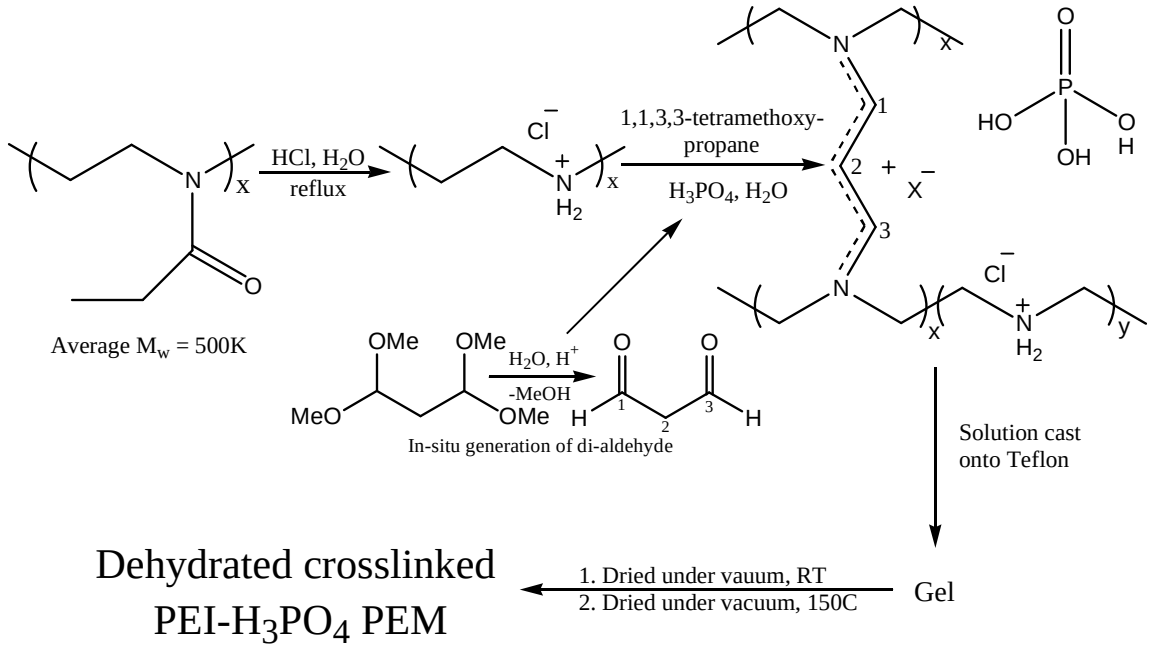


Figure 1: Cross-linked PEI:$H_3PO_4$ synthesis and membrane preparation

compositions in the range of $0 \leq x \leq 7$ moles P per polymer repeat unit (one nitrogen per repeat unit) and theoretical cross-link densities of $2.1 \leq y \leq 8$ moles of N per mole of cross-linker have been prepared and result in stable, freestanding membrane formation. The stiffness of the membranes increases with increasing amounts of cross-linker and decreases with increasing phosphoric acid and water content.

### $^1$H NMR Monitoring of Gel Formation

$^1$H NMR spectroscopy was used to monitor gel formation in a sample with 2.1N:1cross-linker and 0.7P:1N. In place of $H_2O$, $D_2O$ was used as the solvent. This allowed locking to deuterium and improved spectral quality. The concentration of components was identical to that listed in the experimental section. Figure 2 shows a

stack plot of $^{1}H$ NMR spectra from 0 to 10 ppm at different times during gel formation. Before the addition of the 1,1,3,3-tetramethoxy-propane, a spectrum of LPEI-HCl and $H_3PO_4$ dissolved in $D_2O$ was taken. Only the backbone methylene protons were observed. The peak at approximately 4.8 ppm is from the protons in water. Addition of the cross-

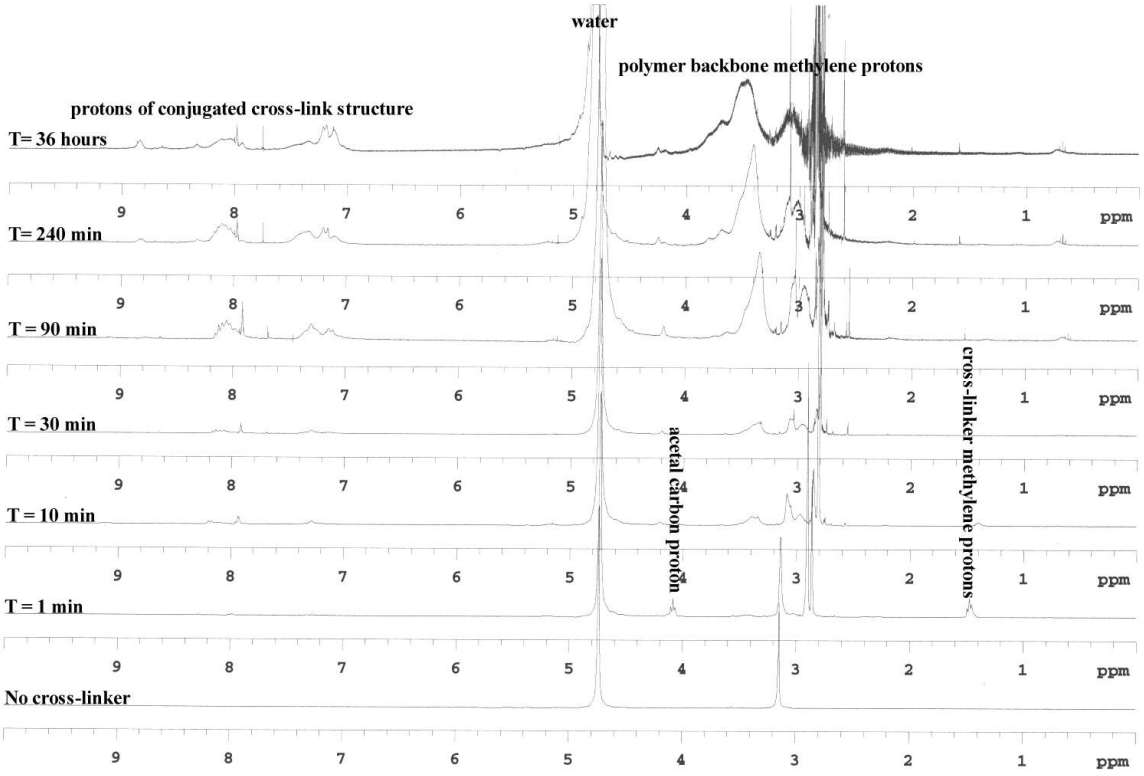


Figure 2: Stack plot of $^{1}H$ NMR spectra at indicated times during gel preparation

linker at T = 1 min resulted in peaks appearing at 1.4 and 4.1 ppm. These peaks are from the cross-linker methylene protons and the cross-linker backbone acetal protons, respectively. Within ten minutes, these peaks disappear and peaks between 2.6 and 3.4 ppm appear. These peaks are likely to be mainly from the methylene protons in the backbone of the modified PEI. Also, peaks above 7 ppm are present indicating the

presence of protons associated with unsaturated groups.[10] These groups are likely to be mainly from the proposed conjugated cross-link structure. At longer times, the peaks above 7 ppm become larger relative to the backbone peaks below 4 ppm indicating an increase in formation unsaturated groups. This implies cross-linking continues after addition of the cross-linker for 30 minutes or more.

**Thermal Properties**

To remove excess water, HCl and any residual organics, membranes were heated at 150 °C under reduced pressure. During the first 16 hours, weight loss is relatively fast, after which, weight loss is slow (0.004 to 0.07 %/hour) (Figure 3). The relative weight

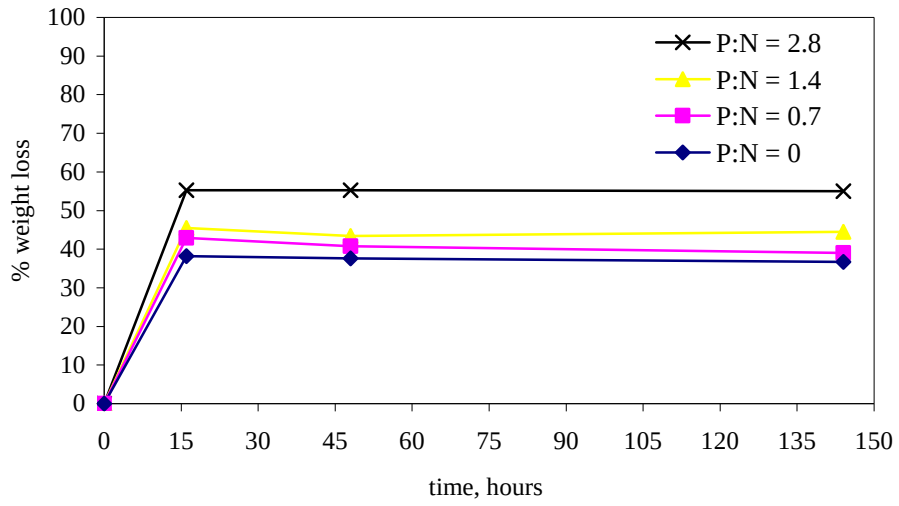


Figure 3: Percent weight loss versus time for xPEI:$H_3PO_4$ samples from P:N = 0 to 2.8 at 150 °C under vacuum over 144 hours

loss of samples with a higher P:N is less than samples with lower P:N. All samples undergo a change of color from amber to darker brown after this heat treatment. Samples

characterized by ionic conductivity, infrared spectroscopy and thermogravimetric analysis (TGA) were dried for ~16 hours at 150 °C under vacuum beforehand. TGA measurements were performed on the membrane materials. Thermograms show that at a scan rate of 5 °C/min under a nitrogen atmosphere residual water loss occurs from room temperature to ~290 °C, followed by significant weight loss associated with polymer degradation and water resulting from the formation of poly(phosphates) $(\text{-OP(O}_3\text{) -})_x$.

**Infrared Spectroscopy**

The structure of the dried polymer matrix was examined with IR. Figure 4 shows a stack plot of LPEI, LPEI:HCl and $\text{xPEI:H}_3\text{PO}_4$ with compositions from P:N = 0 to 2.77.

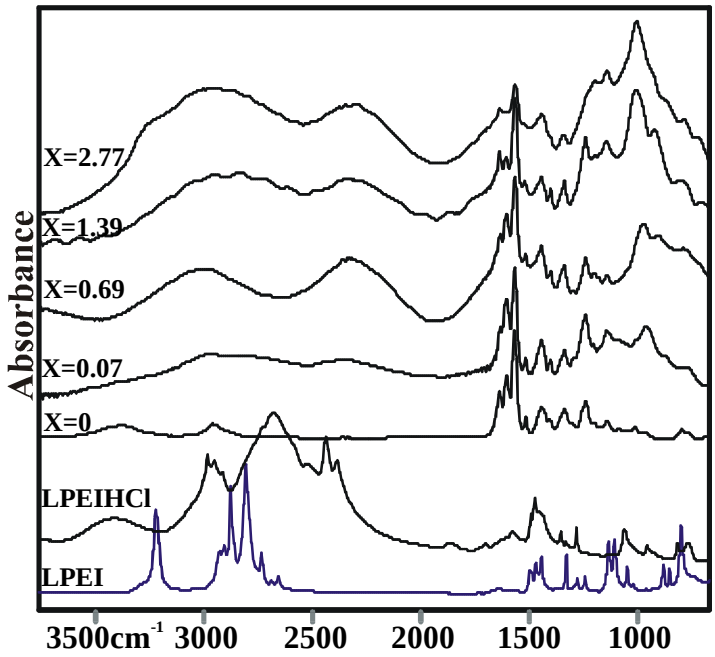


Figure 4: Stack plot, from bottom to top, LPEI, LPEIHCl and xPEI:$H_3PO_4$ samples at 2.1N:1cross-linker at P:N = 0, 0.07, 0.69, 1.39 and 2.77

There are few similarities between the cross-linked sample with no phosphoric acid and the parent polymers LPEI-HCl and LPEI. A diminishing of intensity of peaks related to the N-H stretch and the $NH_2^+$ stretch is observed for the cross-linked material without phosphoric acid indicating that cross-linking and heating of LPEI-HCl results in essential elimination of much of the amine NH and $NH^+Cl^-$. Large bands at 1600 $cm^{-1}$ are related to the unsaturated cross-linker and dominate the cross-linked membranes' spectra. These bands are from a combination of alkene and imine symmetric stretches. Identification of each band has been difficult so model compounds are currently being studied to make positive identifications. With addition of $H_3PO_4$, broad bands from 2000 to 3600 $cm^{-1}$ develop in intensity and area. These are attributed to the $\nu_s$(OH) of $H_3PO_4$ and $H_2O$. Also,

bands from 900 to 1100 $cm^{-1}$ increase in relative intensity and are related to the $\nu_s$(PO) (Figure 5). The multiplicity observed for these

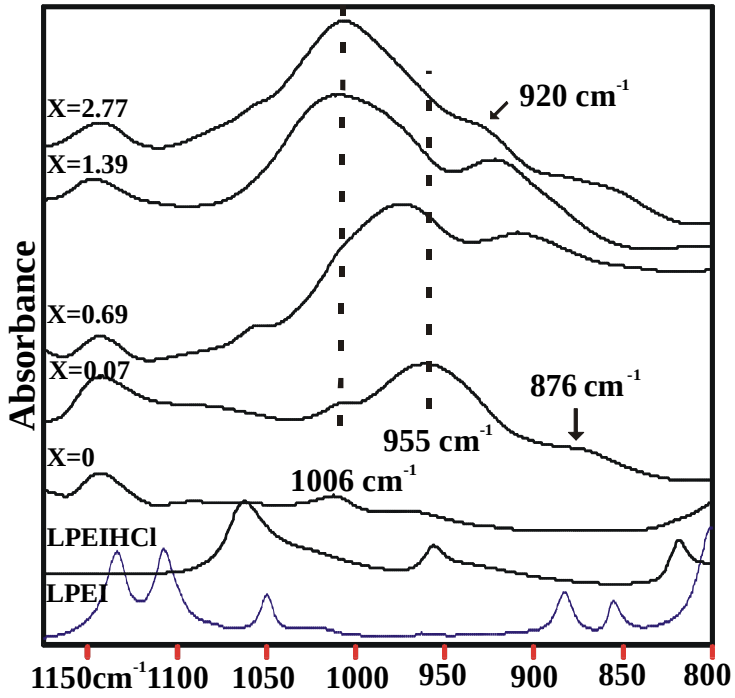


Figure 5: Stack plot, from bottom to top, LPEI, LPEIHCl and xPEI:$H_3PO_4$ samples at 2.1N:1cross-linker at P:N = 0, 0.07, 0.69, 1.39 and 2.77

bands is believed to be associated with different degrees of protonation and self-condensation of $H_3PO_4$. A shift of the $\nu_s$(PO) bands to higher frequency may signify the presence of more protonated phosphates, i.e. $H_3PO_4$,[12] or possibly substituted phosphoric acid.

**$^{31}$P NMR**

Phosphoric acid has been shown to form condensed phosphates at elevated temperatures and in different solvent systems.[13,14] Solid state $^{31}$P NMR was employed to examine the chemical environment of the phosphorous species present in xPEI:$H_3PO_4$. Figure 6 shows a stack of $P^{31}$ spectra from P:N = 0.35 to 4.2 taken with non-

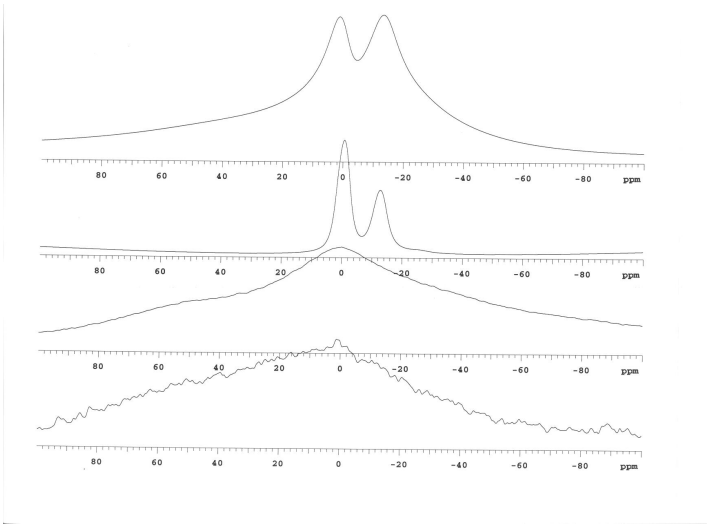


Figure 6: Stack plot of $P^{31}$ NMR spectra for xPEI:$H_3PO_4$ samples from P:N = 0.35 to 4.2 (bottom to top)

spinning samples (intense and numerous spinning side bands posed interpretation problems in spinning samples). At low phosphoric acid compositions, P:N = .35 and 1.4, the only signal seen was a broad mass from ~–150 ppm to ~125 ppm with maxima at 0 ppm. At higher phosphoric acid compositions, P:N = 2.8 to 4.2, spectral resolution increased significantly. Two main peaks were observed at 0 ppm and –13 ppm with a possible small peak at –25 ppm.

While no statement about the state of protonation of phosphoric acid in the xPEI:$H_3PO_4$ membrane samples can be made at high acid composition, the presence of

multiple peaks allows assignment of peaks to the non-substituted, mono-substituted and di-substituted forms of phosphate. 0 ppm has been assigned to the phosphorous of non-condensed 'free' phosphoric acid, while more shielded peaks at –11 and –24 ppm have been assigned to mono-substituted and di-substituted phosphorous, respectively.[13] So a peak at -12 ppm indicates the presence of at least phosphate dimer, $H(OP(O_3))_2OH$ and the endgroup phosphorous atoms of trimer and higher order poly(phosphates), and a peak at ~-24 ppm indicates the presence of phosphate trimer, $H(OP(O_3))_{\geq 3}OH$ and higher order poly(phosphates). From the NMR data at low phosphoric acid, P:N = 0.35 and 1.4, no comment can be made on the state of condensation of phosphoric acid because of the broad peaks. With the two high composition samples, it is clear that there is a significant amount 'free' phosphate in the P:N = 2.8 and 4.2 samples. From integrations of peak areas, Table 1 was prepared. Table 1 lists the peak location and the relative number of total phosphorous atoms determined by the integration ratio followed by the relative number and percentage of molecules that are phosphate monomers, dimers and trimers. The assumptions made include: no tetramer and higher aggregate species are present (because of seemingly low peak area of di-substituted species), a trimer has two phosphorous atoms that would be present at –12 ppm and one at –24 ppm and a dimer phosphorous is represented by the peak at –12 ppm.

**P/N = 2.7**

| Peak, ppm | relative # of total P's | aggregation type | relative # of molecules | relative % of molecules |
|---|---|---|---|---|
| 0 | 60 | monomer | 60 | 76 |
| -12 | 38 | dimer | 17 | 22 |
| -24 | 2 | trimer | 2 | 2 |

**P/N = 4.2**

| Peak, ppm | relative # of total P's | aggregation type | relative # of molecules | relative % of molecules |
|---|---|---|---|---|
| 0 | 38 | monomer | 38 | 58 |
| -12 | 56 | dimer | 22 | 33 |
| -24 | 6 | trimer | 6 | 9 |

Table 1: For samples with P:N = 2.7 and 4.2, peak location, relative number of total phosphorous atoms and relative number and percentage of molecules that are phosphate monomers, dimers and trimers

At P:N = 4.2, an increase in the relative number phosphate dimers and trimers is observed when compared to the P:N = 2.7 sample. This may be because the phosphoric acid present in the P:N = 4.2 sample interacts less with the polymer matrix and more with other phosphoric acid molecules resulting in more condensation. This behavior is more like pure phosphoric acid that can undergo condensation at 150 °C especially in the presence of amine base and reduced pressure. The P:N = 0.35 and 1.4 samples may contain less of the condensed phosphates. Increased interaction with the backbone and less interaction with other phosphates occurs because of the lower phosphoric acid

compositions. The infrared spectra for the samples indicate different species are present as acid composition is changed, but specific vibrational modes associated with aggregate species cannot be correlated with the NMR data at this point.

**Ionic Conductivity**

Proton conductivity measurements for the xPEI:$H_3PO_4$ membranes were taken at 60 °C to 150 °C under vacuum using a four probe geometry and an a.c. method[15] to decrease contact resistances and electrolyte polarization at the electrodes, respectively. Measurements were taken on membranes with 2.1N:1cross-linker and phosphoric acid compositions from P:N = 0.4 to 4.2, as well as samples with P:N = 0.7 and N:cross-linker = 8 to 2. In general, proton conductivity was dependent on phosphoric acid composition, temperature and the cross-link composition. Throughout the 60 to 150 °C range, all samples displayed Arrhenius behavior.

Figure 7 displays ionic conductivity versus temperature from 60 to 150 °C for samples with 2.1N:1cross-linker and varying compositions of phosphoric acid.

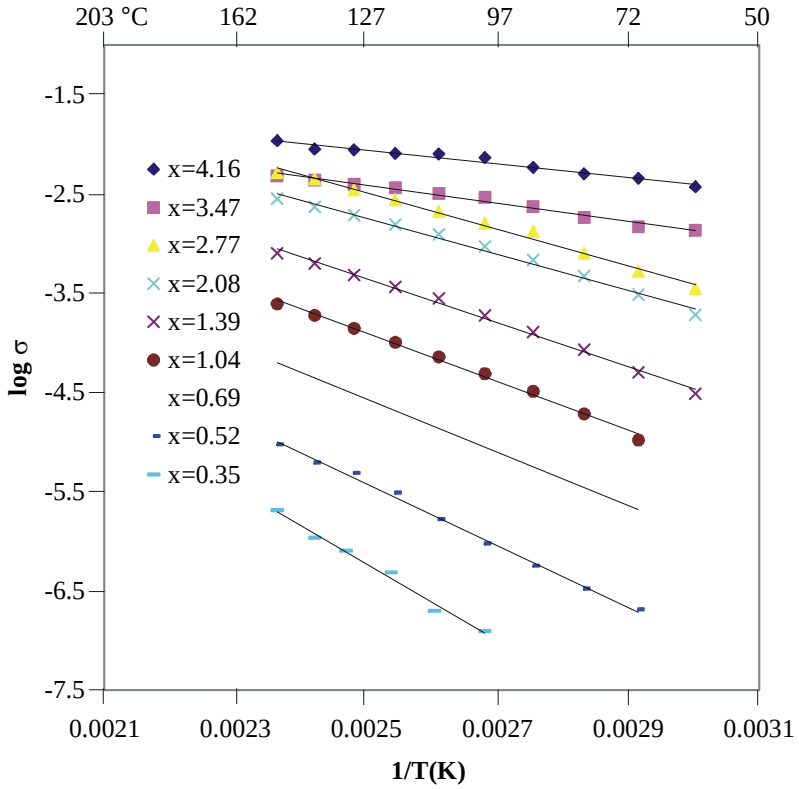


Figure 7: Plots of conductivity versus temperature from 60 to 150 °C for samples with 2.1N:1cross-linker and x(P:N) from 0.35 to 4.16

Conductivity increases approximately five orders of magnitude from low to high acid composition. The dependence of phosphoric acid on conductivity is shown in Figure 8, where the ionic conductivity is plotted versus P:N at 90, 120 and 150 °C for samples with a 2.1N:1crosslinker ratio. Dramatic increases in the ionic conductivity are observed

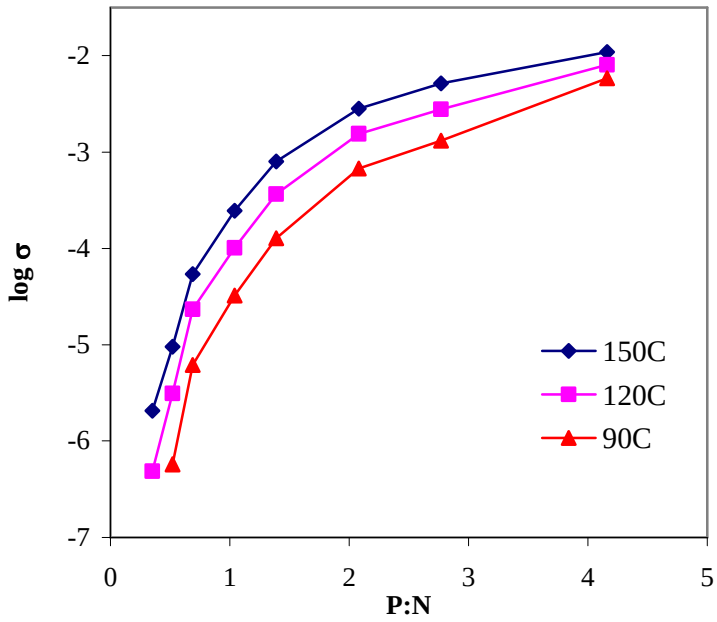


Figure 8: Plots of conductivity versus P:N at 90, 120 and 150 °C for samples with 2.1N:1cross-linker

at P:N ratios less than 2, while above this increases in conductivity are smaller in magnitude. The maximum conductivity observed for the highest acid composition sample was 0.01 S/cm. Table 2 compares the ionic conductivity of the xPEI:$H_3PO_4$ with 4.2P:1N to published Nafion[16], phosphoric acid[17] and phosphoric acid containing PBI[18]. It is uncommon to find non-humidified reported values of conductivity for proton-conducting membranes at temperatures above 100 °C because of membrane dehydration and significant conductivity decreases. All of the cross-linked PEI samples were tested at 0 % relative humidity to provide baseline minimum conductivity values at specific temperatures as humidified atmospheres increase conductivity values and because of uncertainty in the regulation and measurement of humidity.

| sample | T (°C) | Relative Humidity (%) | σ (S/cm) |
|---|---|---|---|
| Nafion | 103 | 100 | 0.00054 |
| $H_3PO_4$ (85 wt. %) | 150 | 0 | 0.568 |
| PBI:$H_3PO_4$ (6.3 P:1 r.u.) | 150 | 5 | 0.0047 |
| PBI:$H_3PO_4$ (6.3 P:1 r.u.) | 150 | 30 | 0.059 |
| XPEI:$H_3PO_4$ (4.2 P:1 N) | 150 | 0 | 0.010 |

Table 2: Comparison of the the ionic conductivity in the proton conducting systems Nafion, $H_3PO_4$, PBI:$H_3PO_4$ and xPEI:$H_3PO_4$

The xPEI:$H_3PO_4$ membrane with high acid composition (4.2P:1N) has a higher conductivity than reported values for very highly acid doped polybenzimidazole even at 5% relative humidity. A 6-fold increase in relative humidity for the polybenzimidazole sample results in a higher conductivity than the xPEI:$H_3PO_4$ membrane. Nafion's conductivity is very highly dependent on humidity above 55 °C, where it begins to decrease from 0.039 S/cm at 60 °C to 0.00054 S/cm at 103 °C at 100% humidity. Above 100 °C, Nafion conductivity decreases sharply.[16, 19]

Also seen in Figure 7, the slope of the ionic conductivity becomes less negative as the conductivity increases. From the slope of the plot, the apparent activation energy for ionic conduction was calculated and shown in Figure 9. This activation energy reflects

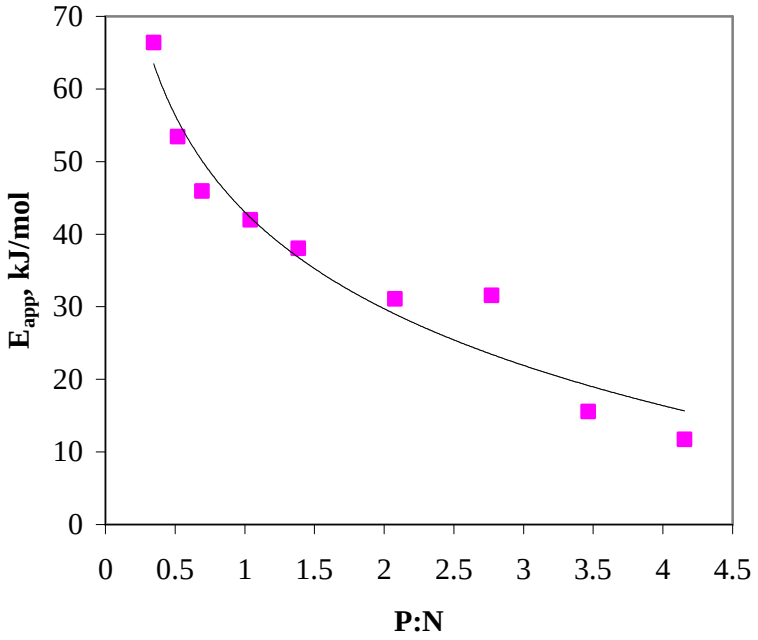


Figure 9: Plot of apparent activation energy for ion conduction versus P:N for xPEI:$H_3PO_4$ samples with 2.1N:1cross-linker

the temperature effect on ion conduction. At a P:N = 4.2, the apparent activation energy for ion conduction is 12 kJ/mol compared with 21 kJ/mol for Nafion membranes[20] and 28 kJ/mol for high phosphoric acid composition poly(benzimidazole)[18] membranes. From Figure 8, a change in the slope of the apparent activation energies is evident and becomes less negative as the P:N ratio increases. Figures 7, 8 and 9 combined suggest that a change in mechanism of ionic conduction occurs as the phosphoric acid composition is increased (Figure 10). At low acid compositions, proton conduction is likely the result of

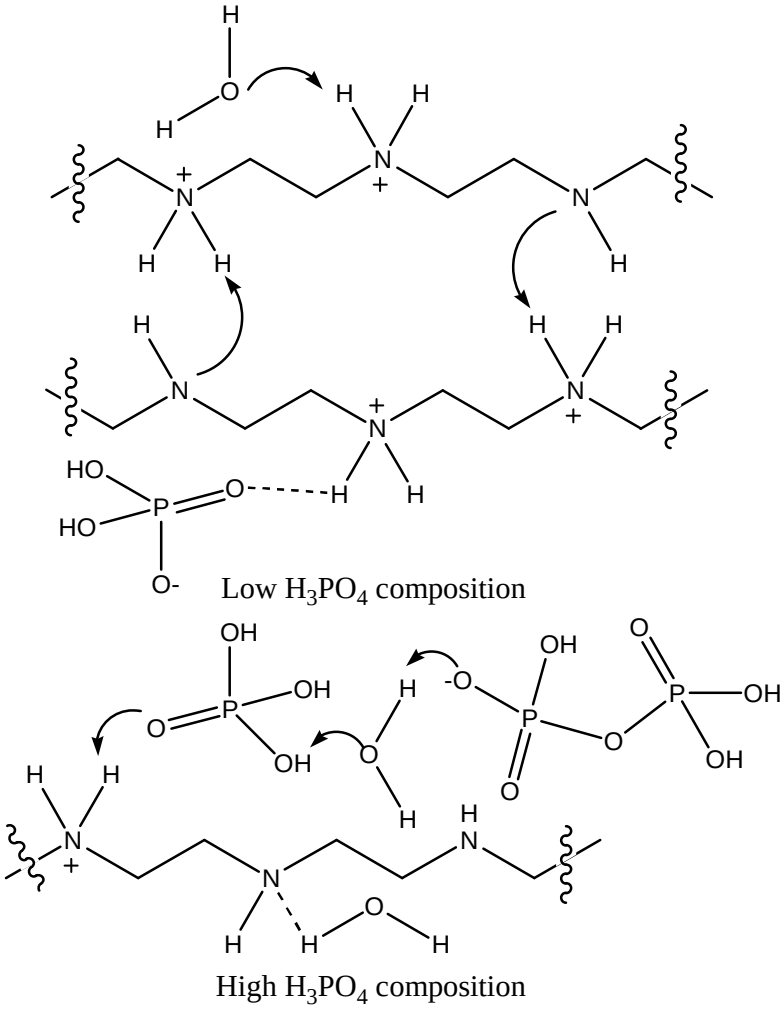


Figure 10: Model for proton conduction at low and high phosphoric acid compositions

significant proton interaction/hopping between the phosphate and the polymer matrix because of the presence of less acid and mobile charge carriers. At higher acid compositions, the number of mobile charge carriers increases, less relative proton interaction with the polymer matrix occurs and proton transport is likely to be more dependent on the diffusional mobility of the additional phosphoric acid. In general, the

mechanism for proton conduction may be more like that in pure phosphoric acid but with the presence of more condensed phosphates.

Examination of the dependence of cross-link density on the ionic conductivity at set phosphoric acid compositions (P:N = 0.7) revealed that conductivity actually increases as theoretical cross-link density increases (Figure 11). This is surprising because usually polymer stiffening occurs with cross-linking.

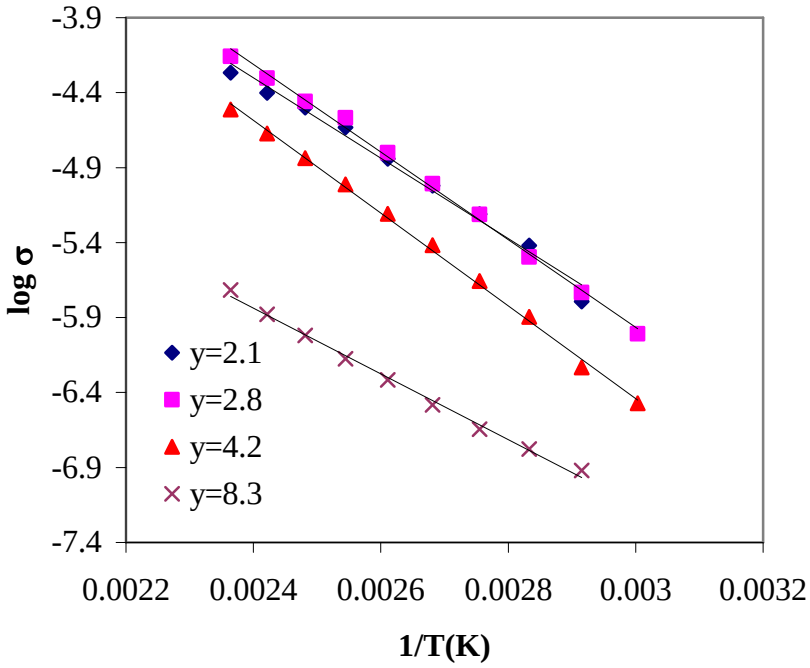


Figure 11: Ionic conductivity versus temperature for xPEI:$H_3PO_4$ samples with P:N = 0.7 and N:cross-linker = 2.1 to 8.3

Although an explanation is not obvious, the cross-link unit may play a role in interacting with the phosphates in some way and result in the generation of more mobile protons. The conductivity of the N:cross-linker = 2 and 3 samples is about the same indicating some limit may have been reached.

**Fuel Cell Testing**

Given the high ionic conductivity, the performance of xPEI:$H_3PO_4$ membranes in a working PEMFC was desired. Membrane electrode assemblies (MEAs) were constructed to fit in a purchased fuel cell that allowed for MEA interchange. As described in the introduction, an MEA consists of three layers: two catalyst layers containing typically platinum on carbon (Pt/C) and electrically conducting carbon sandwiching an electrolyte membrane. Initially, Pt/C was made from literature procedures starting with platinum strips, converting them into chloroplatinic acid with mixtures of $HNO_3/H_2SO_4$, adding a conductive carbon and the chloroplatinic acid to an aqueous solution followed by addition of a reductant and then workup. This yielded Pt/C whose x-ray diffraction data was similar to that in the literature, but was later found not to perform comparably to a sample of commercial Pt/C most likely due to surface area/particle size effects not easily controlled by those with inexperienced in inorganic dimensional morphology. So, two commercial Pt/C catalysts were purchased: one from Aldrich (99%) in a powder form and the other from Electrochem where the platinum was already affixed to an electronically-conducting carbon paper and contained 1 mg Pt/$cm^2$ (20 wt.% Pt/VXC72).

Composite MEAs incorporating xPEI:$H_3PO_4$ into the electrode layers were prepared using the powder-based catalyst but were not as consistent (although fuel cell power output was sometimes as high or higher) as the platinized carbon paper. The MEAs with the platinized carbon paper were assembled by making a mulit-layer sandwich with the component order shown in Figure 12. First a square of polyethylene (Glad Press'n Seal, sticky side up) with a 1 $cm^2$ square cut out of the middle was layed

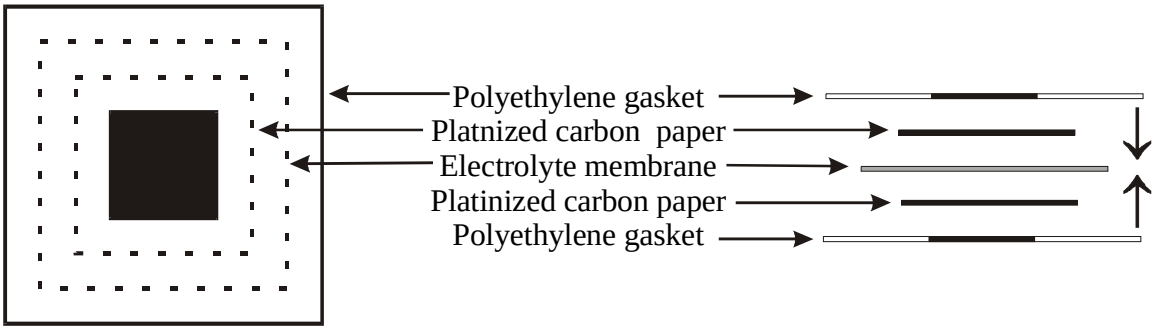


Figure 12: Diagram of a typical MEA prepared showing the different components and component ordering

flat and then the catalyst sheet, electrolyte membrane and catalyst sheet were placed on top with the bottom electrode aligned with the square hole. A top sheet of polyethylene with the same size 1 $cm^2$ square cutout was then placed sticky side down over the MEA assembly and compressed with other polyethylene sheet to form the version of the MEA that was incorporated and tested in the fuel cell.

The fuel cell, including the MEA, and testing apparatus is shown in Figure 13. Gas inlets and exits are marked, and regulators controlled the flow of gas. Current and

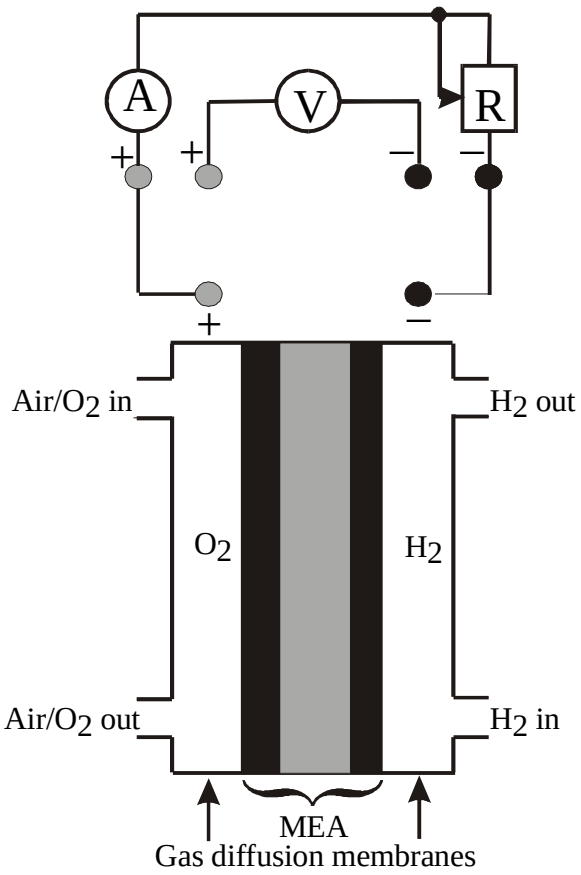


Figure 13: Schematic of the fuel cell setup including the electrical and gas connections

voltage were measured at the fuel cell current collectors with two Kietheley digital multimeters. To measure fuel cell performance under different loads, resistors from 0.1 to 10 Mohm were placed in series with the current-measuring multimeter. Hydrogen (99.9%) was supplied from a regulated tank, while filtered dry air was used as a substitute for pure oxygen.

An MEA with a Nafion® 117 electrolyte membrane was incorporated into the fuel cell and its performance tested to provide a way of comparing data obtained with xPEI:$H_3PO_4$ based MEAs. The Nafion MEA was prepared in the same way as the

xPEI:$H_3PO_4$ MEAs and allowed to run 16 hours with no applied external resistance (other than that of the internal resistance ammeter) before taking performance data. In Figure 14, the current and voltage outputs are plotted at different applied external loads at room temperature after the current and voltage stabilized. With no applied external

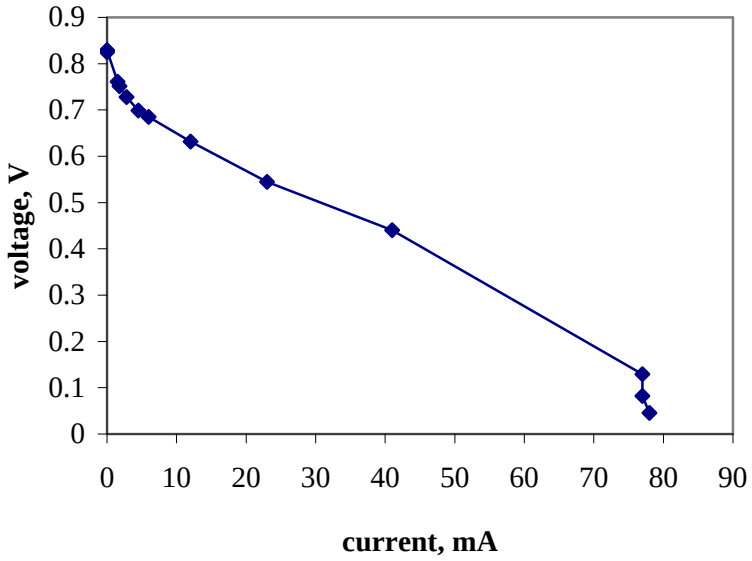


Figure 14: Plot of current versus voltage for fuel cell operating at room temperature with an MEA containing a Nafion 117 membrane

resistance, the cell puts out a current of 78 mA at a voltage of 0.0454 V, while, with increases in the applied resistance, current decreases and voltage increases. The curve resembles Figure 8 presented in Chapter 1 in that, from low to high current, the curve initially decreases significantly in voltage followed by a relatively unchanging slope and then a sharp decrease in voltage. The initial loss in voltage from theoretical of 1.23 V at the open circuit voltage (activation losses) is caused by the slow pace of the reactions taking place on the surface of the electrodes. Voltage is also required to drive the chemical reaction that transfers the electrons to or from the electrode and peroxide and

water formation at the electrodes. The voltage loss associated with the middle region as defined by the relatively unchanging slope is related mainly to the internal resistance of the cell that deals with the ionic resistance of the electrolyte and the electrical resistances of the catalysts and the wiring (ohmic losses). Usually the electrical resistances are small compared to the ionic resistances of the electrolyte. At higher currents, higher conversion of $H_2$ and $O_2$ gases takes place, and the voltage drop is related to supply not meeting demand resulting in fewer reactants remaining on the catalyst. The fuel cell's voltage declines rapidly when the current becomes very high as the electrodes are starved

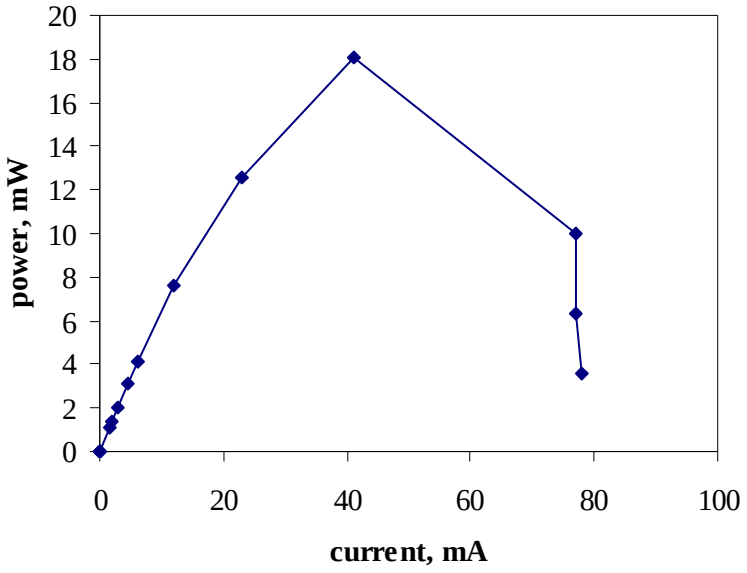


Figure 15: Plot of current versus power for fuel cell operating at room temperature with an MEA containing a Nafion 117 membrane

of gases.[21] The power, in mW, that the fuel cell with the Nafion membrane produces is shown in Figure 15 at different currents. The power reaches a maximum of 18 mW at 41

mA and 0.419 V. The shape of this plot is comparable to other Nafion power curves reported. The DC resistance of the cell was ~500k ohms.

xPEI:$H_3PO_4$ based MEAs were tested in the fuel cell in a manner identical to the Nafion MEAs, i.e. the cell was run with no applied external resistance for 16 hours at room temperature before performance data was taken. Figure 16 shows a plot of the

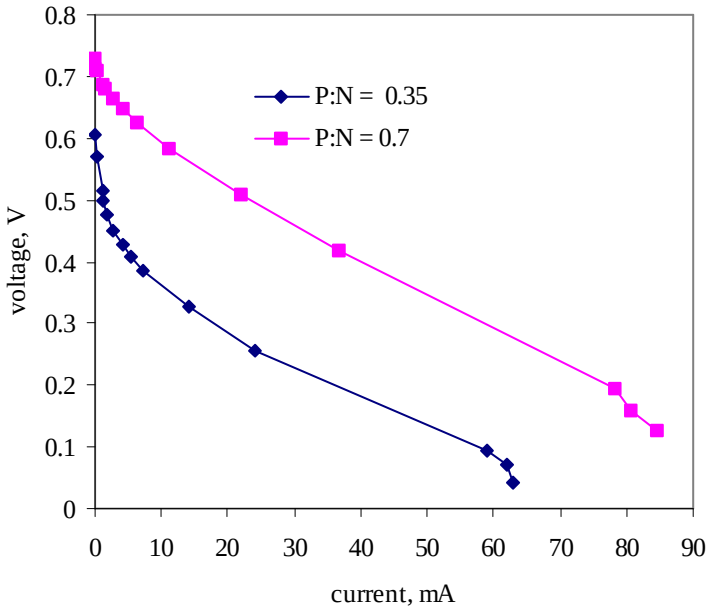


Figure 16: Plots of current versus voltage for a fuel cell operating at room temperature with MEAs containing xPEI:$H_3PO_4$ membranes where P:N = 0.35 and 0.7

current versus the voltage for two MEAs with P:N = 0.35 and 0.70. Overall voltages and currents are higher for the MEA with P:N = 0.70, but the overall curve looks approximately the same. The open circuit voltage for the P:N = 0.70 MEA was a little over 1 V higher than the P:N = 0.35 MEA. The power in milliwatts versus current is presented in Figure 17 and shows that the power output for both MEAs is approximately

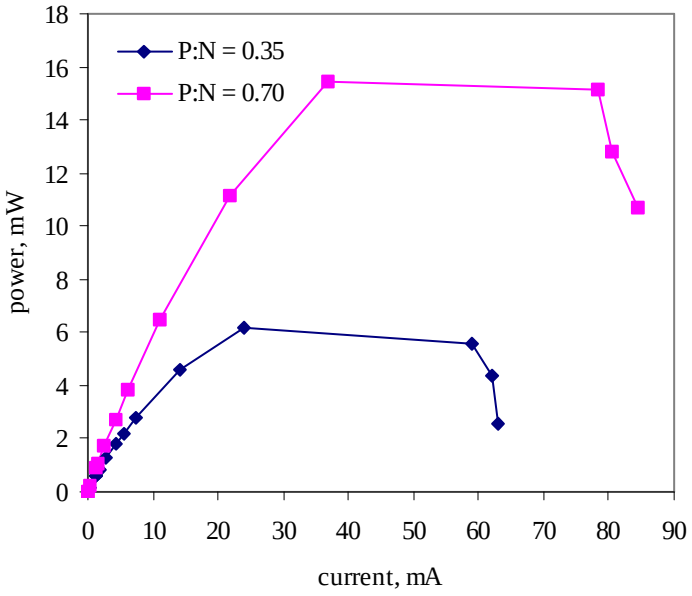


Figure 17: Plots of current versus power for a fuel cell operating at room temperature with MEAs containing xPEI:$H_3PO_4$ membranes where P:N = 0.35 and 0.7

the same in relative performance curve shape. The power maximum for the P:N = 0.35 MEA was ~ 6 mW at 24 mA and 0.26 V, while, for the P:N = 0.70, it was ~ 15 mW at 37 mA and 0.42 V. Cell resistances were ~500k ohms for both the P:N = 0.35 and 0.70 MEA. The DC resistances of the entire fuel cell when both MEAs were incorporated was ~500k ohms for each and was not significantly different than the fuel cell resistance with the Nafion MEA

Direct comparison of the P:N = 0.70 MEA with the Nafion MEA (Figure 18) reveals very similar performance for each. Given that both MEAs were prepared and

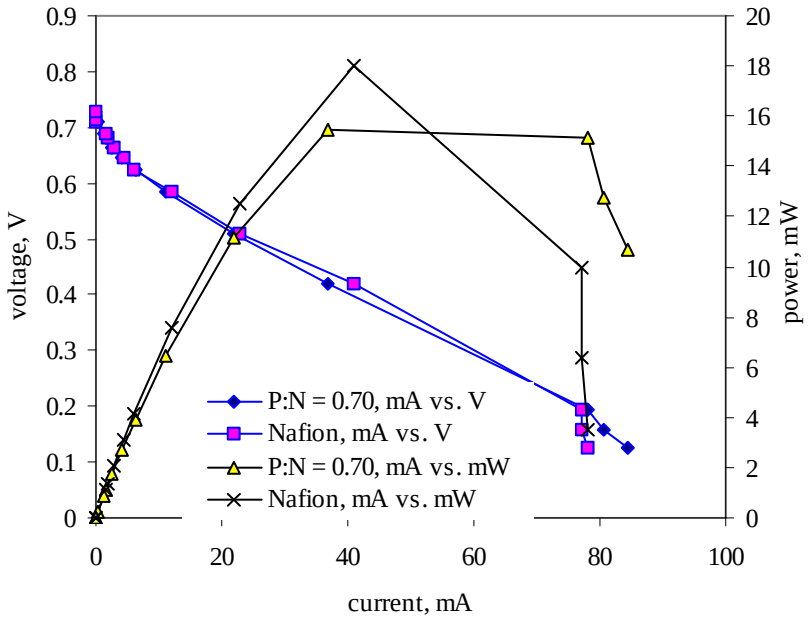


Figure 18: Comparison of the current versus voltage and current versus power plots for MEAs with Nafion 117 and xPEI:$H_3PO_4$ where P:N = 0.7

tested in the same way, this indicates that the xPEI:$H_3PO_4$ conductivity is not a significant issue at low temperatures and phosphoric acid composition. At temperatures above 100 °C, the xPEI:$H_3PO_4$ membranes are likely to perform better than Nafion given Nafion's large dropoff in conductivity.

To better understand the sources of voltage drop from the theoretical OCV, a current interrupt technique was used. The current interruption technique is a simple method that can give qualitative, and in some cases quantitative, information about the magnitude of the activation and ohmic losses contributing to the overall voltage drop from the theoretical OCV. It involves measuring the voltage of a fuel cell at a current at which mass transport voltage drop is negligible and then rapidly opening the circuit and

recording the voltage response. In this region of performance, only activation and ohmic losses are responsible for the voltage drop and the typical form of the voltage response for the current interruption is displayed in Figure 19.

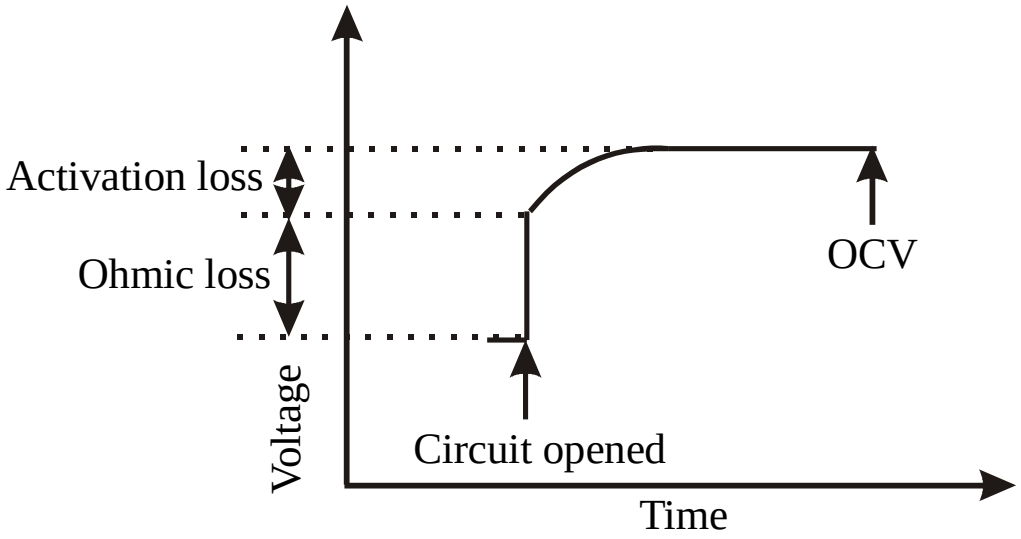


Figure 19: Graph of voltage versus time for a fuel cell after a current interrupt

This behavior results because as the current is suddenly cut off the ohmic losses immediately reduce to zero, while the charge double layer formed as the cell operates takes time to disperse. Ohmic losses related to electrical resistance are considered small in relation to the ionic resistance in PEMFCs, so the ohmic loss from this test is often used to compare voltage drop related to electrolyte membranes.[22-24] The current interrupt test was performed on a Nafion based MEA and an xPEI:$H_3PO_4$ MEA where P:N = 0.70. The ohmic losses for the membranes in the ohmic region of the performance curve are displayed in Figure 20.

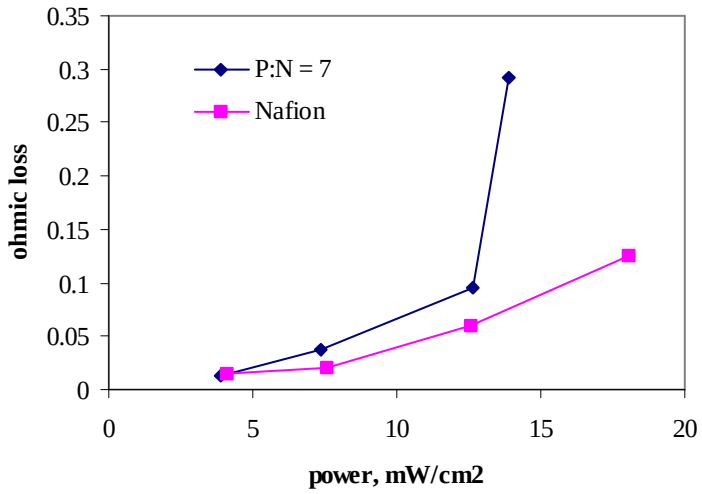


Figure 20: Ohmic loss versus power produced from the fuel cell at room temperature with a Nafion MEA and an xPEI:$H_3PO_4$ MEA where P:N = 0.70

At higher powers, the ohmic loss or ionic resistance becomes larger in the xPEI:$H_3PO_4$ MEA relative to the Nafion MEA. This may cause the xPEI:$H_3PO_4$ membrane to deliver a lower maximum power and implies at higher ionic/electrical currents the xPEI:$H_3PO_4$ membrane cannot handle as high of an ionic current as well at room temperature. Future current interrupt experiments should be performed at elevated temperatures (>100 °C) to evaluate if the ohmic losses for the xPEI:$H_3PO_4$ membrane become less than the Nafion membrane as would be expected given Nafion's characteristic dehydration at elevated temperatures.

**Conclusion**

Thermally and mechanically stable xPEI:$H_3PO_4$ membranes have been made by cross-linking high molecular LPEI-HCl in the presence of aqueous phosphoric acid and

allowing ensuing gel formation and dehydration. Ionic conductivity for these membranes was found to be comparable to the best PBI:$H_3PO_4$ values and much better than Nafion at 150 °C. A change in the way ion conduction occurs is evident over the range of P:N samples with the apparent activation energy decreasing significantly at higher phosphoric acid compositions. IR studies show that a large portion of the protonated amines found in LPEI-HCl are removed possibly by the evolution of HCl during the pre-test thermal treatment as a result of a decreasing of the $pK_a$ of the amine sites through functionalization. Also, a noticeable higher frequency shift of the phosphoric acid P-O stretching bands is evident as the acid composition is increased implying the presence of increased relative concentration of completely protonated phosphate. $P^{31}$ NMR reveals that, at least at high phosphoric acid composition, a significant number phosphorous contain molecules are dimeric or high order phosphates. All this, including the ionic conductivity data, indicate that proton conduction at low phosphoric acid composition is likely to be confined mostly to the backbone as a result of a hopping mechanism promoted by the presence of phosphoric acid and traces of water. At higher acid compositions, proton conduction becomes more diffusion-based as the number of potential charge carriers increases and less interaction of the phosphate species with the immobile polymer matrix occurs resulting in higher conductivity (added acid behaves also like a diluent).

A method of testing the performance of xPEI:$H_3PO_4$ membranes as MEAs in a fuel cell was developed. The performance of Nafion and xPEI:$H_3PO_4$ based MEAs were found to be similar at room temperature indicating that the conductivity of the membranes is sufficient. The xPEI:$H_3PO_4$ membrane makes a slightly larger contribution

to ohmic losses from theoretical OCV as seen by the current interrupt tests. At elevated temperatures (>100 °C), it is expected that the xPEI:$H_3PO_4$ membranes will surpass the performance of Nafion membranes given their thermal stability and higher ionic conductivity. The current fuel cell components cannot survive operation at high temperatures, so construction of a high temperature fuel is necessary. xPEI:$H_3PO_4$ membranes have high potential for serving as the electrolyte membrane in PEMFCs given their high conductivity, stability and low cost.

**References**


1. Mehta, V. Cooper, J.S. *J. Power Sources* **2003**, 114, 32.
2. Calculated using current Aldrich prices for a batch starting with 10 g poly(2-ethyl-2-oxazoline)
3. www.fuelcellstore.com
4. Stecher, P.G. Editor 'The Merck Index of Chemicals and Drugs' Merck & Co., Inc.: Rahway, New Jersey, 1960.
5. Daniel, M.F. Desbat, B. Cruege, F. Trinquet, O. Lassegues, J.C. *Solid State Ionics* **1988**, 28-30, 637.
6. Schoolmann, D. Trinquet, O. Lassegues, J.C. *Electrochim. Acta* **1992**, 37, 1619.
7. Tanaka, R. Yamamoto, H. Kawamura, S. Iwase, T. *Electrochim. Acta* **1995**, 40, 2421.
8. Senadeera, G.K.R. Careem, M.A. Skaarup, S. West, K. *Solid State Ionics* **1996**, 85, 37.
9. Tanaka, R. Yamamoto, H. Shono, A. Kubo, K. Sakurai, M. *Electrochim. Acta* **2000**, 45, 1385.
10. Lloyd, D. McNab, H. *Synth.* **1973**, 12, 791.
11. Lloyd, D. Nyns, C. Vincent, C. A. Walton, D. J. *J. Chem. Soc., Perkin II* **1980**, 10, 1441.
12. Bouchet, R. Siebert, E. *Solid State Ionics* **1999**, 118, 287.
13. Chung, S.H. Bajue, S. Greenbaum, S.G. *J. Chem. Phys.* **2000**, 112, 8515.
14. Chung, S.H. Wang, Y. Greenbaum, S.G. Bzducha, W. Zukowska, G. Wieczorek, W. *Electrochim. Acta* **2001**, 46, 1651.
15. Cahan, B.D. Wainright, J.S. *J. Electrochem. Soc.* **1993**, 140, L185.
16. Summer, J.J. Craeger, S.E. Ma, J.J. DesMarteau, D.D. *J. Electrochem. Soc.* **1998**, 145, 107.
17. Chin, D.T. Chang, H.H. *J. App. Electrochem.* **1989**, 19, 95.

18. Ma, Y.L. Wainright, J.S. Litt, M.H. Savinell, R.F. *J. Electrochem. Soc.* **2004**, 151, A8.
19. Rierke, P.C. Vanderborgh, N.E. *J. Mem. Sci.* **1987**, 32, 313.
20. Slade, R.C.T. Hardwick, A. Dickens, P.G. *Solid State Ionics* **1983**, 9-10, 1093.
21. Winter, M. Brodd, R.J. *Chem. Rev.* **2004**, 104, 4245.
22. Larminie, J. Dicks, A. 'Fuel Cell Systems Explained' John Wiley and Sons Ltd.: West Sussex, England, 2003.
23. Slade, S. Campbell, S.A. Ralph, T.R. Walsh, F.C. *J. Electrochem. Soc.* **2002**, 12, A1556.
24. Lee, C.G. Nakano, H. Nishina, T. Uchida, I. Kuroe, S. *J. Electrochem. Soc.* **1998**, 145, 2747.

## Experimental

### Polymer Synthesis

**Synthesis of LPEI-HCl:** In a 3 L round bottom flask (rbf), 30 g poly(2-ethyl-2-oxazoline) (Aldrich, avg. MW 200k or 500k) was dissolved with 1800 mL of 3 M HCl with stirring. The solution was heated at solvent reflux for 5 days, whereupon the liquid component was removed under reduced pressure using a rotary evaporator. The remaining material was an off-white granular powder and was verified to be LPEI-HCl using NMR. $^{1}$H-NMR ($D_2O$): δ (ppm)- 3.35 (s , variable peak area), 3.18 (s).[1]

**Neutralization of LPEI-HCl to LPEI:** The above LPEI-HCl was then dissolved with 3 L of distilled water and neutralized with NaOH pellets until the pH was >10 (as determined with pH paper). This results in polymer precipitation, so the slurry was heated to ~75 °C with stirring to re-dissolve the polymer and ensure maximum neutralization. The solution was cooled to room temperature usually with an ice bath resulting in re-precipitation of the polymer, LPEI. This was vacuum filtered with a glass funnel containing a glass frit to remove the liquid component containing NaCl and NaOH. The pH of the filtrate should be neutral if no NaOH remains in the polymer, so the pH was of the filtrate was tested. After the first filtration, the pH was never neutral, so the LPEI was placed in a large beaker and 3 L of distilled water was added again followed by heating to dissolution, cooling to room temperature and filtering. When the filtrate was neutral, typically after 3 or more of these cycles, the LPEI-hydrate was dried under vacuum at room temperature overnight. This material was then put into a jar and dried under

vacuum at ~50 °C for 1 day and at ~70 °C for 1 day resulting in anhydrous LPEI. $^{1}$H-NMR ($CD_3OD$): δ (ppm)- 2.65 (4 H); $^{13}$C-NMR ($CD_3OD$) δ (ppm)- 49.8. NMR data was consistent with reported values.[1, 2]

**Synthesis of Poly((*N*-2-cyanoethyl)ethylenimine):** LPEI (3 g, 0.070 mol), synthesized from the above method, and methanol (35 mL) were added to a flask and allowed to dissolve with stirring. Acrylonitrile (3.75 g, 0.071 mol) was then added to this solution, and the reaction solution was heated at solvent reflux for 90 minutes. At this point, the solution became slightly cloudy, and the liquid component was removed under reduced pressure leaving an amber-tinted, highly viscous liquid. Yield: 87 %. Calculated ca. MW: 190k (based on starting average MW for LPEI of 86k). $^{1}$H-NMR ($CD_3OD$): δ (ppm)- 2.90 – 2.75 (q, -C*H*$_2$CN, br), 2.70 – 2.78 (s, -C*H*$_2$C*H*$_2$-, br), 2.58 – 2.48 (t, -NC*H*$_2$CH$_2$CN, br).[3] The above method was used to cyano-ethylate other molecular weight poly(ethylenimine) and non-polymeric amines.

**Synthesis of Diglyme and LiTf Infused TEG Cross-linked PEI Gels**: PEI (indicated by Aldrich to be a mixture of linear and branched chains, $M_w$ = 463), diglyme (99.5% anhydrous), TEG (90%) and LiTf (96%) were obtained from Aldrich and stored in a dry air purge glove box. PEI, TEG and diglyme were used as received. LiTf was dried under reduced pressure at 110°C for 32 hours and stored in a dry air purge glove box. IR and NMR were used to verify the absence of spectroscopically meaningful amounts of water and other contaminants. All gel electrolytes were prepared in a dry air purge glovebox. A typical sample was prepared by adding appropriate amounts of PEI, diglyme and LiTf to

a vial and stirring until complete dissolution of each component occurred. The desired amount of TEG was added, the mixture was stirred to ensure complete dissolution of TEG and the vial was capped. A solid material resulted within thirty minutes to three hours depending on the LiTf and diglyme concentration.[4]

**Synthesis of Poly((*N*-methyl)ethylenimine):** 5 g LPEI (0.12 mol) was dissolved with 50 ml of hot (> 75 °C) distilled water, and then 200 mL of formic acid (88 % solution) and 125 mL of formalin (37 % solution) were added. This solution was heated at solvent reflux for 24 hours. The solution was allowed to cool to room temperature. 150 mL of concentrated HCl was added, and this was stirred for a short period of time. The liquid component was next removed under reduced pressure to yield LPMEI-HCl. A minimal amount of distilled water was added to the flask to dissolve the polymer, and this was passed through a column containing an ion-exchange resin (Amberlite IRA(Cl)) where the chloride content was previously exchanged with hydroxide using a $NaOH_{(aq)}$ solution (exchange was verified using the silver nitrate test on the $NaOH_{(aq)}$ filtrate). The size of the column was determined based on the number of equivalents of anion residing on the resin and the number of repeat units in the LPMEI-HCl sample. The amount of resin actually used was theoretically double what was needed to neutralize the LPMEI-HCl. Still, the polymer needed to pass through the column at least two times for complete exchange. Water was removed under reduced pressure, and the sample was dissolved in benzene or toluene and cooled in an ice bath. The solution was then centrifuged to collect any remaining salts and filtered. The PMEI was isolated by benzene removal under reduced pressure, and the polymer was dried in a vacuum oven at 50 °C. ~ 95 % yield

was obtained. $^{1}$H-NMR (benzene-$d_6$) δ (ppm)- 2.6 (4 H), 2.2 (3 H); $^{13}$C-NMR (benzene-$d_6$) δ (ppm)- 56.4, 43.2.[1, 5]

**Cross-linked PMEI:LiX Electrolyte**: In a small vial, 0.10 g LPMEI (0.0018 RU mol) was dissolved in 1 mL of monoglyme or methanol along with the desired amount of lithium salt (either LiTf or LiTfsi). Cross-linker (1,6-di-bromohexane or 1,4-butane-di-triflate) (0.00009 mol) was added and stirred until dissolution. This solution could then be cast onto a desired substrate. Typically, it was covered to prevent excessive airflow contact, and the liquid component was allowed to evaporate. The material was placed in an oven at 60 °C overnight and resulted in a hardened material that did not re-dissolve in methanol or monoglyme.

**Cross-linked PCEEI:LiX Electrolyte**: Partially cyano-ethylated PEI from 75 to 90 % substitution was prepared in a manner similar to that described above. This material, typically 0.1 g, was then dissolved in 1 mL acetonitrile. To the solution, acrolein was added to fully substitute the non-substituted PCEEI sites. Lithium salt was also added. This solution was stirred, and the solution could immediately be dispensed onto an appropriate substrate, where upon solid cross-linked films were left after solvent evaporation. IR verified essentially complete substitution of PCEEI through this method.

**xPEI:$H_3PO_4$ Electrolyte:** The typical manner of preparation of a cross-linked PEI gel, in this case where x = 0.69, follows. Linear PEI-HCl was prepared by the acidic hydrolysis of poly(2-ethyl-2-oxazoline) (Aldrich, average $M_w$ *ca.* 500,000) as described above. In a

vial, 0.25 g of the PEI-HCl was dissolved in 5 mL water followed by the addition of 0.25 g phosphoric acid (Fisher Scientific, 85%) and stirring. The cross-linker, 0.25 g 1,1,3,3-tetramethoxypropane, was then added, and the vial immediately capped and stirred for 10 minutes. The 1,1,3,3-tetramethoxypropane is not immediately soluble but quickly becomes so as the reaction progresses. The solution was then poured into a Teflonized dish, covered tightly to prevent cross-linker evaporation and then left for two days. Typically, a homogeneous, freestanding gel formed within 24 to 48 hours. The cap was then removed, water was allowed to slowly evaporate for 3 days, and the gel was transferred out of the dish to a dessicator and placed under vacuum until sample evaluation.[6]

**Techniques**

**Infrared Spectroscopy:** IR samples were typically prepared in two ways: 1. a solution of the material was cast onto a salt plate (NaCl, KBr or ZnSe) and the solvent was evaporated or the sample was thermally treated and 2. a drop of the sample was sandwiched between two salt plates and then sealed with tape. Infrared spectra were acquired for samples in either an evacuated or dry air purge atmosphere. Spectra were acquired with a Bruker IFS66V FT-IR spectrometer with a KBr beamsplitter over a range of 4000 – 400 $cm^{-1}$ at a resolution of 1 $cm^{-1}$. Commercially available software (Thermo Galactic, Grams/AI 7.00) was used for spectral analysis. The spectral bands were fitted using a mixed Gaussian-Lorenzian function and a straight baseline.

**Differential Scanning Calorimetry:** Sample solutions were cast into aluminum DSC pans and dried in a dried air purge glovebox overnight followed by 24 hours in a vacuum oven at 50 °C. The samples were then capped with an aluminum DSC pan lid. Thermal data was collected using a Mettler DSC 820 calorimeter with commercially available software from Mettler Toledo (Stare v.6.10) under a dry nitrogen purge. Typically, the samples were cycled between 100 and –100 °C. Sample mass was obtained after the experiment after record pan weights.

**Thermogravimetric Analysis:** Thermograms were obtained with a heating ramp of 10 °C / min under an argon atmosphere with a Dupont 951 Thermogravimetric Analyzer outfitted with Thermal Analysis 2000 software.

**Nuclear Magnetic Resonance Spectroscopy:** $^{1}H$ and $^{13}C$ spectra were obtained using either a Varian 300 or 400 MHz spectrometer. $^{31}P$ spectra were obtained on the Varian 400 MHz spectrometer with a solid state probe.

**Two-probe A. C. Conductivity:** Measurements were obtained by sandwiching samples between two 12.5 mm stainless steel electrodes in an airtight cell. Constant temperatures were maintained using a circulating water/ethylene glycol bath. Impedance measurements were made over the range of 5Hz to 10MHz using an HP 4192A LF impedance analyzer, and impedance plots were fitted using a commercial program (LEVM version 7.1).

**Four-probe A. C. Conductivity:** Measurements were carried out in the 60 – 150 °C range under reduced pressure. Samples were dried at 150 °C under reduced pressure for 16 hours before measurements were taken. Measurements were taken in a glass tube with two stopcocks and four platinum wires fed through the top. The four probe setup consisted of a longitudinal geometry in which two platinum wires were used to apply current to the ends of a sample. Two more platinum wires were used to measure the voltage drop along the film near the center of the sample. A Teflon-coated clamp was used to compress the sample against the four wires. Typical sample dimensions were 1 cm x 0.1 cm x 0.3 cm. After sample insertion, the interior of the glass tube was evacuated with vacuum. This created a very low humidity atmosphere. Heating tape was used to control the temperature inside the tube by applying the tape around the exterior of the glass tube. A Wavetek sweep generator was used in conjunction with a Keithley Model 175 autoranging multimeter and a Keithley Model 169 multimeter to vary the applied frequency between 100 and 500 kHz, measure the voltage and measure the current, respectively. The impedance was plotted versus the a. c. frequency, and the bulk resistance was taken in the frequency independent impedance range of the plot.[7]

Statistical analysis of the error in the ionic conductivity measurements was not done. In general, measurements were repeated once. Reported data was not greater than a half order of magnitude off from the initial measurement. The 4-probe conductivity measurements were compared with the two probe measurements using identical samples and were, in general, less than a half order of magnitude different. Samples tested using the 2-probe configuration were tested for water contamination with IR spectroscopy after measurements. It is not possible to definitively claim very small traces of water or solvent

did not remaining in the samples even if none could be verified using IR spectroscopy. Significant efforts were made to dry samples completely and to keep samples free of contaminants. Other sources of error in the conductivity measurements include incorrect measuring of sample dimensions and instrumental error.

**Li|Polymer Electrolyte|$LiV_3O_8$ Cell Assembly:** Coin cells were assembled by first preparing the individual cell components. The $LiV_3O_8$ paste was prepared by mixing and grinding together, with a mortar and pestle, the following materials: 87 % (by weight) $LiV_3O_8$, 5 % KS6 graphite, 5 % SLP graphite and 3 % Teflon shreds. After compressing this material together, it becomes a cohesive solid that can be made very thin with a rolling pin and a flat surface. A 1.5 cm diameter circle of this material weighing between 6 and 9 mg was cut out with a circle template. The mass was recorded, and the paste was then dried at 110 °C or higher overnight. A 2.2 cm circular sheet of Celgard separator membrane was cut out. A solution of the polymer electrolyte was then prepared (typically 0.10 g PMEI, 0.025 g LiTfsi and 1 ml monoglyme). Each of these components was moved into a dry air purge glovebox. A coin cell bottom (lid with larger diameter) was laid down with a stainless steel metal disk (1.8 cm diameter) inside. The $LiV_3O_8$ cutout was then placed on the metal disk, and then the polymer electrolyte solution was applied until the metal disk area was covered. The solvent was allowed to evaporate for about an hour. The Celgard was then placed on top of the metal disk and more polymer electrolyte solution was added until the Celgard was saturated. This was followed by solvent evaporation for about an hour and then a final dose of solution was applied followed by solvent evaporation for about an hour. The cell was then transferred to a vacuum oven

and dried at ~ 60 °C overnight under vacuum overnight. The same procedure was used when making a cross-linked polymer electrolyte membrane separator except the Celgard was left out. After drying, the cell was transferred to a glovebox with a nitrogen atmosphere where a lithium disk (1.5 cm diameter) and a stainless steel disk was placed on top of the polymer electrolyte infused Celgard. The top of the coin cell was then situated and crimped with the lip of the bottom lid. The cell was then moved to the Arbin Electrochemical Analyzer (AEE) carefully so as prevent shorts. External pressure was applied with a spring-loaded c-clamp with the spring distance acting as the pressure gauge (typically set to 0.60 inch for the springs used). As described before, the force constant of the spring was determined with the use of a force gauge. The cell, outfitted with electrical leads, was then connected with the AEE, and the cell was tested according to a programmed schedule like the one shown below:

| | | | | | | |
|---|---|---|---|---|---|---|
| ✖ | PreRest | 1 | Rest | | | |
| | **Log Limit** | **Step Limit** | **Goto Step** | **Type1** | **Sign1** | **Value1** |
| 1 | ☑ | ☑ | Discharge | PV_CHAN_Step_Time | >= | 01:00:00 |
| ✖ | Rest1 | 2 | Rest | | | |
| | **Log Limit** | **Step Limit** | **Goto Step** | **Type1** | **Sign1** | **Value1** |
| 1 | ☑ | ☐ | | DV_Time | >= | 00:01:00 |
| 2 | ☑ | ☑ | Next Step | PV_CHAN_Step_Time | >= | 00:30:00 |
| ✖ | Discharge | 2 | Current(A) | -1e-005 | | |
| | **Log Limit** | **Step Limit** | **Goto Step** | **Type1** | **Sign1** | **Value1** |
| 1 | ☑ | ☐ | | DV_Voltage | >= | 0.01 |
| 2 | ☑ | ☑ | Next Step | PV_CHAN_Voltage | <= | 1.9 |
| ✖ | Rest2 | 2 | Rest | | | |
| | **Log Limit** | **Step Limit** | **Goto Step** | **Type1** | **Sign1** | **Value1** |
| 1 | ☑ | ☐ | | DV_Time | >= | 00:01:00 |
| 2 | ☑ | ☑ | Next Step | PV_CHAN_Step_Time | >= | 00:30:00 |
| ✖ | Charge | 2 | Current(A) | 1e-005 | | |
| | **Log Limit** | **Step Limit** | **Goto Step** | **Type1** | **Sign1** | **Value1** |
| 1 | ☑ | ☐ | | DV_Voltage | >= | 0.01 |
| 2 | ☑ | ☑ | Next Step | PV_CHAN_Voltage | >= | 3.1 |
| ✖ | Counter | 2 | Set Variable(s) | Reset | Increment | Decrement |
| | **Log Limit** | **Step Limit** | **Goto Step** | **Type1** | **Sign1** | **Value1** |
| 1 | ☑ | ☑ | Rest1 | PV_CHAN_Cycle_Index | <= | 20 |
| 2 | ☑ | ☑ | End Test | PV_CHAN_Cycle_Index | >= | 21 |

Figure 1. Typical schedule for cell cycling on Arbin Electrochemical Analyzer

**MEA Preparation and Fuel Cell Tests:** See Chapter 5.

**Current Interrupt Test:** This test was performed by connecting the voltage leads from the fuel cell to a serial box interface connected to a computer. A program called WinDaq (made by Dataq Instruments) was used to convert the signal into a voltage displayed as a function of time on a computer monitor. This program also allowed saving the time dependent voltage data. The fuel cell voltage was monitored continuously with an applied external resistance and as the current circuit was opened. External resistance was changed with incorporation of different resistors. Data recording was stopped when voltage became steady. The magnitude of the voltage was obtained in the portion of the data in which the fuel cell response to the open circuit was linear. This was taken as the voltage drop associated with ohmic losses.

## References


1. Snow, A.G. 'Synthesis and Spectroscopic Studies of Polymer Electrolyte Hosts: Linear Poly(ethylenimine), Linear Poly(*N*-methylethylenimine) and Linear Poly(2-(2-methoxyethoxy)ethylenimine)' Dissertation, University of Oklahoma, **2002**.
2. Saegusa, T. Ikeda, H. Fujii, H. *Macromolecules* **1972**, 5, 108.
3. Erickson, M. Frech, R. Glatzhofer, D.T. *Electrochem. Acta* **2003**, 48, 2059.
4. Erickson, M. J. Frech, R. Glatzhofer, D.T. *Polymer* **2004**, 45, 3389.
5. Tanaka, R. Ueoka, I. Takaki, Y. Kataoka, K. Saito, S. *Macromolecules* **1983**, 16, 849.
6. Glatzhofer, D. T. Erickson, M.J. Frech, R. *Solid State Ionics*, submitted.
7. Cahan, B.D. Wainright, J.S. *J. Electrochem. Soc.* **1993**, 140, L185.